ABSTRACT

Title of Thesis:	IMPROVING PHYSICS-BASED ENGINEERING FRAMEWORK FOR COMMODITY CLASSIFICATION
	Tejas Rawool, Master of Science, 2026
Thesis Directed By:	Dr. Shuna Ni, Assistant Professor, Department of Fire Protection Engineering

This thesis evaluates and improves a zone-based fire model for predicting Critical Delivered Flux (CDF), a key metric for sprinkler-based fire protection in warehouse environments. Originally validated for Class 2 commodity, the model is extended to four other representative commodities: Class 3, standard plastic, plastic pallet and cartoned meat tray. The model represents rack storage as vertically stacked fuel zones and simulates fire growth and water transport using energy and mass conservation. A two-level hierarchical optimization framework is introduced to improve parameter estimation, classifying parameters as either commodity-specific or test-specific and optimizing them at different levels. This separation enhances parameter consistency and improves the model's adaptability across different commodity types. The enhanced model is validated against experimental data for 5-tier storage configurations and demonstrates good agreement between predicted and experimentally derived CDF values for most commodities except plastic pallets. Two further refinements are

incorporated: (1) commodity-specific tier-to-tier vertical ignition delays are applied to all commodity types to better represent observed vertical fire spread behavior; and (2) a suppression-driven ignition cut-off is applied specifically to the plastic pallet commodity, preventing upper-tier ignition after water application as observed from the experiments. The enhanced model is validated against experimental data for 5-tier rack storage and produces CDF predictions within acceptable accuracy limits for all commodity types. Overall, the proposed framework offers a scalable, physically grounded approach for commodity classification and fire protection design using only two lower-tier tests.

In addition to validating and improving the zone-based model and its implementation, this study examines methods for identifying water application time from test data. Accurate identification is critical, as it defines the transition between free-burn and suppression and governs parameter calibration from lower-tier experiments, with errors propagating into predicted CDF values for high-tier configurations. When direct measurements are unavailable, visual observation of the total HRR curve is the most reliable approach. A sensitivity analysis is also conducted to evaluate the impact of the final test duration, showing that reducing it has minimal effect on both experimentally derived and model-predicted CDF values.

IMPROVING PHYSICS-BASED ENGINEERING FRAMEWORK FOR COMMODITY CLASSIFICATION

by

Tejas Rawool

Thesis submitted to the Faculty of the Graduate School of the
University of Maryland, College Park, in partial fulfilment
of the requirements for the degree of
Master of Science
2026

Advisory Committee:

Assistant Professor Shuna Ni, Chair

Professor Stanislav I Stoliarov, Co-Chair

External Member, Dong Han

Acknowledgements

First and foremost, I would like to express my deepest gratitude to my advisor, Dr. Shuna Ni, for her constant encouragement and frequent, thoughtful feedback throughout this research. Her guidance was instrumental in shaping both the direction and quality of this work. I am especially thankful for the effective research methods she taught me and for the strong work ethic she exemplified, which have profoundly influenced my approach to research and problem-solving. Her mentorship has played a pivotal role in my development as a researcher and engineer.

I would also like to sincerely thank Dr. Dong Han for serving on my advisory committee. His expertise, insightful discussions, and constructive feedback greatly strengthened the modeling framework and interpretation of results presented in this study.

Next, I would like to thank Dr. Stanislav Stoliarov for his continued support and for serving on my advisory committee. His comments, questions, and suggestions during meetings consistently challenged me to think more deeply about my work and helped me refine both my technical reasoning and analytical approach. I am grateful for his time, guidance, and the high standards he encouraged throughout this research process.

I am thankful to the faculty and staff of the Department of Fire Protection Engineering at the University of Maryland for providing a supportive and intellectually stimulating environment. The knowledge gained through coursework, teaching assistant experiences, and interactions with faculty and peers has been invaluable to my academic and professional growth.

Finally, I would like to express my heartfelt gratitude to my family for their unwavering support, encouragement, and belief in me. Pursuing graduate studies far from home comes with its own challenges, and their constant love and reassurance provided the foundation that made this journey possible. I am also deeply thankful to my friends Divya Kamila, Sami Ahmed, and Kashif Ansari for their constant motivation, encouragement, and support throughout my graduate studies. I am equally grateful to my friends and colleagues in the office Subhojit Roy, Maria Mannan, and Yufeng Zheng for creating a positive and engaging work environment and for making daily research both enjoyable and rewarding.

Table of Contents

List of Figures

List of Tables

1. Introduction

Warehouse fires continue to pose a significant risk to life safety and property despite advancements in fire protection technologies. According to the National Fire Protection Association (NFPA) [1], fire departments in the United States responded to an average of approximately 1,500 warehouse structure fires per year between 2018 and 2022, resulting in hundreds of millions of dollars in direct property damage annually. Although warehouse fires represent a relatively small fraction of total structure fires, their consequences are often severe due to high fuel loads, vertically arranged storage, and the inherent challenges of fire detection and suppression in large spaces, and high replacement and remediation costs.

Effective fire protection in warehouse environments relies on an accurate assessment of the fire hazard posed by stored commodities. Commodity classification is a fundamental methodology used to determine appropriate fire protection strategies by categorizing materials and storage configurations according to their fire hazard characteristics. Fire protection standards and guidelines such as the International Fire Code (IFC) [2], NFPA 13 [3], and FM Property Loss Prevention Data Sheets [4] use commodity classification as a primary basis for determining sprinkler system design criteria, including design densities (i.e., minimum water application rates per unit floor area required for fire control or suppression), as well as corresponding protection strategies for storage occupancies.

In practice, many real-world commodities do not clearly meet the classification criteria defined in existing standards or lack sufficient information for unambiguous classification, particularly for products with mixed materials and complex packaging configurations. This challenge is further compounded by the vast number of possible storage arrangements and commodity types encountered in industrial and commercial facilities, which far exceeds what can be systematically addressed through experimental fire testing alone, given that such testing is expensive and time-consuming. Consequently, a robust computational methodology is needed to extend the predictive value of limited experimental data while reducing the number and scale of tests required for new commodity types. Rack storage systems, in particular, present an additional layer of complexity, as they are typically configured with different numbers of vertically stacked fuel layers, commonly referred to as tiers. Lower-tier storage (e.g., two- or three-tier arrays) is smaller in scale, while higher-tier storage (e.g., five-tier arrays) more closely represents the heights encountered in real warehouse environments, yet reliably predicting fire behaviour across different tier configurations from limited lower-tier data remains a key challenge in fire protection engineering. An existing zone-based fire model for predicting the Critical Delivered Flux (CDF), defined as the minimum water application rate required to suppress fire growth, was developed precisely to address this challenge, by calibrating model parameters against lower-tier experimental data and extrapolating predictions to higher-tier storage configurations. Building on this foundation, this thesis presents a systematic extension and refinement of that model, with three primary contributions. First, the model, which was validated for Class 2 commodities, is extended to four additional representative commodities, namely Class 3, standard plastic, cartoned meat tray, and plastic pallet; for each commodity, only lower-tier experimental data are used for model calibration, and the calibrated model is subsequently validated against higher-tier storage configurations. Second, a two-level hierarchical optimization framework is introduced to improve parameter estimation by distinguishing between commodity-specific and test-specific parameters, thereby enhancing model consistency and adaptability across different commodity types. Third, commodity-specific refinements, including tier-to-tier ignition delays and a suppression-driven ignition cut-off for plastic pallets, are incorporated to better capture the observed fire-spread behavior across commodities.

2. Literature Review

Commodity classification is a methodology by which commodities are grouped into distinct classes based on their material properties and fuel geometries for fire protection applications. For each class, a representative commodity is defined, and fire protection strategies for these representative fuels have been established through extensive large-scale testing and accumulated operational experience. Once a commodity is assigned to a class, the protection recommendations associated with the corresponding representative commodity are applied to the commodity of interest. When a new or modified commodity is introduced, the central challenge lies in determining which representative commodity it most closely approximates in terms of fire growth and suppression response. This assessment is inherently complex, as the perceived similarity between commodities depends strongly on the choice of characterization parameters. Accordingly, prior research has emphasized the identification of physically meaningful parameters and the development of experimental and analytical methods to quantify these parameters in a consistent and comparable manner across different commodity types.

The first systematic commodity classification testing procedures were developed in the early 1990s to support the design of automatic sprinkler protection for warehouse storage. Chicarello and Troup [5] proposed a series of large-scale fire suppression tests using fuel arrays configured as two pallet loads long, two pallet loads deep, and two tiers high (2×2×2). In their methodology, the timing of water application was determined based on the calculated activation time of a hypothetical sprinkler, and the measured heat release rates (HRRs) were used in empirical correlations to rank commodities according to fire hazard. This work formed the foundation for modern commodity classification approaches and influenced subsequent experimental methodologies.

Building upon this framework, Arvidson and Lönnermark [6] conducted a series of commodity classification tests aimed at establishing a standardized test methodology for sprinkler protection, aligned with the forthcoming European Standard prEN 12845 [7]. The study had two primary objectives: to establish benchmark experimental data for a range of representative commodities that could be directly related to the classification scheme defined in the standard, and to validate a simplified four-pallet test configuration (2×1×2) as a viable alternative to the original eight-pallet arrangement (2×2×2). Each commodity was tested under three different delivered water application densities, with water application initiated at a convective heat release rate of 2 MW to ensure consistent suppression conditions across tests. The results demonstrated significant differences in fire hazard behavior among the tested commodities. Despite this variability, most commodities showed good agreement with the commodity categories defined in prEN 12845, based on comparisons of measured convective and total heat release rate characteristics. A notable exception was the EUR standard plastic commodity, which the standard classified as Category III but whose measured fire characteristics were consistent with Category IV behavior, leading the authors to recommend a revision to the material factor boundaries in the standard. The authors concluded that the proposed test methodology could be used to test and classify any commercial commodity in accordance with the requirements of prEN 12845.

The previous study relied on overall heat release rate measurements from fires and required two or three sprinklered tests to establish commodity rankings. Building on this framework, Wu [8] presented a series of commodity classification tests using a flame heat flux–based approach with a novel measurement device known as the Heat Flux Pipe, with the aim of developing a more physics-based methodology that could replace multiple sprinklered tests with a single free-burn test. Recognizing that flame heat flux is strongly linked to flame spread and fire growth, the study utilized direct in-flame heat flux measurements obtained with the

Heat Flux Pipe placed at the centerline of the commodity array (2x2x2) to differentiate commodity fire hazards. Initial exploratory sprinklered tests on Class II and Standard Plastic commodities revealed a clear distinction in maximum flame heat flux, with values of approximately 114 kW/m² and 192 kW/m² respectively. Subsequent free-burn tests on Class II, wood pallet, and Standard Plastic commodities showed even larger differences, with maximum centerline flame heat fluxes of approximately 140 kW/m², 190 kW/m², and 440 kW/m², respectively. These results demonstrated that flame heat flux provides a strong basis for distinguishing commodity fire hazards and corresponding protection requirements. The study also confirmed that the Heat Flux Pipe is a robust instrument capable of operating in large-scale fires up to 30 MW and withstanding flame heat flux levels as high as 440 kW/m². By incorporating flame heat flux as a primary driving parameter in flame spread, this approach has the potential to extend the Chicarello and Troup commodity classification methodology to other storage geometries and protection options beyond the original fixed test configuration.

Whereas Wu [8] characterized commodity fire hazards at the full rack-storage scale through flame heat flux measurements, Gollner et al. [9] examined the problem at the bench scale, proposing an approach based on nondimensional analysis of burning behavior using bench-scale material tests on single commodities, focusing on the mass transfer number, commonly referred to as the Spalding B-number. They conducted an experimental study on an individual Group A plastic commodity to investigate its time-varying burning behavior under single-face exposed burning conditions. The mixed nature of the commodity—comprising polystyrene and corrugated cardboard—resulted in three distinct and repeatable stages of combustion. Measurements of flame height, mass-loss rate, and heat flux were used to develop a phenomenological description of the burning process. Time-dependent and time-averaged B-numbers were obtained from mass-loss data using a Nusselt–Grashof–based turbulent convective heat-transfer model. The experimentally extracted B-numbers, which incorporated real heat-transfer effects beyond the idealized thermodynamic definition, reflected changes in combustion behavior as different constituent materials became involved in the fire. However, significant variability between tests resulted in large uncertainties, limiting the quantitative usefulness of the extracted parameters. Although the study demonstrated that B-number–based analysis can capture the complex burning behavior of mixed-material commodities, its application to commodity classification remained a future direction, as high experimental uncertainties precluded definitive quantitative conclusions.

Overholt et al. [10] further advanced B-number–based approaches by developing a physics-based flame spread prediction methodology applicable across multiple scales. In their work, the early stages of large-scale warehouse fires were modeled by decoupling heat and mass transfer processes. Bench-scale experiments were conducted to measure mass-loss rates and extract B-numbers for representative fuels, specifically corrugated cardboard and polystyrene. Corrugated cardboard was identified as a critical contributor to early flame spread in warehouse fires, while polystyrene represented a highly hazardous plastic commodity. The experimentally determined B-numbers were then used to model in-rack flame heights in large-scale rack storage configurations ranging from 6.1 to 9.1 m in height. Good agreement was observed between flame spread model predictions and large-scale experimental flame height measurements during the initial stages of fire growth, particularly when flame spread was dominated by corrugated cardboard surfaces. These studies demonstrated the value of nondimensional parameters in linking bench-scale material properties to large-scale fire behavior, and the authors identified sprinkler activation and suppression performance as promising directions for future application of this framework.

To address the need for a systematic, suppression-based classification metric, Xin and Tamanini [11] conducted fifty-six fire suppression tests to develop a physically based framework for commodity classification in sprinkler protection, using representative fuels including Class 2–4 commodities, standard plastic commodity, cartoned meat trays, plastic pallets, and exposed meat trays. The framework was grounded in a conceptual analysis of rack storage fire growth and suppression, in which flame heat transfer governs fire spread. Upon sprinkler activation, only a fraction of the discharged water, defined as the Actual Delivered Density (ADD), penetrates the fire plume to reach the fuel surface; this ADD must equal or exceed the Critical Delivered Flux (CDF), defined as the minimum water flux required to prevent further fire growth, for suppression to succeed. CDF values were determined experimentally via linear interpolation between controlled and out-of-control test data, and subsequently combined with an empirical ADD–SDF correlation to compute the Sprinkler Discharge Flux (SDF) required for each commodity. The resulting SDF-based rankings were validated against FM Global Data Sheet 8-1 [4] and full-scale sprinkler test results, showing good agreement for most commodities, with larger discrepancies noted for Class 3 and 4 commodities attributed to the use of loosely packed representative fuels. Suppression correlations further confirmed that the SDF-based ranking remained consistent across different fuel array heights, supporting the use of 3-tier array measurements to project protection requirements for taller storage configurations.

Further research by Xin [12] investigated the effect of storage height on CDF across 2- and 5-tier rack storage configurations for six representative commodities: cartoned low-combustibility (Class 2), cartoned cellulosic (Class 3), cartoned unexpanded plastic (CUP), cartoned expanded plastic (CEP), uncartoned unexpanded plastic (UUP) and uncartoned expanded plastic (UEP), building on 3-tier data from prior work [11] to provide a complete dataset spanning storage heights of approximately 3 m to 7.5 m. The experimental results revealed that CDFs of cartoned commodities increased linearly with storage height, consistent with a global energy balance analysis showing that the CDF is proportional to storage height under surface-dominated lateral fire spread. In contrast, uncartoned plastic commodities (UUP and UEP) exhibited nonlinear CDF growth with storage height, attributable to their distinct burning characteristics: volumetric fire growth and fuel melting for the UUP commodity, and fuel burnout combined with water shielding effects for the UEP commodity. Based on these findings, Xin proposed a CDF-based commodity classification scheme in which new commodities are ranked by comparing their CDF values with those of representative fuels within each class, with cartoned and uncartoned commodities treated in separate categories given their fundamentally different responses to fire growth and water suppression. This provides a physically grounded link between experimental suppression data and established sprinkler protection requirements.

To reduce reliance on large-scale fire testing, Han and Xin [13] developed a zone-based model for CDF prediction. Large-scale fire suppression tests, particularly for higher-tier storage configurations, are expensive, time-consuming, and resource-intensive. Conducting full-scale tests for every commodity type across all relevant storage heights is not practically feasible. The zone-based model addresses this challenge by calibrating model parameters using only two lower-tier experiments — one uncontrolled and one controlled fire test and then predicting the CDF for higher-tier configurations computationally, thereby significantly reducing the experimental burden required for commodity classification. The model was validated against experimental data for Class 2 commodity and demonstrated good predictive performance, confirming its potential as a cost-effective tool for commodity classification. However, its applicability to other commodity types within the FM classification hierarchy remained unvalidated. The present study builds on this framework by extending and improving the zone-based model to cover a broader range of representative commodities and by introducing a more robust parameter estimation strategy to enhance model generalizability.

3. Description of the Zone-Based Model and Its implementation

This section describes the zone-based model used in the present study and its implementation for CDF prediction. Section 3.1 presents the model formulation, including the governing equations for fire spread and water transport between storage tiers. Section 3.2 describes how the model is implemented in practice, covering the parameter optimization procedure and the use of optimized parameters to predict CDF values in higher-tier storage configurations.

3.1 Description of the Zone-Based Model

The zone-based model conceptualizes the fuel domain (the storage of commodities on the rack) as a series of fuel zones, each representing a tier of commodities, as shown in Fig. 1. The ignition is assumed to occur at the bottom level, and fire spreads vertically before initiating horizontal flame spread in the upper zones with a minor ignition delay. It is further assumed that sufficient burning surface area exists to allow indefinite horizontal fire spread unless suppressed by water application.

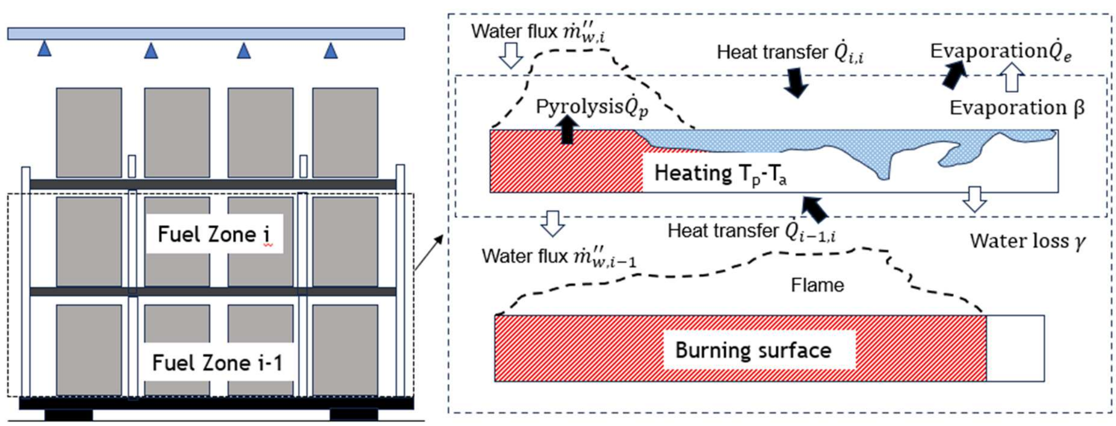

Figure 1 Representation of the zone-based model for commodity classification. Solid arrows represent energy flow and open arrows represent mass flow [13]

In the present modeling approach, fire spread is governed by an energy conservation equation applied over the burning surface area. The overall chemical HRR from all fuel zones is given by $Q_{total} = p_4 \sum_{i=1}^{n} A_i$. Here p_4 ($p_4 = \dot{m}_f'' \, \Delta H_c$ is the power flux of the material); A_i is the burning surface area of zone i (m^2); $\dot{m}_f''$ is mass flux of fuel (kg/m ^{2}·s); and ΔH_c is the heat of combustion of fuel (kJ/kg) used in the burning.

Water is applied uniformly to the topmost zone once the chemical Heat Release Rate (HRR) reaches a prescribed activation threshold. Water transport between zones is modeled within the burning areas under the assumption of mass conservation. Water applied to the topmost zone flows downward through successive zones and undergoes partial or complete evaporation within the burning areas. For simplicity, the model does not account for prewetting caused by water transport over non-burning areas, although this simplification introduces uncertainty, as prewetting may significantly affect the fire behavior of some commodities.

As discussed earlier, the fire spread rate $\frac{dA_i}{dt}$ governed by the energy conservation equation, as shown in Eq. 1.

$$\alpha_{i,i}\dot{m}_f''A_i\Delta H_c + \alpha_{i-1,\ i}\,\dot{m}_f''A_{i-1}\Delta H_c = \rho c\left(T_p - T_a\right)\delta\frac{dA_i}{dt} + \dot{m}_f''A_i\Delta H_p + \dot{m}_{ei}''A_i\Delta H_e \tag{1}$$

In Eq. 1, the terms at the left side represent heat transfer from zone i to itself and that from zone i-1. The first term on right hand side represent energy required for material to sensible heat from ambient temperature to pyrolysis temperature. And the second and third term on right hand side represent energy absorption during pyrolysis and water evaporation process respectively. In Eq. 1, $\alpha_{i,i}$ is the heat transfer fraction from zone i to itself and $\alpha_{i-1,\ i}$ is the energy transfer from zone i-1 to zone i. ρ is the fuel density, c is the heat capacity, T_p is pyrolysis temperature T_a is ambient temperature, δ is fuel depth, ΔH_p is heat of pyrolysis, $\dot{m}_{ei}''$, water evaporation flux and ΔH_e is the heat of evaporation, respectively. Eq. 1 can be rearranged as

$$\frac{dA_i}{dt} = \frac{A_i + p_2 A_{i-1}}{p_1} - \frac{A_i}{p_3} \tag{2}$$

Here $p_1 = \frac{\rho c(T_p - T_a)\delta}{\dot{m}_f'' \alpha_{i,i}\Delta H_c - \dot{m}_f'' \Delta H_p}$, $p_2 = \frac{\alpha_{i-1,i}\dot{m}_f'' \Delta H_c}{\alpha_{i,i}\Delta H_c \dot{m}_f'' - \dot{m}_f'' \Delta H_p}$ and $p_3 = \frac{\rho C(T_p - T_a)\delta}{\dot{m}_e''(\Delta H_e)}$. For simple materials, p_1 represents the ignition delay and p_3 represent the suppression delay. Parameter p_2 represents the ratio of heat transfer to zone i from zone i and i-1. The value of p_2 is approaching unity with $\alpha_{i,i} = \alpha_{i-1,i}$ and $\Delta H_c >> \Delta H_p$. When i=1 in Eq. 2, the burning surface area $A_{i-1} = 0$ representing a non-combustible floor. For the initial condition, A_i in Eq. 2 is set to a constant value A_{ini}. A time shift $t_{ini} = t_{shift}$ is for accounting ignition time delay due to vertical fire spread.

The mass conservation equation for water transport between zones can be written as

$$\dot{m}_{w,i-1}'' A_{i-1} = (\dot{m}_{w,i}'' A_{i-1} - \dot{m}_{e,i}'' A_i)(1 - \gamma) \tag{3}$$

In Eq.3, the left-hand side represents mass flow rate onto zone i-1 and the right-hand side terms stand for the water loss caused by evaporation and transport. γ in Eq. 3 is the water transport loss ratio. The evaporation is assumed to be proportional to the burning surface area in zone *i* with a mass flux $\dot{m}_{e,i}'' = \beta\, \dot{m}_{w,i}''$. The transport loss is assumed to be proportional to the remaining water after evaporation. The parameters used in the model for Class 2 commodity are either determined using the optimization process or preset based on literature data.

3.2 Implementation of the Zone Model

The zone-based model involves seven parameters governing fire spread and suppression behaviour: p_1, p_3, p_4, β, γ, tshift, and A_{ini}. Since p_3 depends on $\dot{m}_e''$, which varies between tests, it cannot be directly used as an optimization parameter. Instead, the composite parameter $p_5 = p_3 \times \dot{m}_e'' = \frac{\rho c(T_p - T_a)\delta}{(\Delta H_e)}$ is independent of $\dot{m}_e''$ and is therefore independent of test conditions. It is thus used in place of p_3. Following the approach of [13], three parameters are preset based on physical reasoning: γ (water loss ratio, preset to 0.1), p_4 (power flux, preset to 0.24 MW/m²), and Aini (initial fire spread area, preset to 0.01 m²). The values of γ and p_4 are estimated based on experimental data and material properties [13], while A_{ini} is assigned a small value to minimise its influence on the chemical HRR during suppression. The remaining four parameters, p_1, p_5, t_{shif} and β, are determined through optimization against lower-tier (2-tier or 3-tier) experimental data, as shown in Table 1.

The optimization is performed in two sequential phases. In the first phase, free-burn experimental data are used to optimize p_1 and t_{shift}, targeting the best possible agreement between predicted and measured chemical HRR during the free-burn phase. The optimized values of p_1 and t_{shift} are then carried over to the second phase, in which p_5 and β are further optimized against the suppression-phase data to best match the chemical HRR after water application. This two-phase approach decouples the free-burn and suppression behaviors, improving both the stability and physical interpretability of the optimization.

Table 1 Description of model parameters and corresponding method of determination [13]

Parameters	Physical representation	Method
p_1 (s)	Ignition delay	Opt. in free burn
p_5 (kg/m^2)	Suppression delay (p_3) x evaporation flux ($\dot{m}_e''$)	Opt. in suppression
β	Water evaporation ratio	Opt. in suppression
γ	Water loss ratio	Preset to 0.1
p_4 (MW/m^2)	Power flux	Preset to 0.24 (optimized in two-level framework, Section 8)
t_{shift} (s)	Time shift accommodating vertical fire spread	Opt. in free burn
A_{ini}(m^2)	Initial condition for fire spread in fuel zones	Preset to 0.01

The optimization framework is implemented in Python using the differential evolution algorithm [15], a global optimization method well-suited for nonlinear and multi-parameter problems. The algorithm iteratively evolves a population of candidate parameter sets within predefined bounds through mutation, recombination, and selection, ultimately converging on the parameter set that minimizes the objective function. The fitness/objective function plays a crucial role in guiding this optimization by quantifying the discrepancy between model predictions and experimental measurements. There are two separate fitness functions used in the optimization process. In the free-burn optimization, the fitness function follows Eq. 4, which includes a penalty term to account for potential misalignment in the water application time.

$$Fitness = \sqrt{\frac{1}{N}\sum_{i=1}^{N} (HRR_{exp,i} - HRR_{model,i})^2} + |WAT - t_0| \quad (4)$$

where the term $HRR_{exp,i}$ is the experimental heat release rate at point i while $HRR_{model,i}$ refers to the modeled heat release rate at the same point. Additionally, WAT represents the water application time in a test, while t_0 is the initial value of the time vector after water application in the model; N is the number of data points for comparison.

However, in the suppression fitness function (Eq. 5), the penalty term $|\mathrm{WAT} - t_0|$ is excluded. Instead, the objective shifts toward minimizing the root-mean-square error (RMSE) between the experimental and modelled heat release rates to closely match the HRR curve after water application.

$$Fitness = \sqrt{\frac{1}{N}\sum_{i=1}^{N} (HRR_{exp,i} - HRR_{model,i})^2} \quad (5)$$

With the parameters obtained from the optimization, the average values of p_1 and p_5 are used to estimate the CDF for higher-tier storage racks. The water evaporation ratio for high-tier storage racks is estimated through interpolation of trends observed in lower-tier experimental data. Normalized CDF (NCDF) values (the ratio of the CDF required to control a fire to the actual applied water flux) are plotted against the water evaporation ratio (β) for lower tiers, and the critical β value where NCDF equals 1 is identified. This critical β is then used in the zone model to estimate the CDF for higher tiers. t_{shift} is assumed to be zero for the estimation of CDF value for high-tier storage. This assumption is physically justified because t_{shift} only moves the HRR curve along the time axis without altering the fire growth rate or suppression behaviour. Since the CDF is determined by the steady-state condition at which the applied water flux is just sufficient to suppress fire growth (i.e., the HRR curve becomes horizontal), the absolute timing of fire ignition does not influence the predicted CDF value. With the average values of p_1 and p_5, together with the identified critical critical β, the zone-based model is again run for high-tier storage. The applied water flux is incrementally increased by 0.001 mm/min until the HRR curve becomes horizontal, and the water flux at which this occurs is determined as the CDF for that high-tier storage.

4. Methods for Identifying Water Application time

Most of the test data does not specify the time of water application (WA), which is a required input for the implementation of the zone model. When water application effectively controls the fire, the HRR curve begins to decline. However, if the fire is not controlled, the HRR curve may initially decline but subsequently rise again, potentially resulting in an uncontrolled fire. To address this limitation, we propose the following methods for identifying the water application time for tests where the WA time is unknown: 1) Visual observation using the total heat release rate data; 2) Visual observation using the convective heat release rate data; 3) Curve smoothing using a consistent window size; 4) Using Sprinkler Activation Temperature Model (SATM); and 5) Based on water flow rate drop in pipelines.

4.1 Description of different methods for estimating water application times

Visual Observation Using Total Heat Release Rate (VOTHRR). In this method, the point of water application is identified through visual inspection of the total heat release rate curve. The experimental total HRR data is plotted against time to generate a comprehensive visualization of fire growth and suppression. We then examine the plotted curve to detect the earliest local maximum point, representing the peak HRR value after the initial impact of water application on the fire. This peak indicates the moment when water application begins to suppress the fire, leading to a sustained decline in HRR. The key criterion for identifying this point is that, after the local maximum, a series of consecutive HRR data points must show a decreasing trend, signalling the onset of fire suppression. This method provides an intuitive approach to estimating water application time, leveraging the clear visual cues of fire behavior as reflected in the total HRR curve (see Figure 2 (a) and (b) for examples). In some cases, the water application rate is too low to cause a noticeable drop in HRR values, making it difficult to pinpoint the water application time through visual inspection alone (see Figure 2 (c) Exp.

HRR curve with WA flux of 6.1 mm/min for an example). In such instances, we compare the test with other cases of the same commodity and tier but under larger water application fluxes (see Figure 2 (c) Exp. HRR curve with WA flux of 16.3 mm/min for an example), as their free-burn phases should align, and water application times are likely to be similar. Based on this comparison, we select a point on the curve where the HRR either stabilizes or shows a brief, subtle decline, using these patterns to approximate the water application time more accurately.

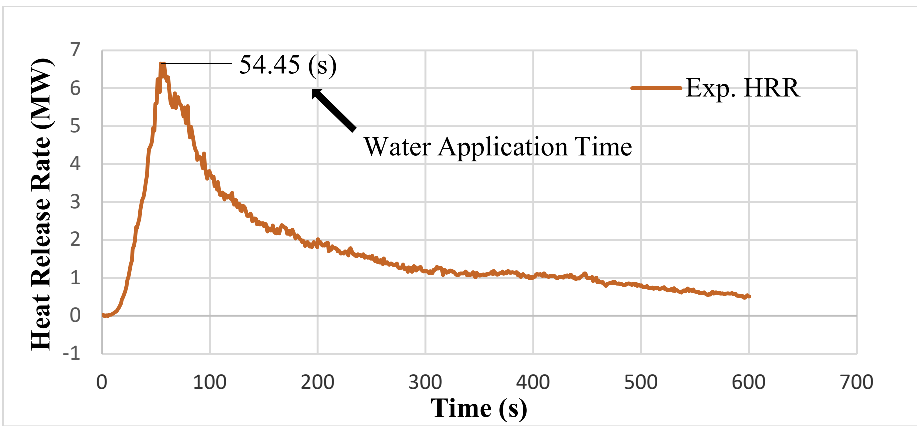

(a) Water Application time for Class 3, 2 tier Commodity Test (WA=4.1 mm/min)

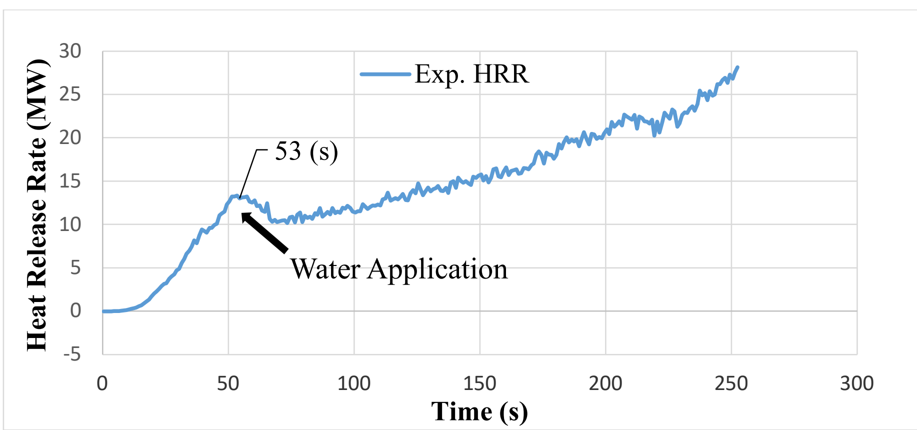

(b) Water Application time for CMT, 3 tier Commodity Test (WA=12.2 mm/min)

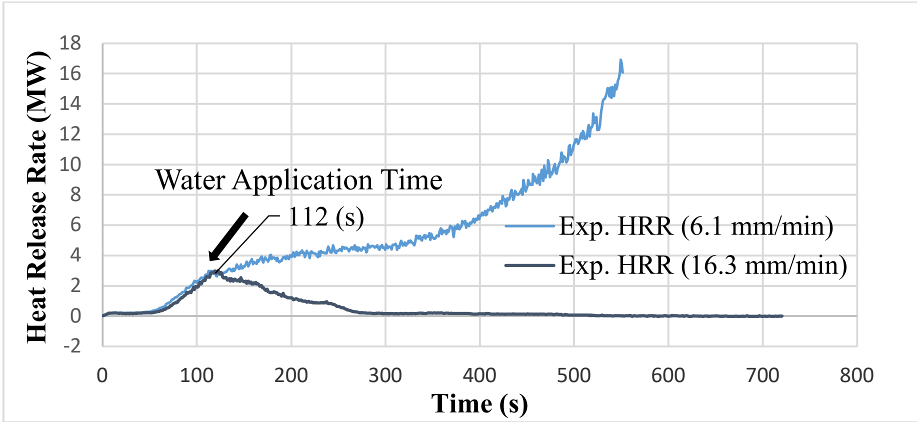

(c) Water Application time for Plastic Pallets, 2 tier Commodity Test

Figure 2 Determination of Water Application time by visual observation

Visual Observation Using Convective Heat Release Rate (VOCHRR). Similar to the THRR-based approach, this method relies on visual analysis of the convective HRR curve. By plotting convective HRR data against time, the fire's convective energy output is depicted, highlighting the dynamics of heat transfer and suppression. We identify the earliest local maximum point on the convective HRR curve, following the same principle as the THRR method: the point after which a sequence of decreasing HRR values is observed, occurring after water application. The convective HRR curve can offer additional insights into fire suppression effectiveness, as it directly reflects the portion of heat release most influenced by water application. This visual observation method complements the total HRR approach, offering an alternative perspective on identifying the water application time.

Curve Smoothing and Derivative Analysis Method (CSDA). The HRR data contains noise, making it challenging to accurately identify the water application time. In this section, we address this by smoothing and differentiating the experimental HRR curve to locate the zero-slope point as the water application time. The detailed procedure for this method is outlined below. **Step 1**: Plot the experimental HRR Curve: Generate a plot of the HRR curve using the experimental data. **Step 2**: Apply Smoothing: Use the Savitzky-Golay filter (window size = 5, polynomial order = 2) to smooth the HRR curve and reduce noise. This window size is optimized based on all test data by comparing the method's results with WAT identified through visual observation. **Step 3**: Differentiate the HRR Curve: Compute the time derivative of the smoothed HRR curve to highlight trends in the rate of change. **Step 4**: Smooth the Differentiated Curve: Apply the Savitzky-Golay filter again (window size = 31, polynomial order = 2) to smooth the differentiated curve. **Step 5**: Identify the Zero-Slope Point: Locate the point where the smoothed differentiated curve is zero, excluding the initial and final regions where the slope is also zero. The water application points for all commodities were identified using the procedure outlined above, Fig. 3 shows an example of the method. The blue line represents the original HRR curve, the red line is the smoothed HRR curve derived from the experimental data, the green line shows the differentiated curve of the smoothed HRR, and the gray line represents the final smoothed differentiated curve. The black vertical lines indicate the water application points predicted by the proposed method.

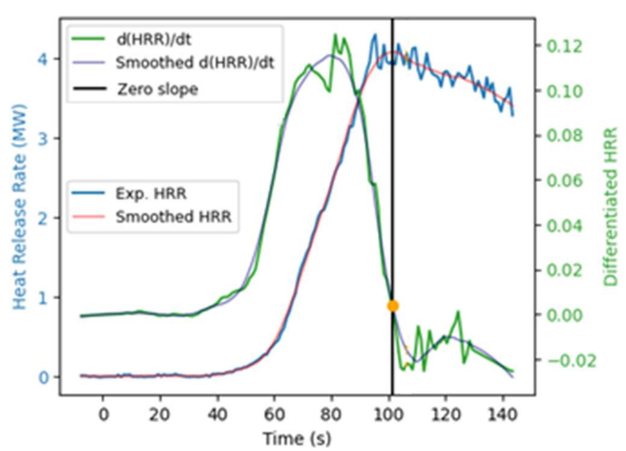

Figure 3 Water Application Points for Class 2, 2 tier Commodity Test (WA=4.1 mm/min) using CSDA method

Determination of WA time Based on Sprinkler Activation Temperature (SAT). In the fire tests on rack storages, the water application time is determined by the gas temperature at a virtual sprinkler, positioned 10 ft above the top of the rack storage. When the gas temperature at this location exceeds 287°C, the water application system is triggered. Instead of directly measuring the gas temperature during the tests, it is calculated using an empirical model for ceiling flows from rack storage fires [13]. This approach begins by determining the fire's virtual origin, which serves as the reference point for characterizing the fire plume. Using convective heat release rate (HRR) data, the centerline excess temperature and velocity of the plume are computed, providing a detailed thermal and flow profile of the fire. By tracking temperature changes over time, the activation point—when the temperature around the sprinkler surpasses 287°C—is identified. It is important to note that there is an inherent delay in actual water application after the calculated temperature exceeds 287°C. This delay consists of 1–2 seconds for system operation and an additional 3–5 seconds for water to flow into the pipes.

Determination of WA Time Using Water Flow Rate Drop in Pipelines (WFRD). Another method to estimate the water application time on the HRR curve is based on the data about the water flow rate recorded in the water application system. The water initially flows along a bypass loop until the application nozzles are activated, at which point the flow rate drops to the designed level. The WAT was determined by identifying the midpoint between the two steady states—before and after water activation—which, in the provided example, occurs at approximately 47 seconds (as shown in Figure 4). However, this actual WAT does not correspond directly to the WAT on the HRR curve due to a delay in gas transport, typically ranging from 30 to 40 seconds, depending on fire size.

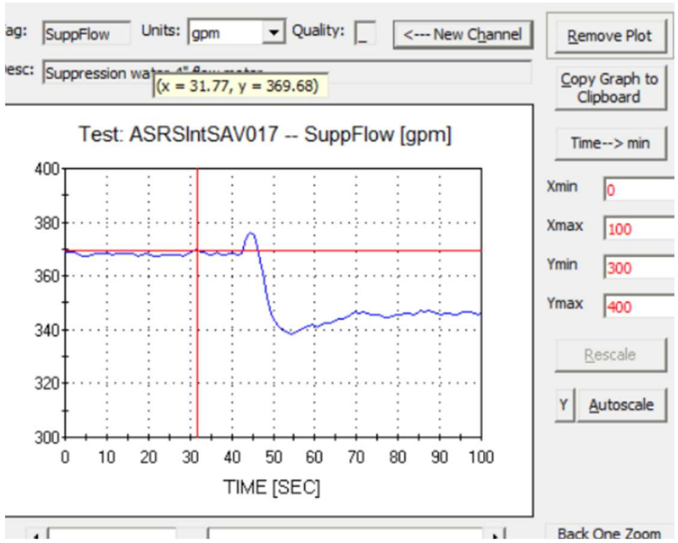

Figure 4 Water flow rate drop before and after water activation using WFRD method

4.2 Comparison of Water Application Time Using Different Methods

Tables 2–6 summarize the water application times determined using all those methods discussed above, including visual observation based on total and convective HRR data, curve smoothing, the sprinkler activation model, and water flow rate drop. These tables provide a comprehensive comparison. The results indicate that all methods generally yield similar water application times.

The two visual observation methods based on total and convective HRR closely align, as the test data for these variables are time-shifted by 33 seconds for total HRR and 9 seconds for convective HRR to maintain a consistent fire development timeline. To improve consistency, the curve smoothing method employs an optimized window size to ensure the identified water application times closely match those determined through visual observation. As a result, the curve smoothing method generally aligns well with visual approaches in most tests. However, due to varying noise levels in the data, a single window size is not universally effective, and in some cases, the identified water application time may be unreliable.

As discussed, the SAMT and water flow rate drop methods exhibit inherent delays or early responses. Given the robustness and consistency of visual observation using total or convective HRR, the visual observation method will be adopted for further analysis to determine water application times. While minor time shifts may persist despite corrections, our zone model incorporates a t_{shift} parameter to account for this variability. In practice, the exact water application time is not our primary concern; rather, we focus on identifying the point that segments the HRR curve into the free-burning and suppression phases. The visual observation method is sufficient for this purpose. Additionally, for CFD estimation of high-tier rack storage fires, only a few lower-tier fire tests are used to estimate model parameters. Although visual observation is not automated, it remains a practical approach given the limited number of tests required. In most cases, the water application point is clearly identifiable in the HRR curves, making manual identification straightforward. In this report, all water application times are determined through visual observation of the total HRR.

Table 2 Comparison of water application time for Class 2 commodity

Test	**Tier**	**WA rate (mm/min)**	**VOTHRR (s)**	**VOCHRR (s)**	**CSDA (s)**	**SAT (s)**	**WFRD (s)**
1	2	4.1	102	67.45	61.45	58	68
2	2	8.2	106	70.45	68.45	65	78
3	3	4.1	103	NAN	69.45	54	76
4	3	6.1	86	55.45	54.45	49	64
5	3	8.1	135	NAN	NAN	NAN	NAN
6	3	12.2	95	61.45	60.45	51	NAN
7	3	18.4	93	62.45	61.45	54	72
8	5	6.1	78	62.45	61.45	56	66
9	5	8.2	90	72.45	71.45	70	83
10	5	10.2	85	68.45	67.45	66	74

Table 3 Comparison of water application time for Class 3 commodity

Test	Tier	WA rate (mm/min)	VOTHRR (s)	VOCHRR (s)	CSDA (s)	SAT (s)	WFRD (s)
1	2	4.1	96	51.45	49.45	42	54
2	2	6.1	60	57.45	57.45	53	71
3	2	12.1	54	51.45	51.45	45	60
4	3	6.1	45	41.45	41.45	38	52
5	3	10.1	58	51.45	46.45	43	54
6	3	12.1	52	49.45	48.45	44	51
7	3	18.2	50	49.45	46.45	42	56
8	5	12.1	47	47.45	46.45	44	52
9	5	18.2	48	49.45	49.45	47	59
10	5	24.4	36	38.45	38.45	37	49

Table 4 Comparison of water application time for Standard plastic commodity

Test	Tier	WA rate (mm/min)	VOTHRR (s)	VOCHRR (s)	CSDA (s)	SAT (s)	WFRD (s)
1	2	4.1	75	102.45	58.45	53	66
2	2	6.1	56	55.45	54.45	50	57
3	2	10.1	76	52.45	51.45	48	60
4	2	16.3	54	47.45	47.45	45	56
5	3	12.1	43	40.45	40.45	37	48
6	3	14.2	47	43.45	NAN	NAN	53
7	3	18.4	51	52.45	47.45	46	60
8	3	26.5	48	45.45	45.45	44	53
9	5	20.4	42	34.45	33.45	32	50
10	5	24.5 (0)	53	43.45	42.45	32	58
11	5	24.5 (1)	65	64.45	63.45	61	76
12	5	28.6 (0)	39	33.45	32.45	31	43
13	5	28.6 (1)	38	32.45	32.45	32	45

Table 5 Comparison of water application time for Plastic pallet commodity

Test	Tier	WA rate (mm/min)	VOTHRR (s)	VOCHRR (s)	CSDA (s)	SAT (s)	WFRD (s)
1	2	6.1	112	115.45	109.45	98	112
2	2	10.1	129	125.45	104.45	120	129
3	2	16.3	122	119.45	90.45	108	122
4	3	6.1	144	NAN	115.45	109	139
5	3	10.1	212	NAN	135.45	120	158
6	3	12.2	188	NAN	140.45	131	154
7	3	14.3	140	NAN	122.45	118	146
8	3	24.5	138	NAN	122.45	110	155
9	3	40.8	119	NAN	103.45	100	126
10	5	40.8	225	225.45	179.45	225	238
11	5	51.0	194	184.45	159.45	NAN	210
12	5	61.2	183	197.45	160.45	202	208

Table 6 Comparison of water application time for Cartoned MT commodity

Test	Tier	WA rate (mm/min)	VOTHRR (s)	VOCHRR (s)	CSDA (s)	SAT (s)	WFRD (s)
1	2	4.1	78	69.45	56.45	50	63
2	2	6.1	58	54.45	54.45	50	59
3	2	10.1	56	47.45	47.45	43	60
4	2	16.3	51	47.45	47.45	43	58
5	3	12.2	53	53.45	52.45	36	48
6	3	14.2	57	55.45	53.45	42	50
7	3	15.5	50	53.45	53.45	41	52
8	3	18.3	51	51.45	50.45	34	50
9	5	20.4	47	35.45	35.45	34	50
10	5	24.5 (0)	61	39.45	39.45	37	47
11	5	24.5 (1)	45	34.45	33.45	32	49
12	5	28.6	44	40.45	39.45	39	51

5. Calculation of CDF from Test Data

This section presents the methodology for estimating Critical Delivered Flux (CDF) from experimental data and evaluates the influence of final time selection on the resulting estimates. Section 5.1 outlines the CDF calculation procedure using paired uncontrolled and controlled HRR data, while Section 5.2 evaluates the effect of final time selection. The results show that CDF estimates for a given tier are only minimally affected by endpoint selection for class 2 commodity.

5.1 Description of the Calculation Method

In the previous section, we frequently discussed the concept of the Critical Delivered Flux (CDF). Here, we provide a summary of the procedure to estimate the CDF from experimental data. To determine the CDF, the Water Application and Apparatus (WAA) tests must establish two distinct fire protection scenarios: an uncontrolled fire and a controlled fire. These scenarios are achieved by varying the applied water flux levels. The calculation of the CDF is based on a mathematical model illustrated in Fig. 5. Using the integrated chemical HRR and the applied water flux, the CDF is determined through the equation provided in [11].

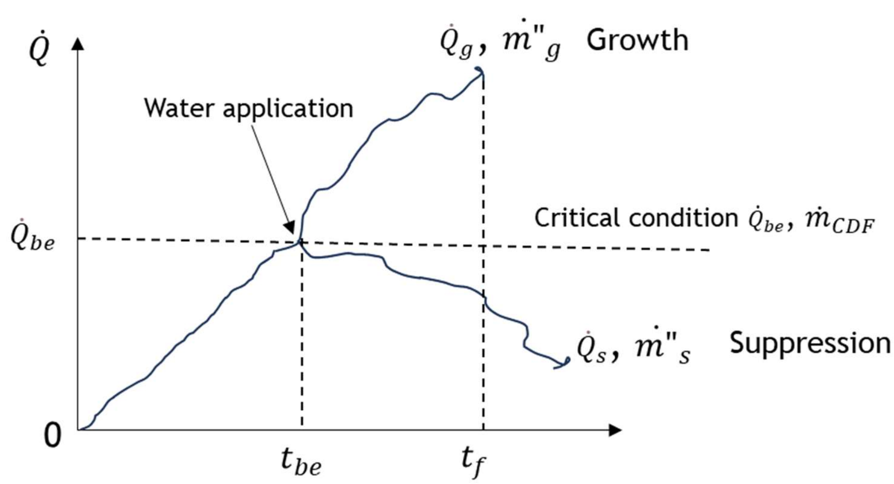

Figure 5 Mathematical illustration for the CDF calculations

$$CDF = \dot{m}_g'' - \frac{\Delta Q_g - \Delta Q_{be}}{\Delta Q_{g-}\Delta Q_s}\left(\dot{m}_g'' - \dot{m}_s''\right) \quad (6)$$

In Eq. (6), ΔQ_s and ΔQ_g are total chemical heat release during the suppression of uncontrolled and controlled fires respectively. $\dot{m}_g''$ and $\dot{m}_s''$ are the applied water fluxes corresponding to uncontrolled and controlled fires. The quantity $\Delta Q_{be} = (t_f - t_{be})\dot{Q}_{be}$ is the hypothetical energy that would have been released if the fire had remained at a constant HRR of $\dot{Q}_{be}$ (the HRR at the moment of water application) throughout the entire suppression period from t_{be} to t_f.

5.2 Effect of endpoint selection

Using the method described in Section 5.1, CDF was determined for all commodities under both uncontrolled and controlled scenarios. The analysis focuses on HRR curves that approach horizontal asymptotes and evaluates the sensitivity of the calculated CDF to the selection of the final time t_f after the free-burn phase (see Figure 6 for details).

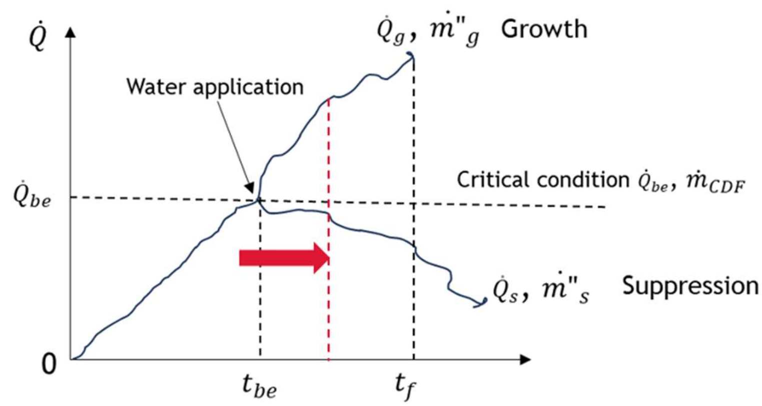

Figure 6 Illustration for shifting the final time point

Figure 7 illustrates the effect of shifting the final time point on the estimated CDF values across all commodities and tier configurations. While some variation is observed, the overall impact on CDF estimates remains minor. The x-axis denotes the amount of time added to the point where the two curves begin to diverge (referred to as the common curve separation point). A value of 50 corresponds to 50 seconds after this separation point—this is used as the common final time for comparison. Other values on the x-axis indicate further time shifts, in 50-second increments, extending toward the true common final time for both curves. The bracketed values in the figure represent the applied water flux, measured in mm/min.

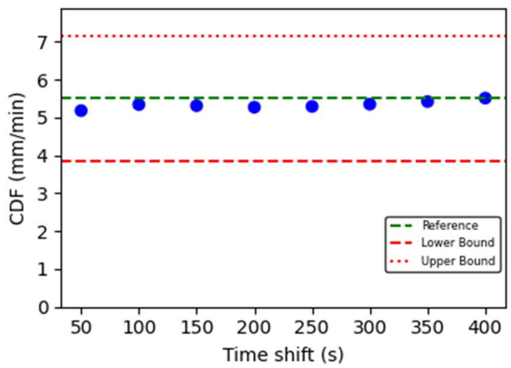

(a) Class 2, 3 tiers (4.1 vs 6.1)

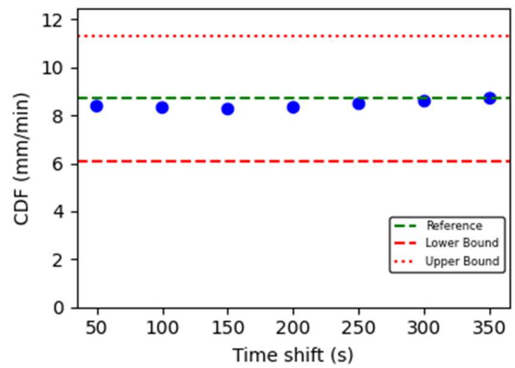

(b) Class 2, 5 tiers (6.1 vs 10.2)

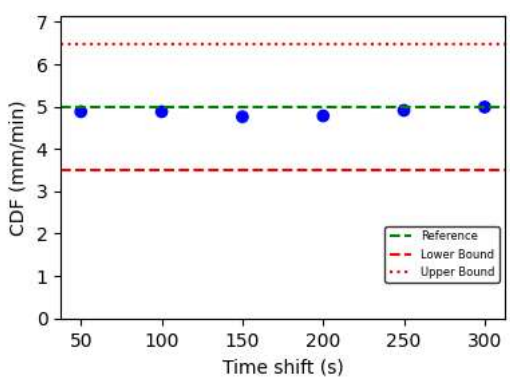

(c) Class 3, 2 tiers (4.1 vs 6.1)

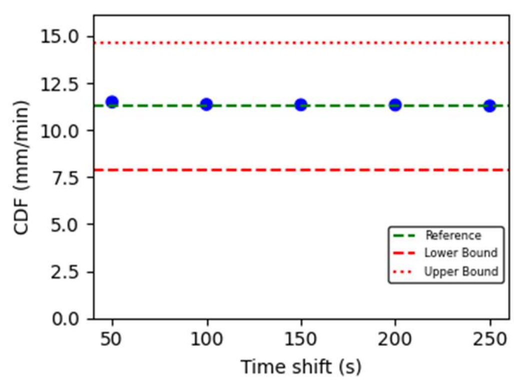

(d) Class 3, 3 tiers (10.2 vs 12.2)

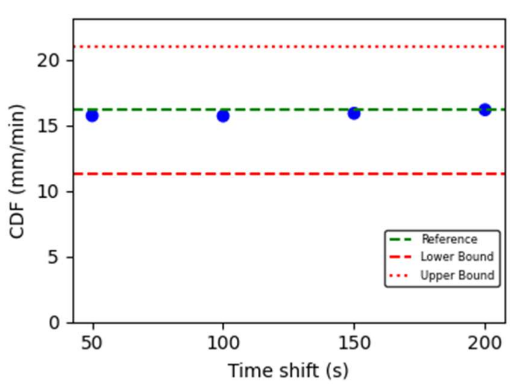

(e) Class 3, 5 tiers (12.2 vs 18.4)

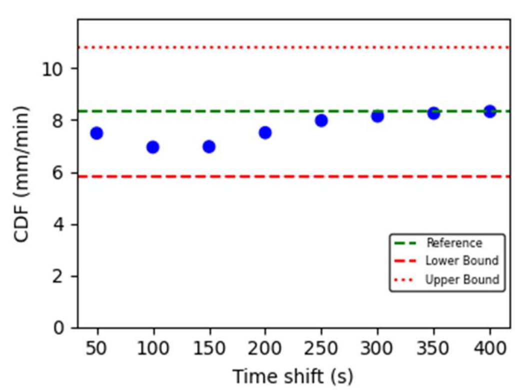

(f) Standard Plastic, 2 tiers (6.1 vs 10.2)

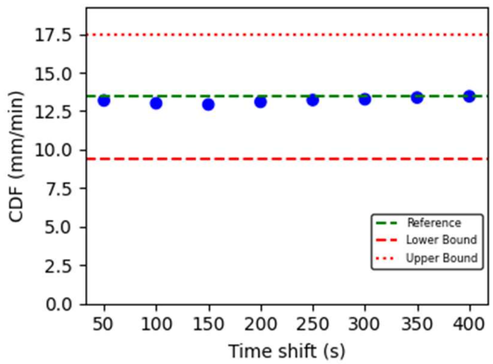

(g) Standard Plastic, 3 tiers (12.2 vs 15.5)

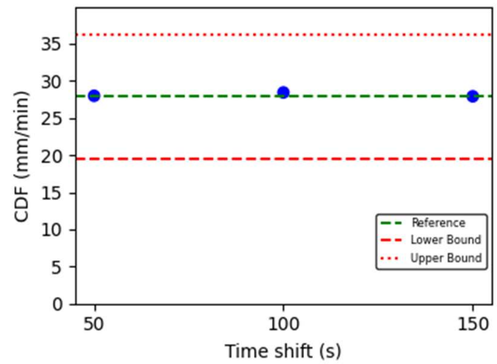

(h) Standard Plastic, 5 tiers (24.5 vs 28.6)

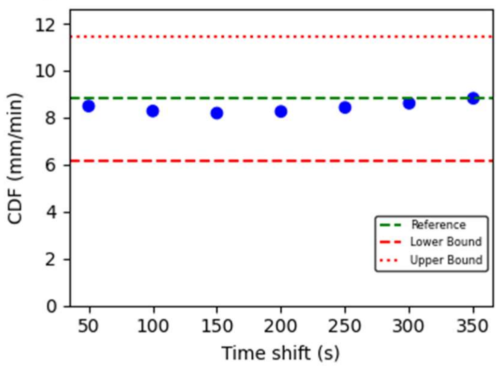

(i) Plastic Pallets, 2 tiers (6.1 vs 10.2)

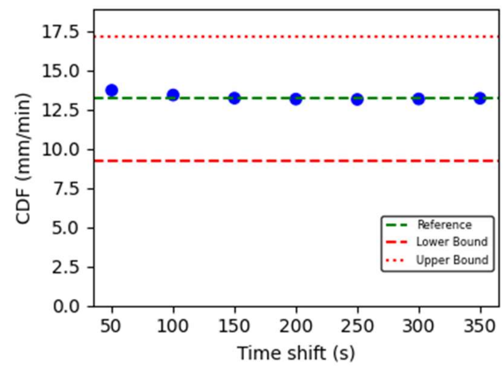

(j) Plastic Pallets, 3 tiers (12.2 vs 14.3)

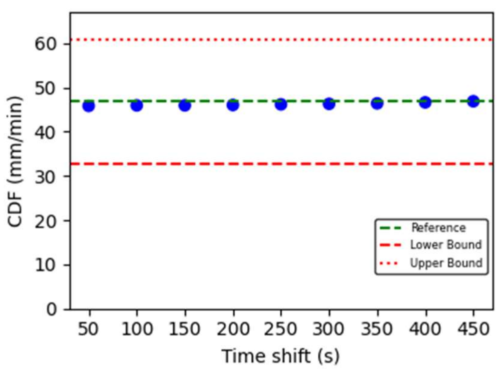

(k) Plastic Pallets, 5 tiers (40.8 vs 51)

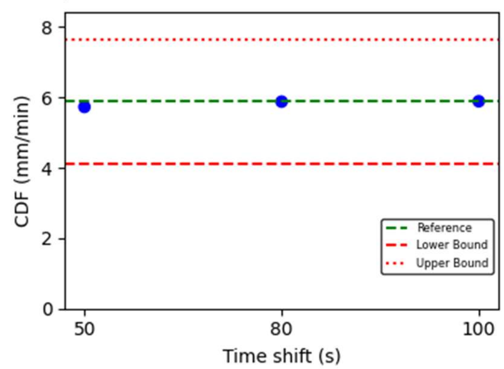

(l) CMT, 2 tiers (4.1 vs 6.1)

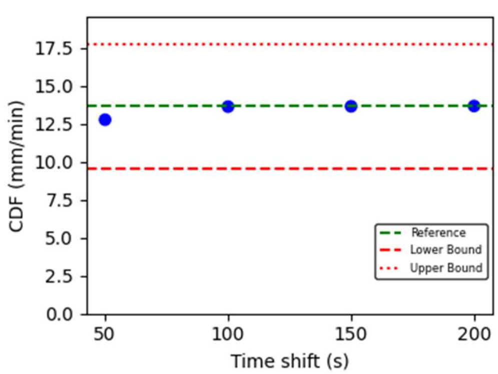

(m) CMT, 3 tiers (12.2 vs 14.3)

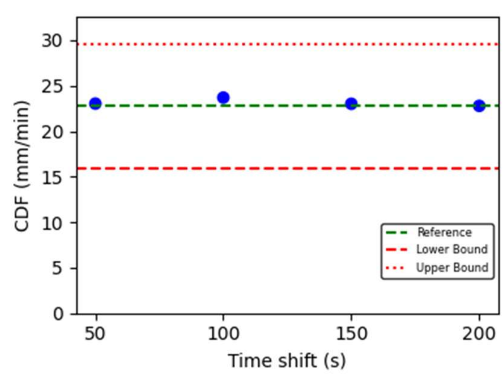

(n) CMT, 5 tiers (20.4 vs 24.5)

Figure 7 Illustration of effect of shifting final time point on the CDF values (The solid blue circles in the subplots represent the calculated CDF values corresponding to each selected final time point)

The conclusion from Figure 7 is further validated by comparing the variation of the CDF values for Class 2, 5-tier rack storage as a function of the final time shift with the experimentally measured CDF values for this rack storage configuration, as shown in Table 7. As shown in Figure 9(i), the experimental data for the Class 2, 5-tier rack storage with a water application rate of 8.2 mm/min produced an almost horizontal HRR curve after the free burning stage, suggesting that the applied water rate closely matches the true CDF value. The computed CDF values in Table 7 are based on test data on Class 2, 5 tiers, 6.1 mm/min and 10.2 mm/min. As shown in Table 7, adjusting the final time has a minimal impact on the true CDF value, with the highest observed percentage difference being only 6.2%, compared to the true CDF value. This indicates that the CDF computation remains stable even when the final time point is adjusted up to 350 seconds from the common curve separation time point.

Table 7 Comparison of experimental CDF vs computed CDF after final time shift for class 2, 5 tier

Experimental CDF (mm/min)	Final Time Shift (s)	Computed CDF (mm/min)	Percentage difference (%)
8.2	50	8.38	2.19
8.2	100	8.42	2.68
8.2	150	8.26	0.73
8.2	200	8.33	1.58
8.2	250	8.48	3.42
8.2	300	8.58	4.63
8.2	350	8.71	6.22

The analysis shows that for HRR vs. time curves where there are no significant drops immediately after water application, but a substantial drop occurs after a short period — as seen in Figure 8 — it is more accurate to discard the data following the significant drop and shifting the final time point closer to the end of the free-burn phase can provide a better estimation of the CDF. For instance, when comparing the uncontrolled case with a WA rate of

12.2 mm/min with the controlled WA rate of 24.5 mm/min for plastic pallets, three tiers, using a common final time for both scenarios gives a computed CDF of 6.6 mm/min (see Figure 8(a)), which is unrealistic because in an uncontrolled case with a WA rate of 12.2 mm/min, the CDF must be greater than that. However, by shifting the final time point closer to where the curve behavior stabilizes, the computed CDF becomes 14.3 mm/min (see Figure 8(b)), which more accurately falls within the expected range of CDF values. In conclusion, shifting the final time rather than using a common final time provides a better estimation of the CDF for HRR curves where the behavior appears unusual.

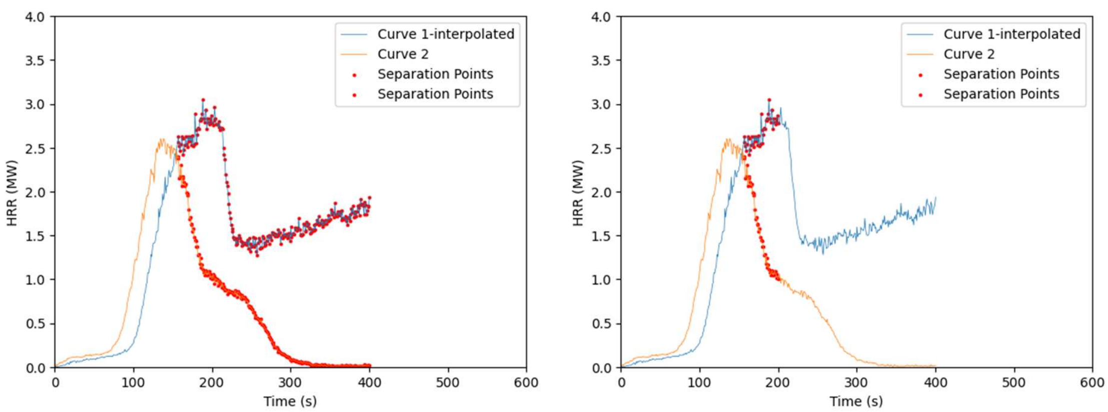

(a) Using common final time Point

(b) Using adjusted final time point

Figure 8 Effect of Final Time Point Adjustment on CDF Estimation for Plastic Pallets, 3 tier

6. Validation of Zone Model and Sensitivity Analysis of CDF Prediction for Class 2 Commodity

This section validates the zone-based model for Class 2 commodities and evaluates the impact of final time (t_f) adjustment on parameter optimization and CDF prediction. Section 6.1 validates the zone-based model for Class 2 commodity and its ability to predict CDF for higher-tier storage using lower-tier test data. Section 6.2 examines the effect of adjusting the final time (t_f) to the midpoint of the suppression phase, and the results demonstrate that optimized parameters except t_{shif} remain consistent, and that CDF predictions are unaffected.

6.1 Validation and Replication of Zone Model Results for Class 2 Commodity

Fig. 9 shows a comparison of the chemical heat release rate between experimental data and model-predicted results for Class 2 commodity, based on the optimized parameters for each test. The values shown in the caption are the water application flux for that test. A distinct inflection point is observed in the curves, marking the moment of water application. This inflection point clearly delineates the transition between the free-burn regime and the suppression regime, highlighting the impact of water application on fire dynamics. Table 8 summarizes the optimized zone model parameters for each Class 2 commodity test. The highlighted columns on the right side for p_1, t_{shift}, p_5 and β values represent the results reported by Han and Xin [13]. As the chemical heat release rate data used in Han et al [13] includes a 33-second time shift, while the data we used are already shifted by 33 seconds, this explains why the parameters optimized during the free-burning phase (p_1 and t_f) differ from results in Han et al [13], whereas those optimized using the data from suppression phase (p_5 and t_{shift}) are similar.

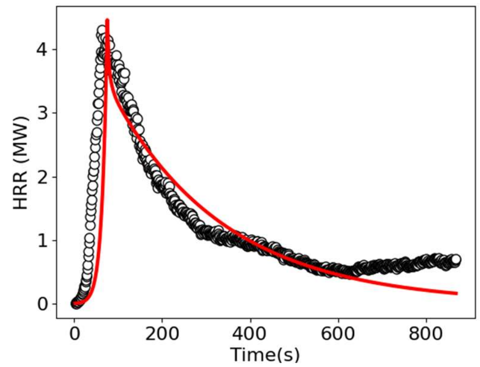

(a) 2 tiers, 4.1 mm/min

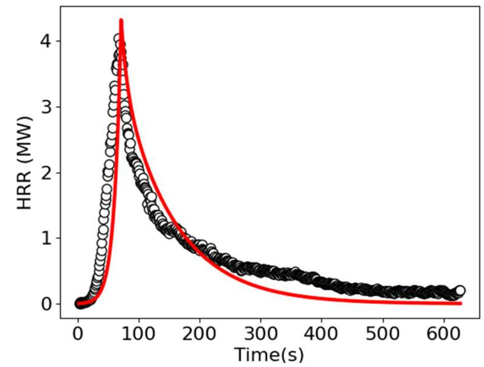

(b) 2 tiers, 8.2 mm/min

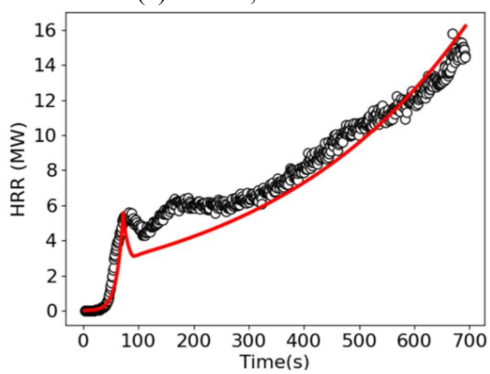

(c) 3 tiers, 4.1 mm/min

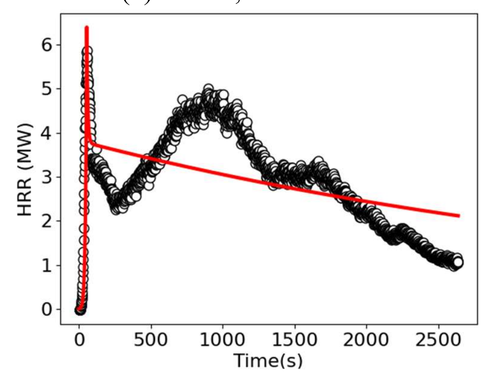

(d) 3 tiers, 6.1 mm/min

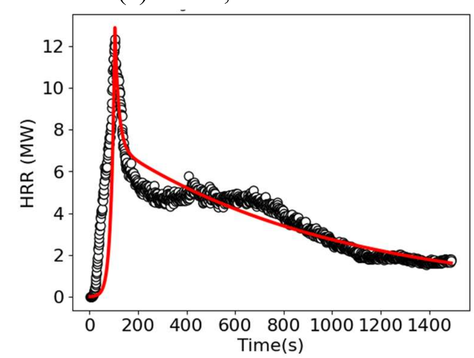

(e) 3 tiers, 8.1 mm/min

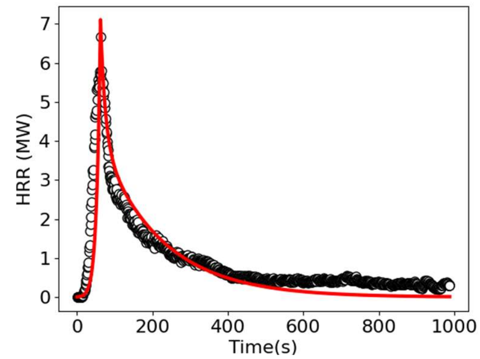

(f) 3 tiers, 12.2 mm/min

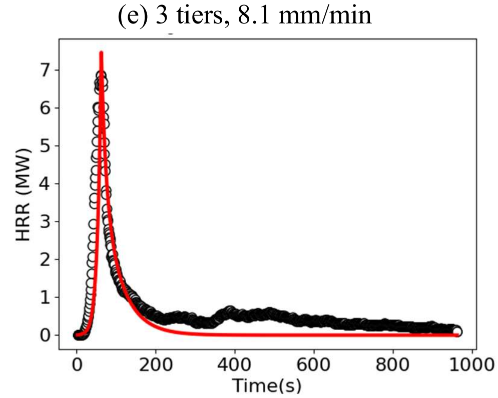

(g) 3 tiers, 18.4 mm/min

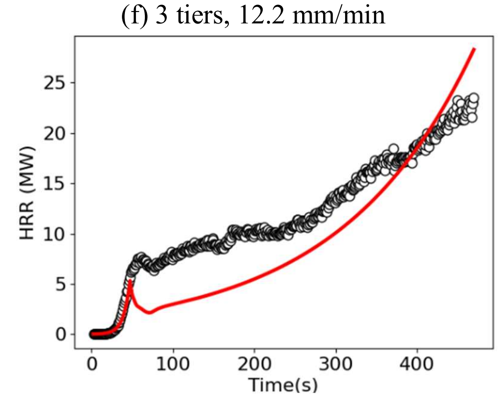

(h) 5 tiers, 6.1 mm/min

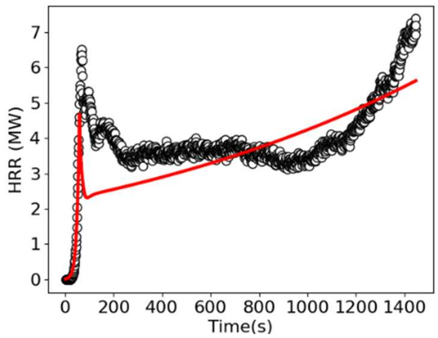

(i) 5 tiers, 8.2 mm/min

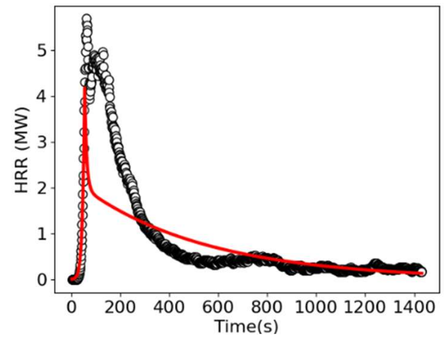

(j) 5 tiers, 10.2 mm/min

Figure 9 Comparison of chemical HRR between experimental measurements and model predictions based on the original zone-based model with a single-level optimization framework for the Class 2 commodity. The values shown in each subplot caption indicate the corresponding water application flux for that test.

Table 8 Optimized zone model parameters for each Class 2 commodity test using the original zone-based model with a single-level optimization framework (The highlighted columns in right side of p_1, t_{shift}, p_5 and β values are results by Han and Xin [13].)

Test	Tier	WA rate (mm/min)	WA Time (s)	HRR at WA (MW)	p_1 (s)		t_{shift} (s)		p_5 (kg/m²)		β	
1	2	4.1	102	5.6	12.69	29.9	0.52	1	0.17	0.40	0.39	0.42
2	2	8.2	106	5.4	12.03	27.6	1.14	6	0.16	0.37	0.17	0.20
3	3	4.1	103	7.0	14.53	21.8	0.08	1	0.19	0.29	0.68	0.67
4	3	6.1	86	6.0	10.60	17.7	0.24	1	0.14	0.24	0.35	0.35
5	3	8.1	135	12.0	7.72	11.0	1.49	21	0.10	0.15	0.35	0.35
6	3	12.2	95	8.8	12.28	19.3	1.22	1	0.16	0.26	0.14	0.14
7	3	18.4	93	9.2	11.76	18.7	1.34	1	0.16	0.25	0.09	0.11
8	5	6.1	78	6.4	11.77	15.2	0.71	22	0.16	0.20	1	0.98
9	5	8.2	90	5.8	15.48	16.1	1.34	32	0.21	0.21	0.51	0.51
10	5	10.2	85	5.1	13.19	13.5	5.16	37	0.18	0.18	0.33	0.33

Fig. 10 shows the correlation between the water evaporation ratio and the NCDF for Class 2 commodity. This relationship enables the estimation of the water evaporation ratio at the point where NCDF=1. To validate the zone model's capability to estimate the critical delivered flux (CDF) for higher-tier storage levels based on optimized parameters derived from lower-tier fire test data, we used the parameters from 2-tier and 3-tier tests, along with their corresponding predicted β values (where NCDF=1), to estimate the CDF for higher-tier storage. Furthermore, we used the average optimized parameters from all lower-tier tests (including both 2-tier and

3-tier storages), along with the average β values (where NCDF=1) from the 2-tier and 3-tier tests, to estimate the CDF for higher tiers. Table 9 provides a summary of all the results, along with the calculated CDF values based on the test data. The results indicate that the estimations based solely on the 3-tier storage test data yielded the most accurate outcomes.

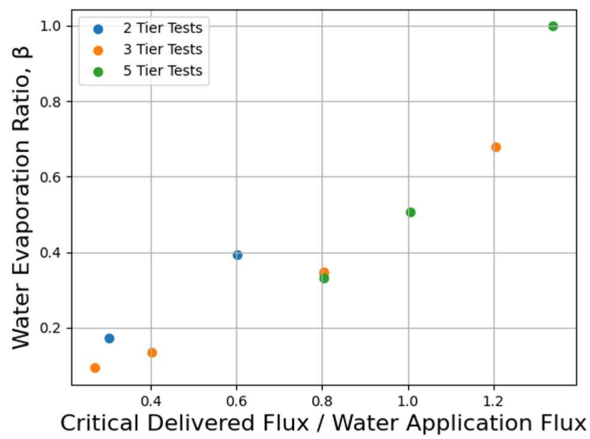

Figure 10 Correlation between water evaporation ratio and normalized critical delivered flux for class 2 commodity based on the original zone-based model and the single-level optimization framework

Table 9 Predicted CDF values for class 2 commodity in 5-tier storage racks based on the original zone-based model and the single-level optimization framework

Commodity	**Number of Tiers**	**Predicted value using the model (mm/min)**	**Calculated value from experiment (mm/min)**
Class 2	2	7.22	8.23
	3	8.20	

6.2 Effect of endpoint selection on parameter optimization

This section investigates the effect of adjusting the final time t_f(as discussed in Section 5.2) to the midpoint of the suppression phase on parameter optimization and the resulting CDF values. Figures 11 and 12 and Tables 10 and 11 present results obtained under this adjusted final time. Specifically, Fig. 11 compares the chemical heat release rate between experimental data and model predictions for Class 2 commodity, while Table 10 summarizes the optimized zone model parameters. Overall, the optimized parameters are consistent with those obtained using the total experimental time (Table 8), with the only difference in t_{shift}, which is assumed to be zero in high-tier predictions and does not affect the estimated CDF values. As shown in Fig. 12, the relationship between the water evaporation ratio and NCDF is used to determine the value of β at NCDF = 1 and provides the basis for estimating CDF. Following the methodology in Section 6.1, parameters derived from lower-tier tests were used to predict CDF values for higher-tier storage configurations, with the results summarized in Table 11. The agreement between the predicted values in Table 11 and those in Table 9 confirms that adjusting t_f to the midpoint of the suppression phase does not influence the estimated CDF values for higher-tier configurations.

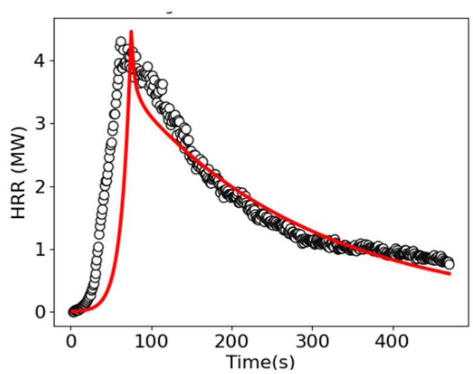

(a) 2 tiers, 4.1 mm/min

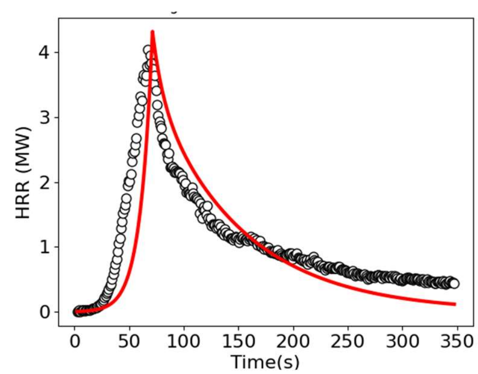

(b) 2 tiers, 8.2 mm/min

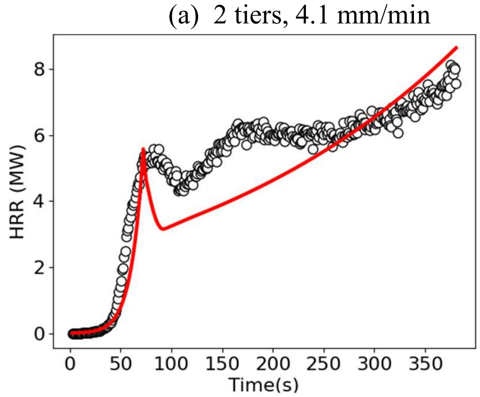

(c) 3 tiers, 4.1 mm/min

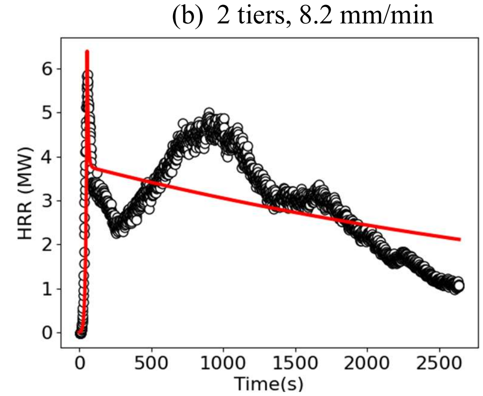

(d) 3 tiers, 6.1 mm/min

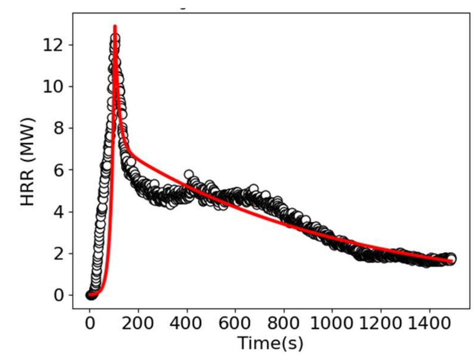

(e) 3 tiers, 8.1 mm/min

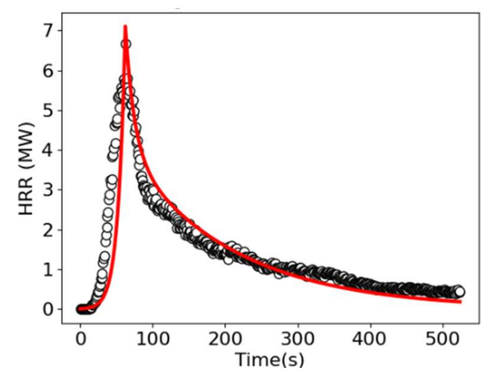

(f) 3 tiers, 12.2 mm/min

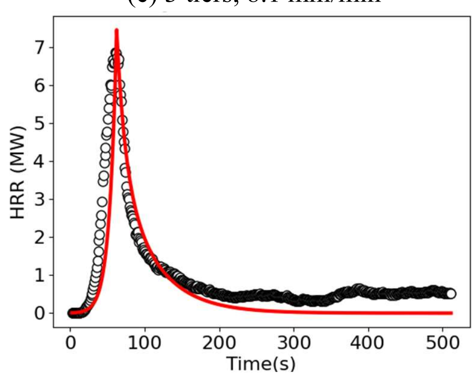

(g) 3 tiers, 18.4 mm/min

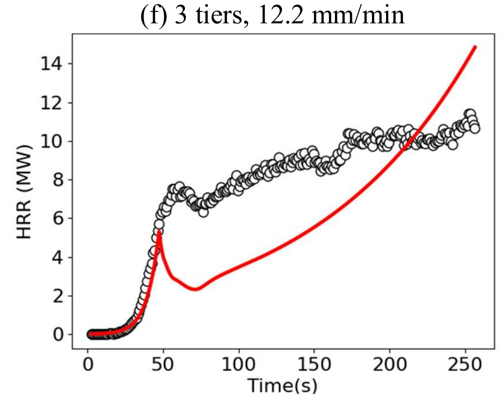

(h) 5 tiers, 6.1 mm/min

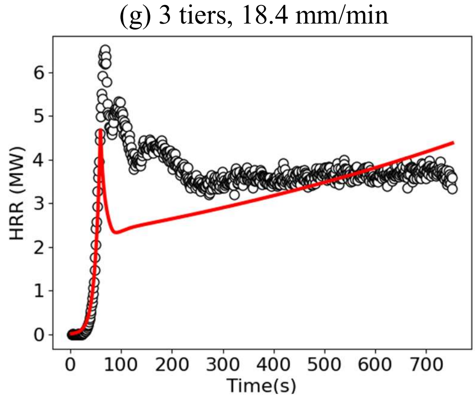

(i) 5 tiers, 8.2 mm/min

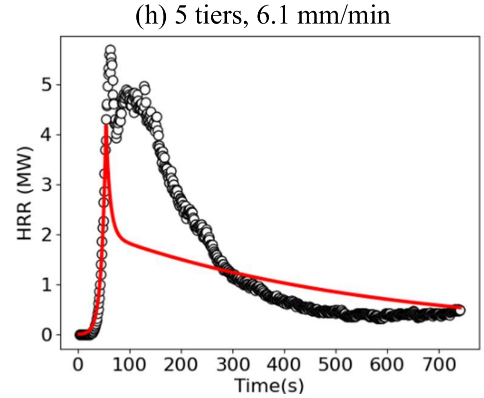

(j) 5 tiers, 10.2 mm/min

Figure 11 Comparison of chemical HRR between experimental measurements and model predictions for the Class 2 commodity using the original zone-based model with a single-level optimization framework, with adjusted final time t_f. The values shown in each subplot caption indicate the corresponding water application flux for that test.

Table 10 Optimized zone model parameters for each Class 2 commodity test, using the original zone-based model with a single-level optimization framework, with adjusted final time t_f. (The highlighted columns in right side of p_1, t_{shift}, p_5 and β values are values obtained in Section 6.1.)

Test	Tier	WA rate (mm/min)	WA Time (s)	HRR at WA (MW)	p_1 (s)		t_{shift} (s)		p_5 (kg/m²)		β	
1	2	4.1	102	5.6	12.7	12.7	0.55	0.52	0.17	0.17	0.39	0.39
2	2	8.2	106	5.4	12.0	12.0	0.42	1.14	0.16	0.16	0.17	0.17
3	3	4.1	103	7.0	14.5	14.5	1.19	0.08	0.19	0.19	0.67	0.68
4	3	6.1	86	6.0	10.6	10.6	1.41	0.24	0.14	0.14	0.34	0.35
5	3	8.1	135	12.0	7.7	7.7	0.02	1.49	0.10	0.10	0.35	0.35
6	3	12.2	95	8.8	12.3	12.3	0.48	1.22	0.16	0.16	0.14	0.14
7	3	18.4	93	9.2	11.8	11.8	1.26	1.34	0.16	0.16	0.09	0.09
8	5	6.1	78	6.4	11.7	11.7	0.06	0.71	0.16	0.16	0.96	1
9	5	8.2	90	5.8	15.5	15.5	0.36	1.34	0.21	0.21	0.51	0.51
10	5	10.2	85	5.1	13.2	13.2	5.16	4.71	0.18	0.18	0.33	0.33

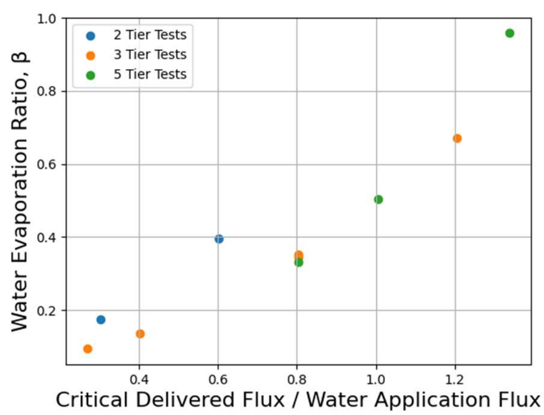

Figure 12 Correlation between water evaporation ratio and normalized critical delivered flux divided by water application flux for each Class 2 commodity test, using the original zone-based model with a single-level optimization framework, with adjusted final time t_f .

Table 11 Predicted CDF values for Class 2 commodity in 5-tier storage racks, using the original zone-based model with a single-level optimization framework, with adjusted final time t_f.

Commodity	Number of Tiers	Predicted value using the model (mm/min)	Calculated value from experiment (mm/min)
Class 2	2	7.22	8.23
	3	8.20	

7. Model validation for different commodities

FM [4] classifies commodities by fire hazard, from noncombustible materials (lowest hazard) to uncartoned expanded plastics (highest hazard). In the study [13], Han and Xin validated the proposed zone model exclusively for Class 2 commodity. In this section, we extend the validation to assess whether the proposed zone model is applicable to other types of commodities. For parameters where the commodity-specific values are uncertain, such as p_4, A_{ini}, and γ, we will refer to the values used for Class 2 commodity. However, the four designated parameters (p_1, p_5, t_{shift} and β) will be specifically optimized during the implementation of the zone model.

7.1 Estimations from All Lower-tier Experimental Data

7.1.1 Parameters Optimized from Experimental data of Class 3 commodity

Fig. 13 shows a comparison of chemical heat release rate between experimental data (trajectory with small circles) and modelled results (red color lines) for class 3 commodity based on the optimized model parameters for each test. The comparison is provided for tests with different numbers of storage tiers (2 tiers, 3 tiers, and 5 tiers) under different water fluxes. An earliest local maximum is observed on the curves, indicating the moment of water application. This earliest local maximum effectively demarcates the transition between the free-phase and the suppression phase, highlighting the influence of water application on the fire dynamics. The results demonstrate that the model successfully captures the major trends observed in the experimental data of Class 3 commodity. This alignment is particularly significant for commodity classification, as it validates the model's ability to replicate the critical aspects of fire behavior under suppression conditions. Table 12 summarizes the optimized zone model parameters for each Class 3 commodity test.

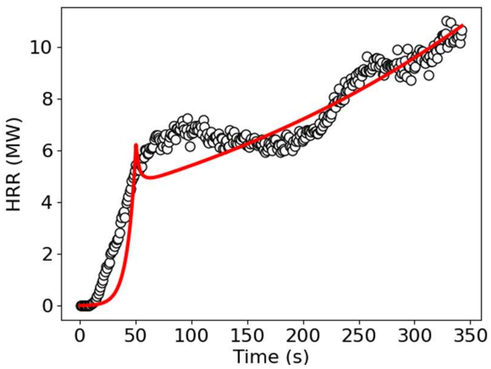

(a) 2 tiers, 4.1 mm/min

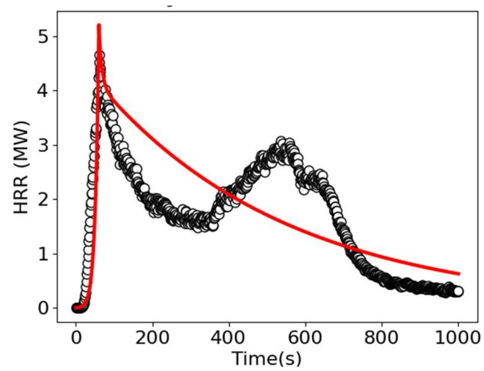

(b) 2 tiers, 6.1 mm/min

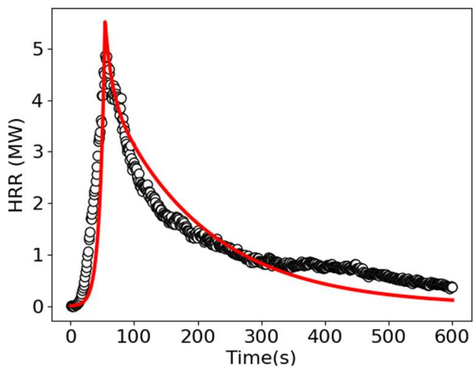

(c) 2 tiers, 12.2 mm/min

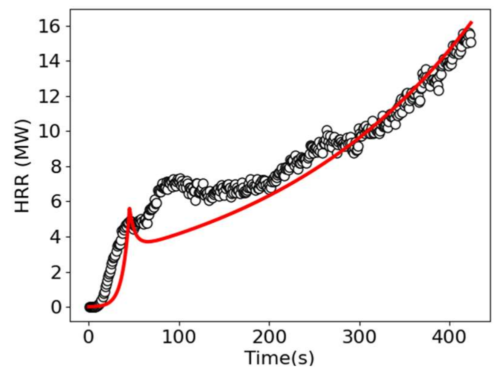

(d) 3 tiers, 6.1 mm/min

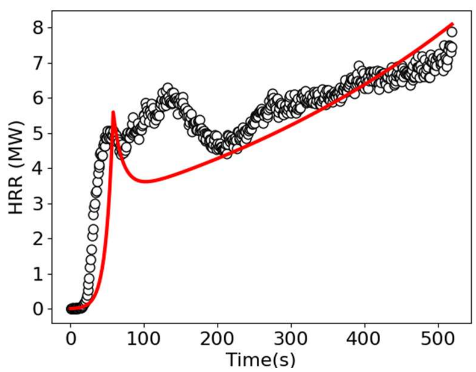

(e) 3 tiers, 10.2 mm/min

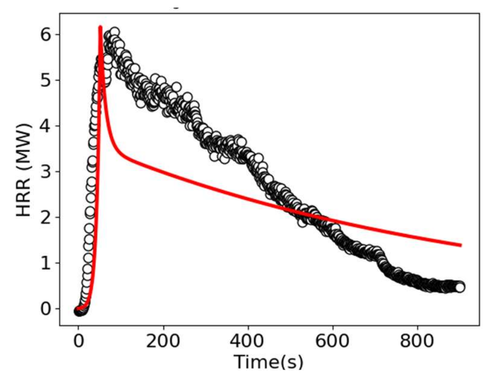

(f) 3 tiers, 12.2 mm/min

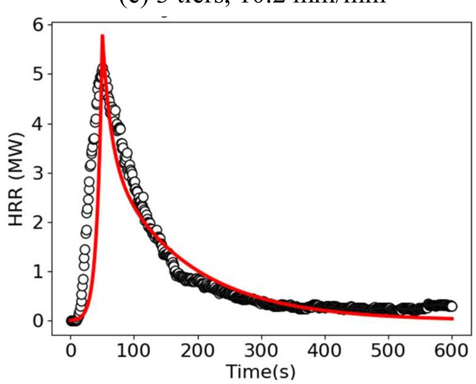

(g) 3 tiers, 18.4 mm/min

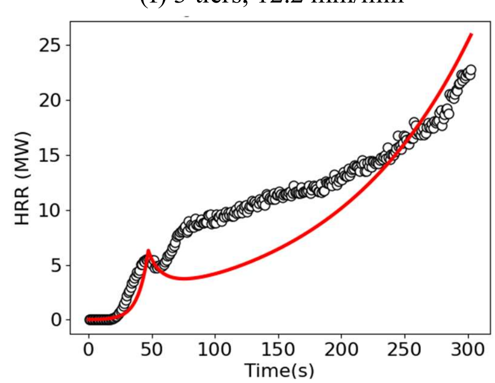

(h) 5 tiers, 12.2 mm/min

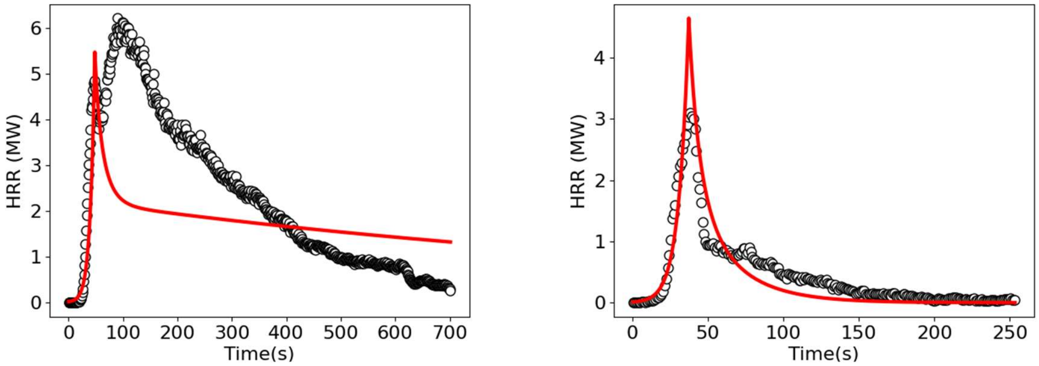

(i) 5 tiers, 18.4 mm/min (j) 5 tiers, 24.5 mm/min

Figure 13 Comparison of chemical HRR between experimental measurements and modeled results for Class 3 commodity, based on the original zone-based model with a single-level optimization framework .

Table 12 Optimized zone model parameters for each Class 3 commodity test, based on the original zone-based model with a single-level optimization framework

Test	Number of Tiers	WA rate (mm/min)	WA Time (s)	HRR at WA (MW)	p_1 (s)	t_{shift} (s)	p_5 (kg/m^2)	β
1	2	4.1	96	7.5	8.07	1.49	0.11	0.37
2	2	6.1	60	6.4	10.08	1.10	0.13	0.22
3	2	12.1	54	6.7	8.93	1.12	0.12	0.10
4	3	6.1	45	6.7	9.12	0.01	0.12	0.33
5	3	10.1	58	6.9	11.93	0.27	0.16	0.16
6	3	12.1	52	7.5	10.45	0.75	0.14	0.13
7	3	18.2	50	7.0	10.14	1.48	0.14	0.08
8	5	12.1	47	7.6	11.95	1.30	0.16	0.21
9	5	18.2	48	6.7	12.54	1.33	0.17	0.12
10	5	24.4	36	6.2	9.80	0.35	0.13	0.11

7.1.2 Parameters Optimized from Experimental data of Standard Plastic Commodity

Fig. 14 presents a comparison of the chemical heat release rates between experimental data and modeled predictions for Standard Plastics commodity based on the optimized model parameters for each test. The experimental data are represented by trajectories marked with small circles, while the model predictions are shown as a red line plot. The comparison is provided for tests with different numbers of storage tiers (2 tiers, 3 tiers, and 5 tiers) under different water fluxes. Similar to the results for Class 3 commodity tests, an earliest local maximum is observed on the curves, indicating the time of water application. This earliest local maximum effectively demarcates the transition between the free-burn phase and the suppression phase, highlighting the influence of water application on the fire dynamics. The results demonstrate that the model successfully captures the major trends observed in the experimental data of standard plastic commodities. Table 13 summarizes the optimized zone model parameters for each standard plastic commodity test.

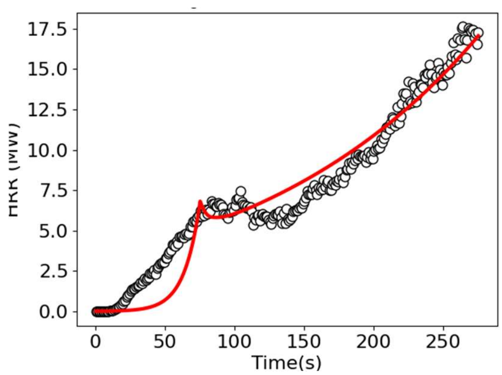

(a) 2 tiers, 4.1 mm/min

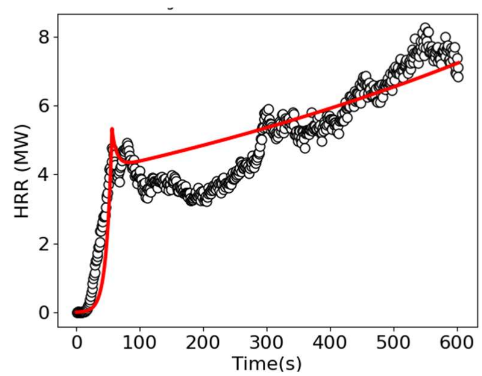

(b) 2 tiers, 6.1 mm/min

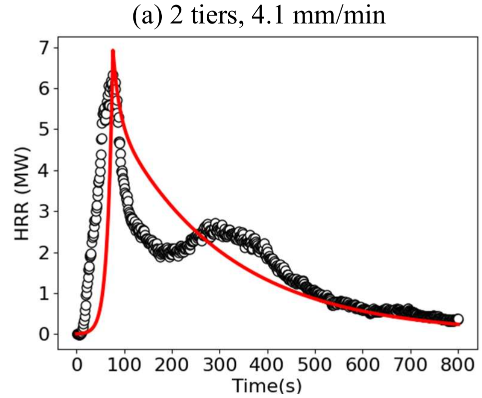

(c) 2 tiers, 10.2 mm/min

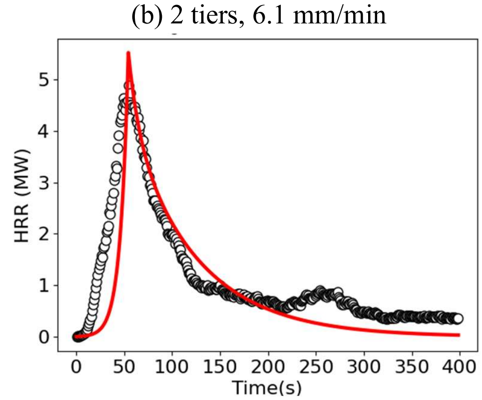

(d) 2 tiers, 16.3 mm/min

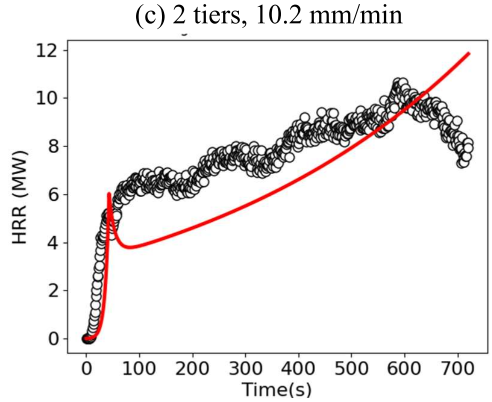

(e) 3 tiers, 12.2 mm/min

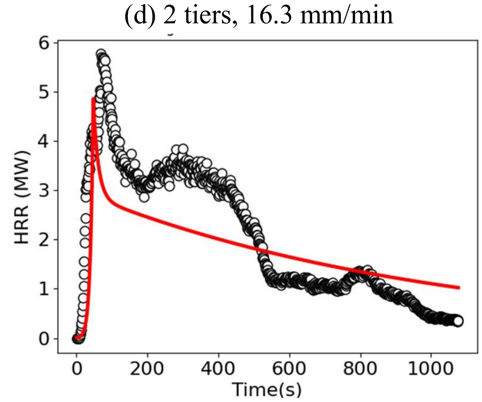

(f) 3 tiers, 15.5 mm/min

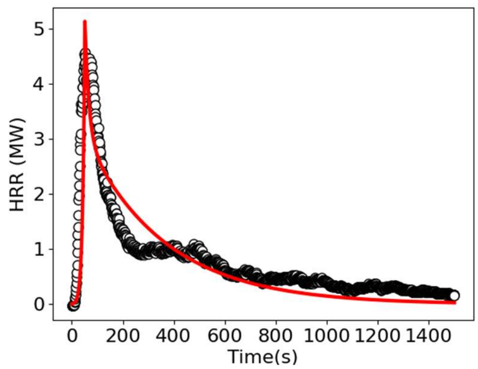

(g) 3 tiers, 18.4 mm/min

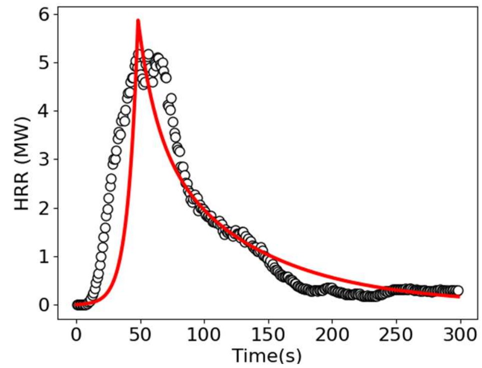

(h) 3 tiers, 26.5 mm/min

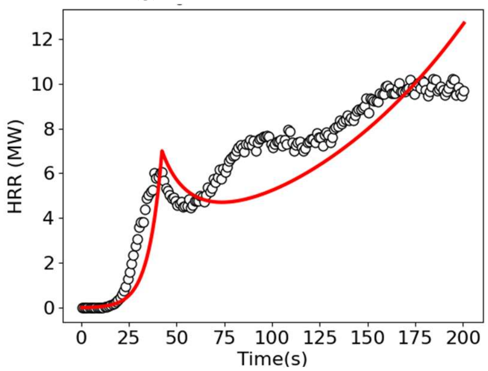

(i) 5 tiers, 20.4 mm/min

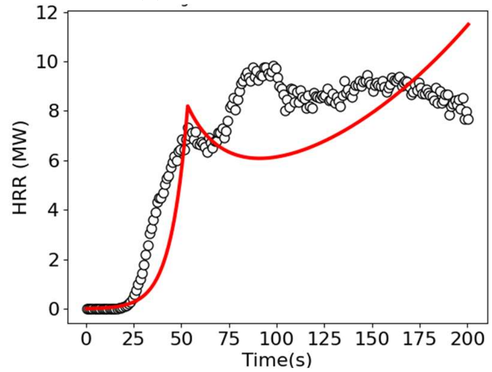

(j) 5 tiers, 24.5 mm/min

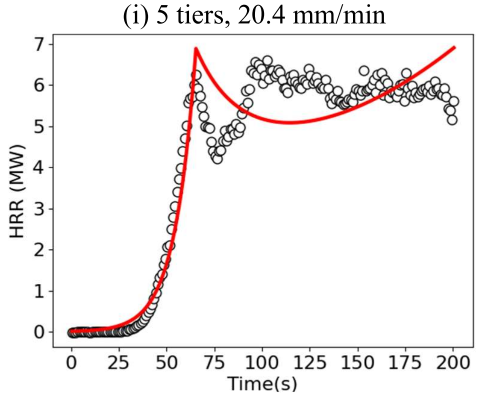

(k) 5 tiers, 24.5 mm/min

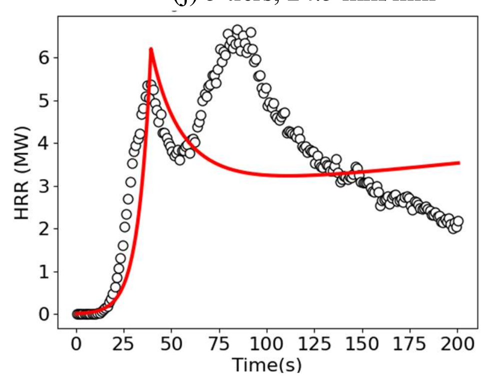

(l) 5 tiers, 28.6 mm/min

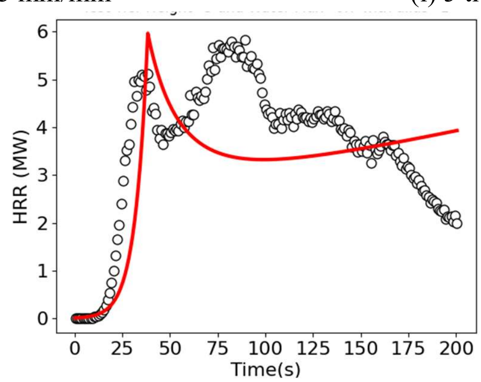

(m) 5 tiers, 28.6 mm/min

Figure 14 Comparison of chemical HRR between experimental measurements and modeled results for standard plastic commodity, based on the original zone-based model with a single-level optimization framework.

Table 13 Optimized zone model parameters for each standard plastic commodity test, based on the original zone-based model with a single-level optimization framework.

Test	Number of Tiers	WA rate (mm/min)	WA Time (s)	HRR at WA (MW)	p_1 (s)	t_{shift} (s)	p_5 (kg/m^2)	β
1	2	4.1	75	8.5	12.19	1.34	0.16	0.35
2	2	6.1	56	6.5	9.33	0.03	0.12	0.22
3	2	10.1	76	8.7	12.33	1.07	0.16	0.12
4	2	16.3	54	6.7	8.93	1.34	0.12	0.08
5	3	12.1	43	7.2	8.57	0.61	0.11	0.12
6	3	14.2	47	5.9	9.80	0.17	0.13	0.09
7	3	18.4	51	6.3	10.57	1.35	0.14	0.08
8	3	26.5	48	7.1	9.69	1.43	0.13	0.05
9	5	20.4	42	8.3	10.40	0.51	0.14	0.09
10	5	24.5 (0)	53	10	12.96	1.15	0.17	0.07
11	5	24.5 (1)	65	8.6	16.55	0.34	0.22	0.07
12	5	28.6 (0)	39	7.3	9.82	1.15	0.13	0.06
13	5	28.6 (1)	38	7.0	9.62	0.65	0.13	0.06

7.1.3 Parameters Optimized from Experimental data of Plastic Pallets Commodity

Plastic pallets are classified as uncartoned and unexpanded plastics. Fig. 15 presents a comparison of the chemical heat release rates between experimental data and modeled predictions for plastic pallet commodity based on the optimized model parameters for each test. The experimental data are represented by trajectories marked with small circles, while the model predictions are shown as a red line plot. The comparison is provided for tests with different numbers of storage tiers (2 tiers, 3 tiers, and 5 tiers) under different water fluxes. Similar to the results for the other commodities, an earliest local maximum is observed on the curves, indicating the time of water application. This earliest local maximum effectively demarcates the transition between the free-burn regime and the suppression regime, highlighting the influence of water application on the fire dynamics. The results demonstrate that the model successfully captures the major trends observed in the experimental data of plastic pallet commodity. Table 14 summarizes the optimized zone model parameters for each plastic plastic commodity test.

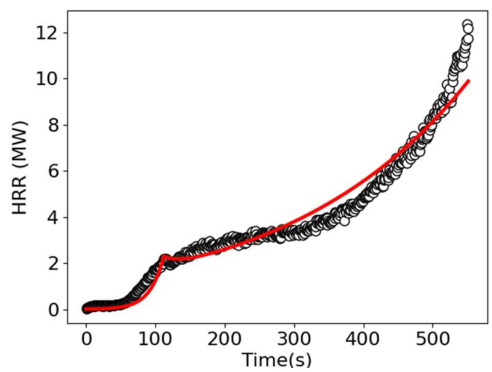

(a) 2 tiers, 6.1 mm/min

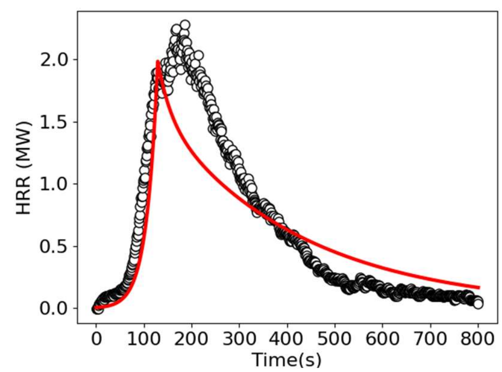

(b) 2 tiers, 10.2 mm/min

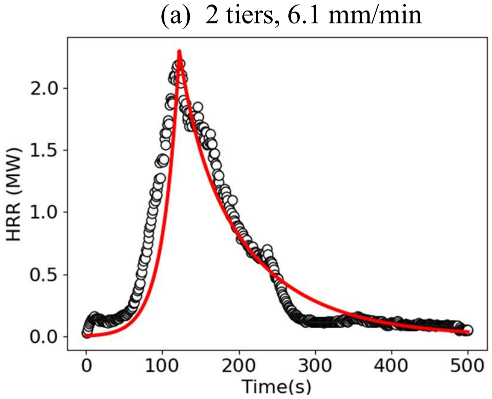

(c) 2 tiers, 16.3 mm/min

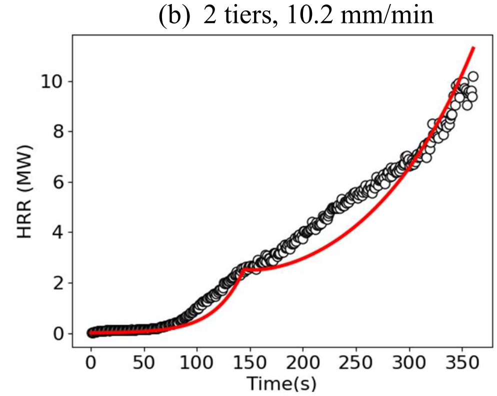

(d) 3 tiers, 6.1 mm/min

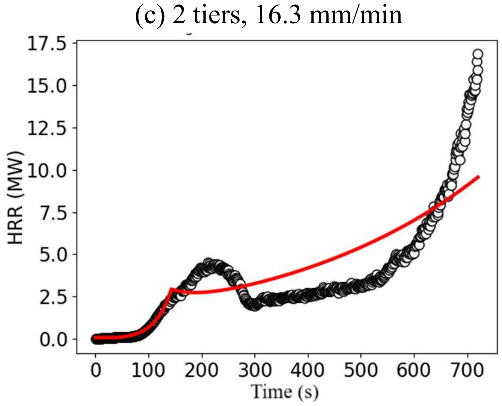

(e)   3 tiers, 10.2 mm/min

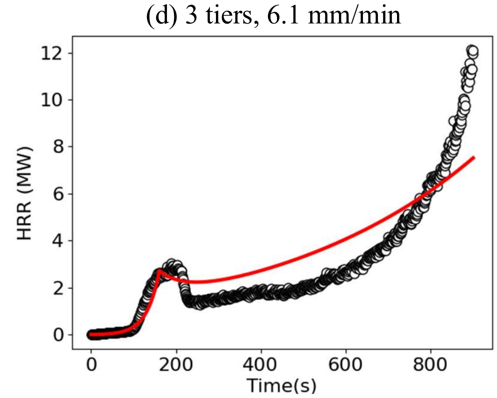

(f) 3 tiers, 12.2 mm/min

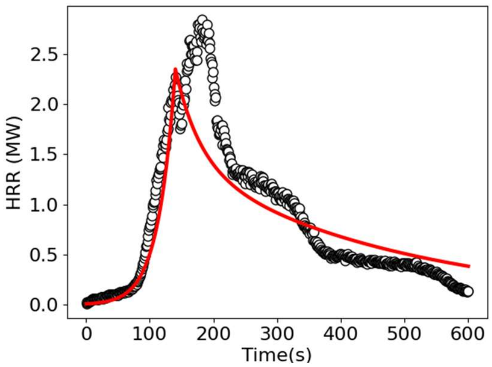

(g) 3 tiers, 14.3 mm/min

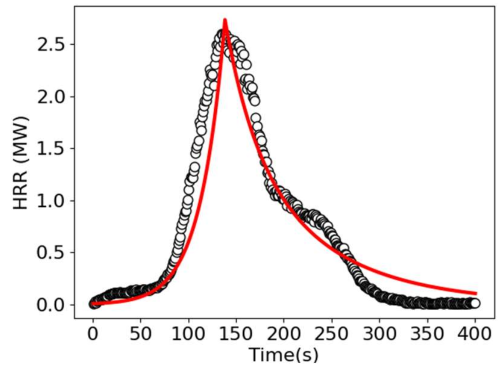

(h) 3 tiers, 24.5 mm/min

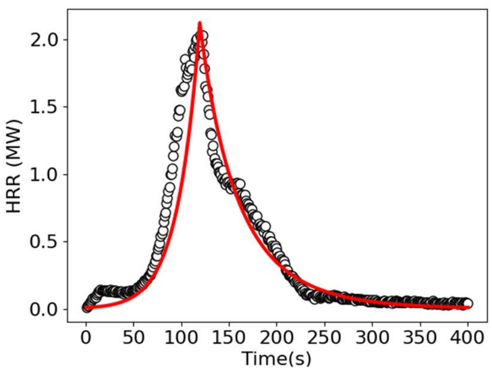

(i) 3 tiers, 40.8 mm/min

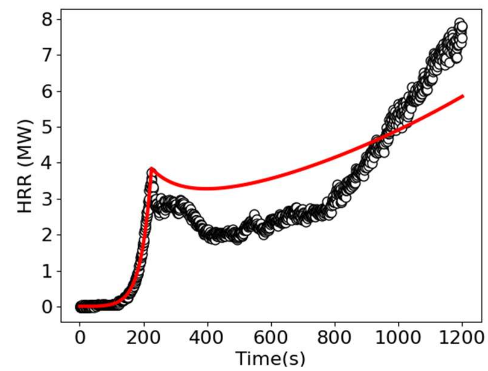

(j) 5 tiers, 40.8 mm/min

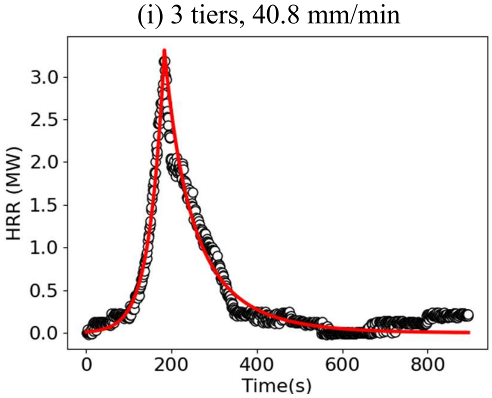

(k) 5 tiers, 51.0 mm/min

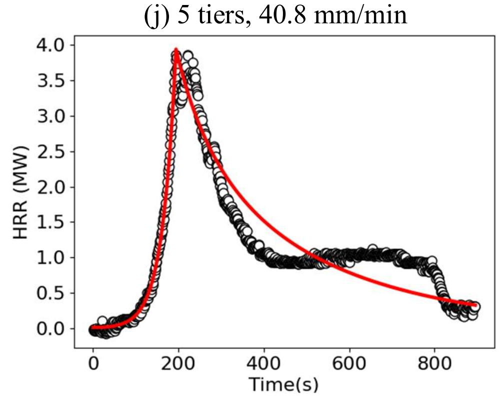

(l) 5 tiers, 61.2 mm/min

Figure 15 Comparison of chemical HRR between experimental measurements and modeled results for plastic pallet commodity, based on the original zone-based model with a single-level optimization framework.

Table 14 Optimized zone model parameters for each plastic pallet commodity test, based on the original zone-based model with a single-level optimization framework.

Test	Number of Tiers	WA rate (mm/min)	WA Time (s)	HRR at WA (MW)	p_1 (s)	t_{shift} (s)	p_5 (kg/m^2)	β
1	2	6.1	112	3	22.15	1.11	0.30	0.20
2	2	10.1	129	2.6	26.31	0.20	0.35	0.13
3	2	16.3	122	3	24.20	0.85	0.32	0.08
4	3	6.1	144	3.3	35.27	1.36	0.47	0.23
5	3	10.1	212	4.0	38.94	0.24	0.52	0.14
6	3	12.2	188	3.6	38.95	0.85	0.52	0.12
7	3	14.3	140	3.1	34.75	0.04	0.46	0.11
8	3	24.5	138	3.6	33.26	0.94	0.44	0.07
9	3	40.8	119	2.8	30.04	0.33	0.40	0.04
10	5	40.8	225	5.1	51.20	49.50	0.68	0.04
11	5	51.0	194	5.3	50.08	22.30	0.67	0.03
12	5	61.2	183	4.4	54.80	0.99	0.73	0.05

7.1.4 Parameters Optimized from Experimental data of Cartoned Meat Tray (CMT) commodity

Fig. 16 shows a comparison of the chemical heat release rates between experimental observations and model predictions for CMT commodities. Similar to previous cases, the experimental data are represented by trajectories marked with small circles, while the model predictions are depicted as a red line plot. The comparison is provided for tests with different numbers of storage tiers (2 tiers, 3 tiers, and 5 tiers) under different water fluxes. Similar to the results for the other commodities, the free burn regime and suppression regime can be notice with the earliest local maximum of the curve. This earliest local maximum clearly separates the free-burn regime from the suppression regime, emphasizing the impact of water application on the fire's behavior and growth. The results demonstrate that the model successfully captures the major trends observed in the experimental data of CMT commodity. Table 15 is a summary of the optimized parameters based on the test data of CMT commodity.

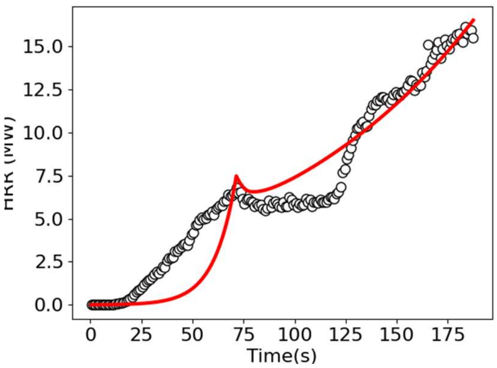

(a) 2 tiers, 4.1 mm/min

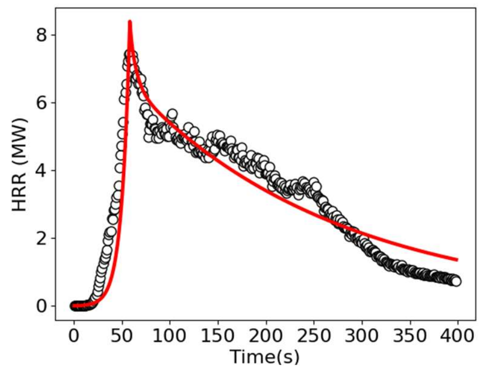

(b) 2 tiers, 6.1 mm/min

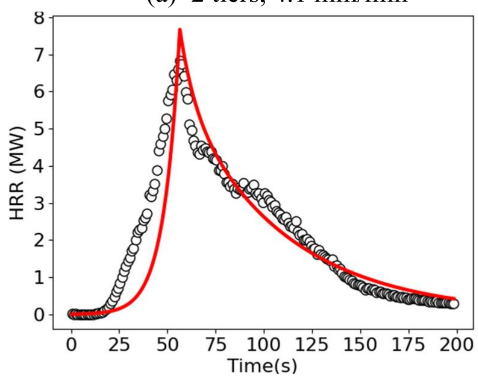

(c) 2 tiers, 10.2 mm/min

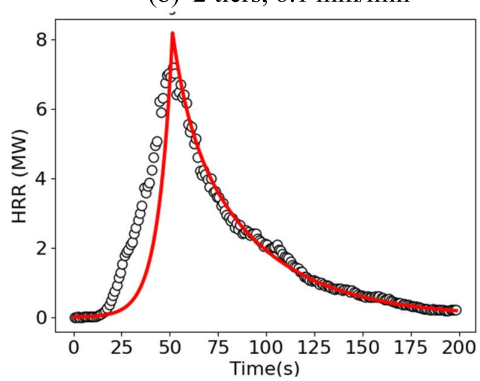

(d) 2 tiers, 16.3 mm/min

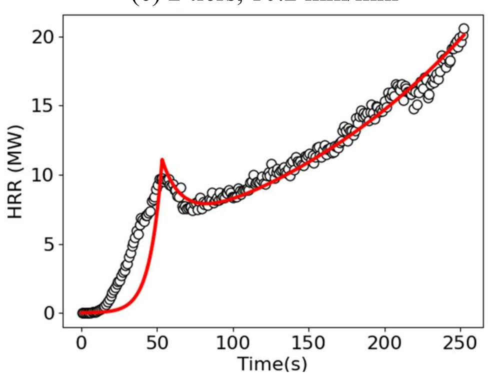

(e) 3 tiers, 12.2 mm/min

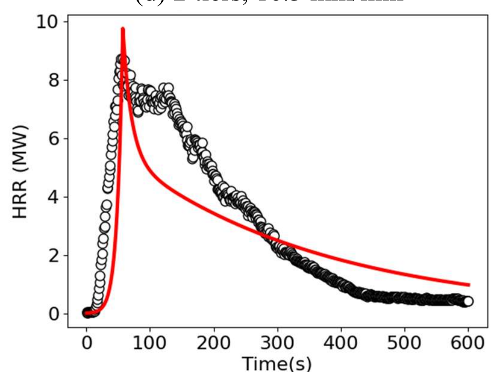

(f) 3 tiers, 14.3 mm/min

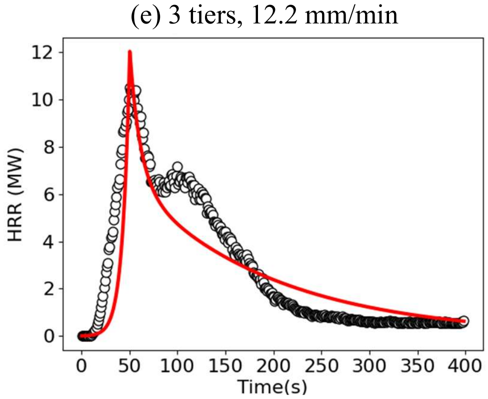

(g) 3 tiers, 15.5 mm/min

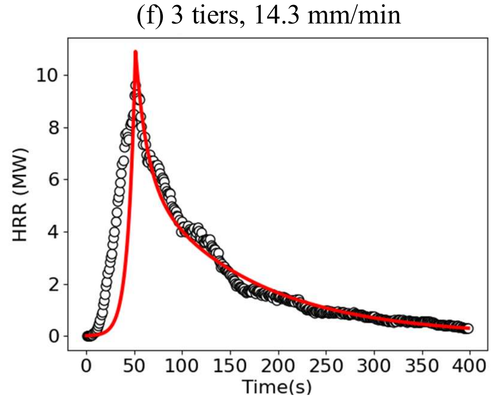

(h) 3 tiers, 18.4 mm/min

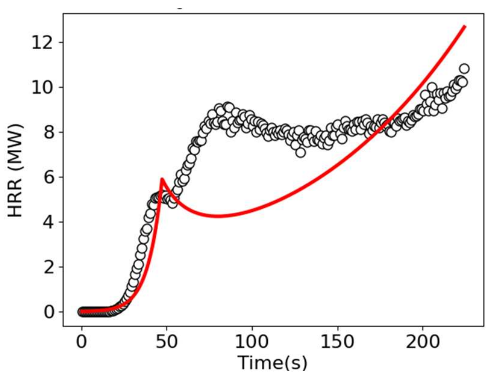

(i) 5 tiers, 20.4 mm/min

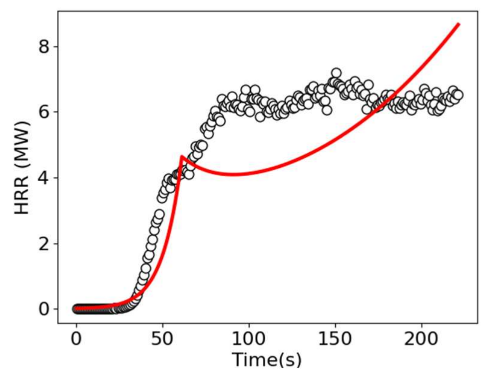

(j) 5 tiers, 24.5 mm/min

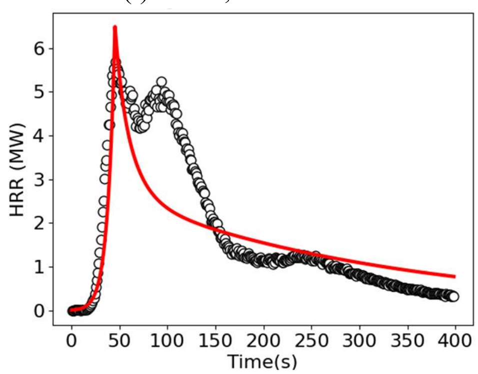

(k) 5 tiers, 24.5 mm/min

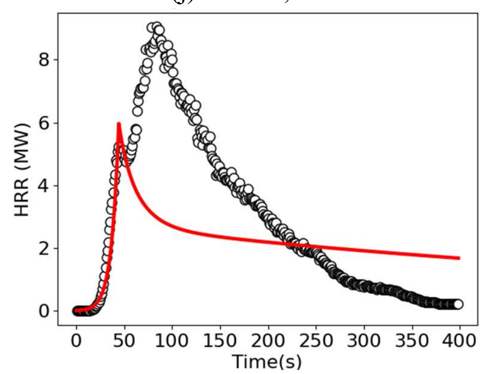

(l) 5 tiers, 28.6 mm/min

Figure 16 Comparison of chemical HRR between experimental measurements and modeled results for cartoned MT commodity, based on the original zone-based model with a single-level optimization framework.

Table 15 Optimized zone model parameters for each cartooned MT commodity test, based on the original zone-based model with a single-level optimization framework.

Test	Number of Tiers	WA rate (mm/min)	WA Time (s)	HRR at WA (MW)	p_1 (s)	t_{shift} (s)	p_5 (kg/m^2)	β
1	2	4.1	71	9.3	11.35	1.33	0.15	0.34
2	2	6.1	58	10.2	9.01	0.99	0.12	0.23
3	2	10.1	56	9.3	8.80	0.84	0.12	0.14
4	2	16.3	51	9.8	7.89	0.93	0.11	0.08
5	3	12.2	53	13.4	9.67	0.51	0.13	0.12
6	3	14.2	57	11.9	10.66	1.20	0.14	0.11
7	3	15.5	50	14.4	8.97	0.85	0.12	0.10
8	3	18.3	51	13.1	9.31	0.45	0.12	0.08
9	5	20.4	47	7.1	20.58	0.04	0.27	0.09
10	5	24.5	61	5.8	25.20	0.62	0.34	0.07
11	5	24.5	45	7.8	11.35	1.17	0.15	0.08
12	5	28.6	44	7.1	20.65	0.43	0.28	0.07

7.1.5 Critical Delivered Fluxes for Different Types of Commodities

The experimental CDF values of different commodities are calculated based on the above-described procedure in Section 5.1 and summarized in Table 16. It can be noted here that as the number of tiers increases within the commodity the CDF values increase. The increase in the CDF values with tier heights shows the increase of water flux within the same commodity.

Table 16 Critical Delivered Flux (CDF) values for different types of commodities and tiers obtained from the experimental values

Commodity type	Number of Tiers	CDF values calculated by Yibing (mm/min)
Class 2	2	2.46
	3	4.92
	5	8.2
Class 3	2	5.33
	3	11.07
	5	20.09
Standard Plastics	2	7.38
	3	14.35
	5	23.78
Plastic pallets	2	9.43
	3	12.71
	5	43.05
Cartoned MT	2	6.56
	3	13.94
	5	27.06

Fig. 17 shows the correlation between the water evaporation ratio (β) and the normalized critical delivered flux (NCDF), defined as the ratio of the Critical Delivered Flux (CDF) required to control the fire to the actual applied water flux. When the NCDF exceeds 1, the fire is expected to remain uncontrolled, whereas values below 1 indicate a controlled fire scenario. For Class 3, standard plastic, and cartoned MT commodities, the evaporation ratios vs. NCDF for tier 3 and tier 5 configurations are within close range of one another but deviate from that for the tier 2 configuration, suggesting different suppression characteristics for the tier 2 configuration. However, for plastic pallets, the evaporation ratios vs. NCDF for tier 2 and tier

3 are closely aligned, while that for tier 5 shows a distinct deviation, indicating a variation in suppression behavior at the highest storage level.

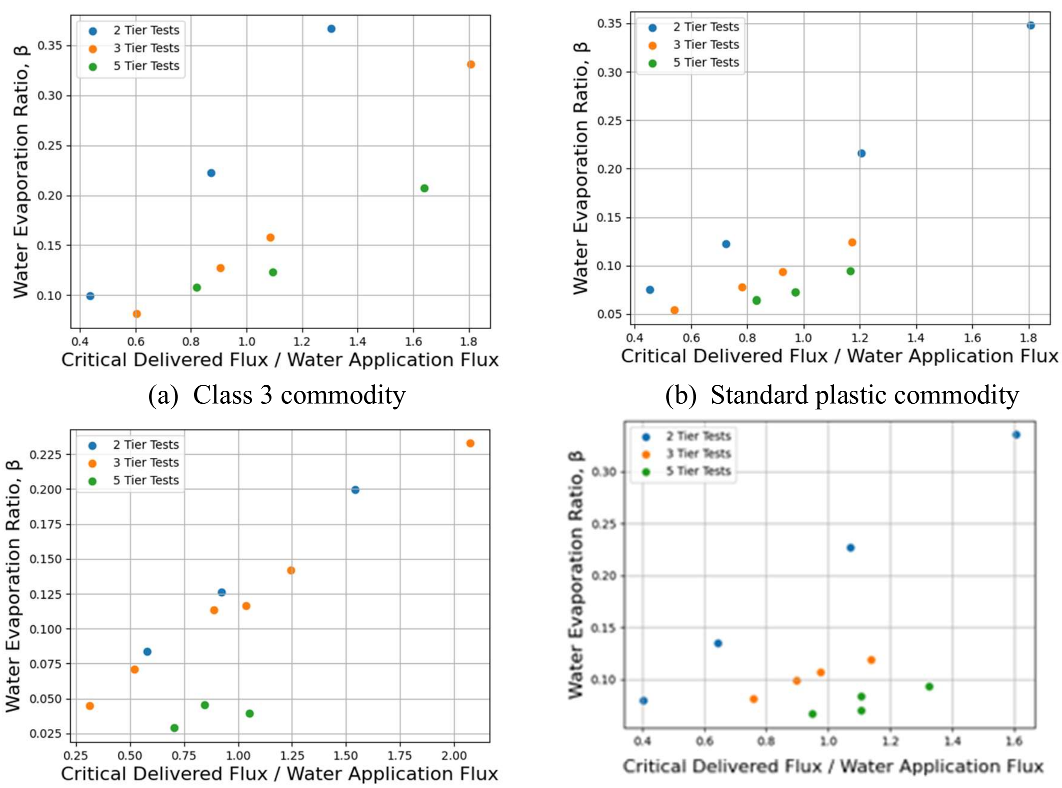

(a) Class 3 commodity (b) Standard plastic commodity

(c) Plastic pallet commodity (d) Cartoned MT commodity

Figure 17 Correlation between water evaporation ratio and normalized critical delivered flux across different commodities, based on the original zone-based model with a single-level optimization framework.

The same methodology described in Section 6.1 was applied to estimate the CDF for all commodities, using parameters from lower-tier tests to predict higher-tier storage configurations. The relationship between the water application ratios and the NCDF values allows us to estimate the water evaporation ratio when NCDF =1. Table 17 provides a summary of estimated CDF for 5-tier storage using the zone model. While estimations based on 3-tier storage test data produced better results compared to the 2-tier data, the overall deviation between the model-predicted CDF and the CDF calculated in Xin[12] is less than 30% except for plastic pallets. This deviation is considered reasonable for industrial fire protection applications. A potential explanation for the significant deviation in the plastic pallet data is the difference in fire dynamics between cartoned and non-cartoned commodities as explained in section 10.

Table 17 Predicted CDF values for different commodities from tier 2 and tier 3 tests, based on the original zone-based model with a single-level optimization framework.

Commodity	Number of Tiers	Predicted value using the model (mm/min)	CDF values calculated by Yibing (mm/min)
Class 2	2	7.22 (12%)	8.2
	3	8.20 (0%)	
Class 3	2	11.25 (44%)	20.09
	3	15.67 (22%)	
Standard Plastics	2	14.02 (41%)	23.78
	3	20.20 (15%)	
Plastic Pallets	2	17.02 (60%)	43.05
	3	18.43 (57%)	
Cartoned MT	2	13.01 (52%)	27.06
	3	19.92 (26%)	

7.2 Parameter Optimization Using Two Lower-Tier Cases: One Controlled and One Uncontrolled with the Smallest Water Flux Difference

In Section 7.1, the CDF of the 5-tier configuration was calculated using parameters optimized from all the lower-tier data. However, in practice, the objective is to minimize the number of tests required while still achieving reliable results. Therefore, in this section, we refine our approach by using data from only two 2-tier cases or two 3-tier cases — one controlled and one uncontrolled with the smallest water flux difference. These limited datasets are used to optimize the parameters, and the resulting CDF is calculated.

7.2.1 Parameters Optimized from Experimental Data of Class 2 Commodity

Fig. 18 shows a comparison of the chemical heat release rate between experimental data and modeled results obtained using optimized parameters for the selected 3-tier Class 2 commodity tests. Table 18 summarizes the optimized zone model parameters for those tests.

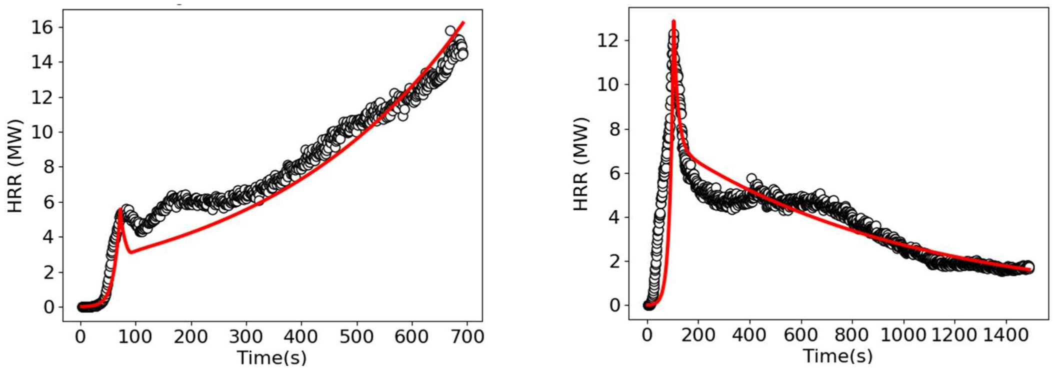

(a) 3 tiers, 4.1 mm/min (b) 3 tiers, 8.1 mm/min

Figure 18 Comparison of chemical HRR between experimental measurements and modeled results for Class 2 commodity, using the original zone-based model with a single-level optimization framework.

Table 18 Optimized zone model parameters for Class 2 commodity, using the original zone-based model with a single-level optimization framework.

Number of Tiers	WA rate (mm/min)	WA Time (s)	HRR at WA (MW)	p_1 (s)	t_{shift} (s)	p_5 (kg/m^2)	β
3	4.1	103	7.0	14.5	1.38	0.19	0.68
3	8.1	135	12.0	18.7	0.122	0.25	0.23

7.2.2 Parameters Optimized from Experimental data of Class 3 Commodity

Fig. 19 shows a comparison of the chemical heat release rate between experimental data and modeled results obtained using optimized parameters for the selected 2-tier and 3-tier Class 3 commodity tests. Table 19 summarizes the optimized zone model parameters for those modelled tests.

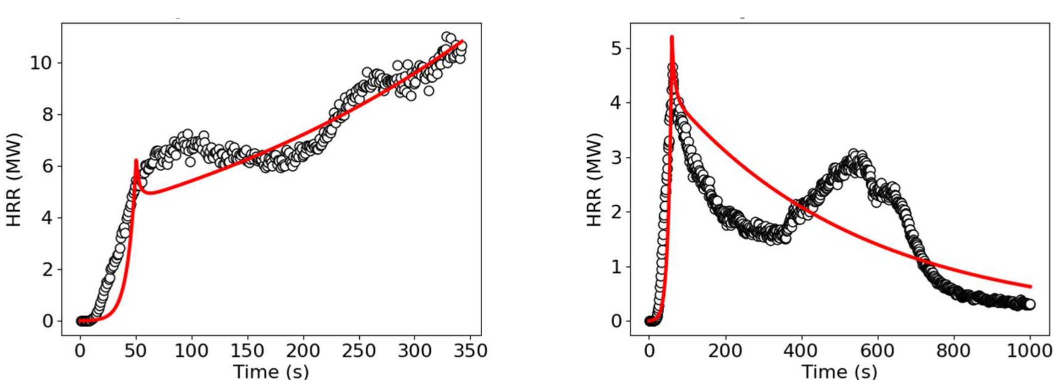

(a) 2 tiers, 4.1 mm/min (b) 2 tiers, 6.1 mm/min

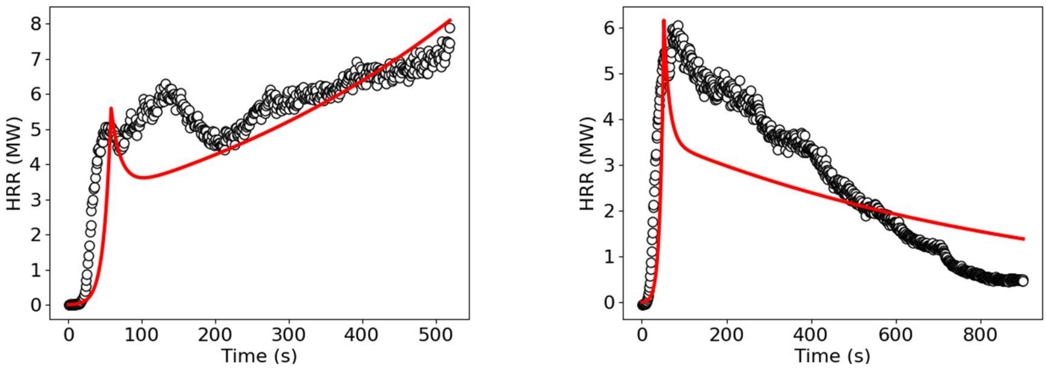

(c) 3 tiers, 10.1 mm/min (d) 3 tiers, 12.1 mm/min

Figure 19 Comparison of chemical HRR between experimental measurements and modeled results for Class 3 commodity, using the original zone-based model with a single-level optimization framework .

Table 19 Optimized zone model parameters for Class 3 commodity, using the original zone-based model with a single-level optimization framework.

Number of Tiers	**WA rate (mm/min)**	**WA Time (s)**	**HRR at WA (MW)**	p_1 **(s)**	t_{shift} **(s)**	p_5 **(kg/m^2)**	**β**
2	4.1	96	7.5	8.07	1.05	0.11	0.37
2	6.1	60	6.4	10.08	0.52	0.13	0.22
3	10.1	58	6.9	11.92	1.49	0.16	0.16
3	12.1	52	7.5	10.45	0.47	0.14	0.13

7.2.3 Parameters Optimized from Fire Tests on Standard Plastic Commodity

Fig. 20 compares the chemical heat release rate between experimental data and modeled results obtained using optimized parameters for the selected 2-tier and 3-tier Standard Plastic commodity tests. Table 20 summarizes the optimized zone model parameters for those selected tests.

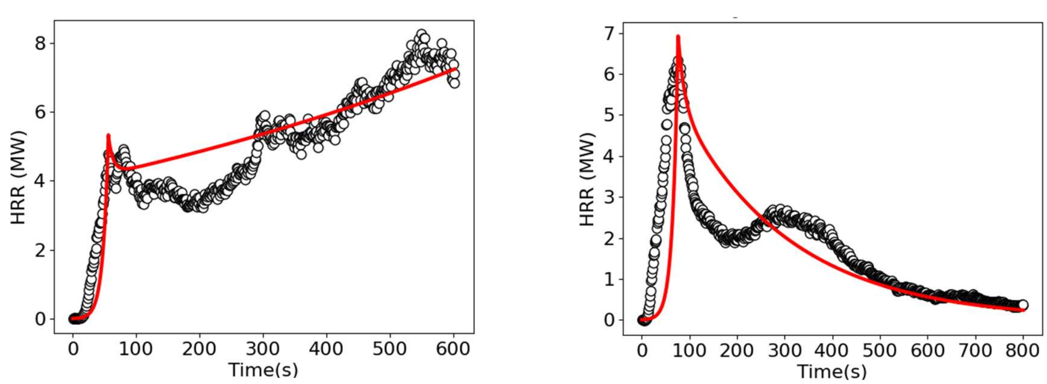

(a) 2 tiers, 6.1 mm/min, Case 1

(b) 2 tiers, 10.2 mm/min, Case 1

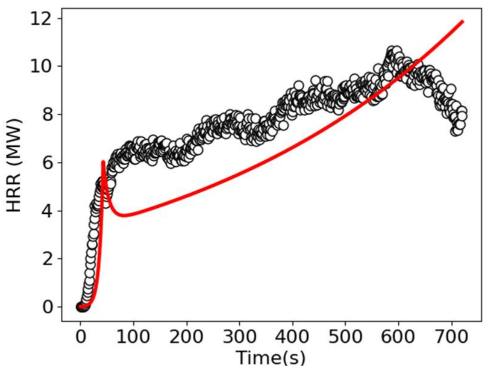

(c) 3 tiers, 12.1 mm/min

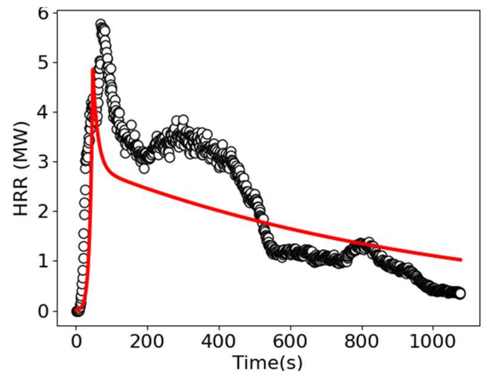

(d) 3 tiers, 14.2 mm/min

Figure 20 Comparison of chemical HRR between experimental measurements and modeled results for standard plastic commodity, using the original zone-based model with a single-level optimization framework.

Table 20 Optimized zone model parameters for standard plastic commodity, using the original zone-based model with a single-level optimization framework.

Number of Tiers	WA rate (mm/min)	WA Time (s)	HRR at WA (MW)	p_1 (s)	t_{shift} (s)	p_5 (kg/m^2)	β
2	6.1	56	6.5	9.33	1.26	0.12	0.22
2	10.2	76	8.7	12.33	1.40	0.16	0.12
3	12.1	43	7.2	8.57	1.4	0.11	0.12
3	14.2	47	5.9	9.80	1.02	0.13	0.09

7.2.4 Parameters Optimized from Experimental data of Plastic Pallet Commodity

Fig. 21 compares the chemical heat release rate between experimental data and model results obtained using optimized parameters for the selected 2-tier and 3-tier Plastic Pallet commodity tests. Table 21 summarizes the optimized zone model parameters for those selected tests.

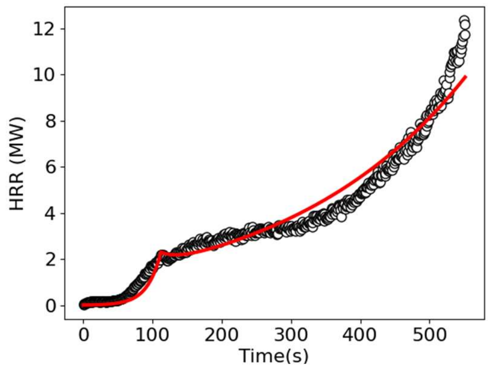

(a) 2 tiers, 6.1 mm/min

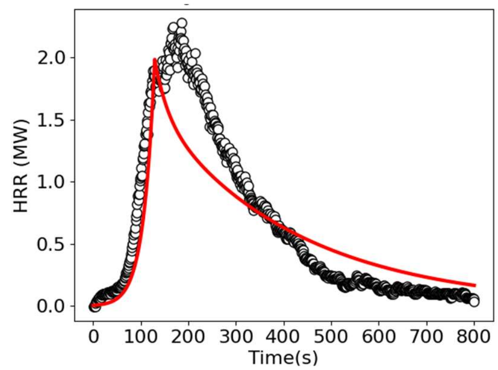

(b) 2 tiers, 10.2 mm/min

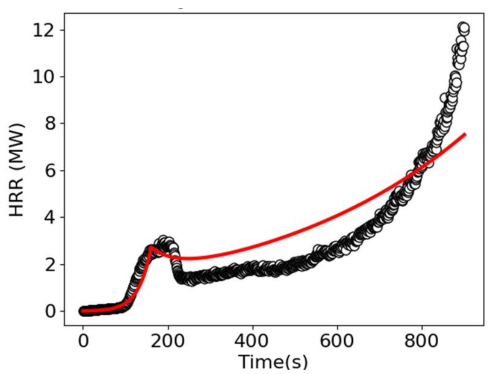

(c) 3 tiers, 12.2 mm/min,

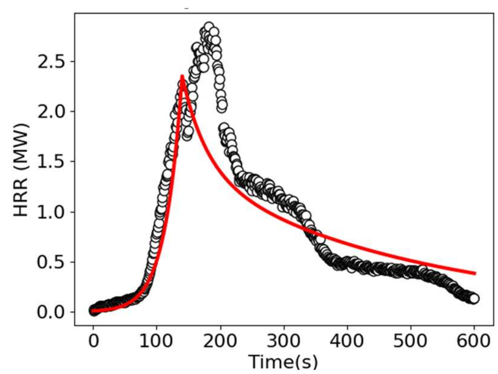

(d) 3 tiers, 14.3 mm/min,

Figure 21 Comparison of chemical HRR between experimental measurements and modeled results for plastic pallet commodity, using the original zone-based model with a single-level optimization framework.

Table 21 Optimized zone model parameters for plastic pallet commodity, using the original zone-based model with a single-level optimization framework.

Number of Tiers	**WA rate (mm/min)**	**WA Time (s)**	**HRR at WA (MW)**	p_1 **(s)**	t_{shift} **(s)**	p_5 **(kg/m²)**	**β**
2	6.1	112	3	26.31	0.61	0.35	0.13
2	10.2	129	2.6	22.51	0.76	0.30	0.2
3	12.2	188	3.6	38.95	0.84	0.52	0.12
3	14.3	140	3.1	34.75	0.14	0.46	0.11

7.2.5 Parameters Optimized from Experimental data of Cartoned Meat Tray (CMT) Commodity

Fig. 22 compares the chemical heat release rate between experimental data and modeled results obtained using optimized parameters for the selected 2-tier and 3-tier CMT commodity. Table 22 summarizes the optimized zone model parameters for those selected tests.

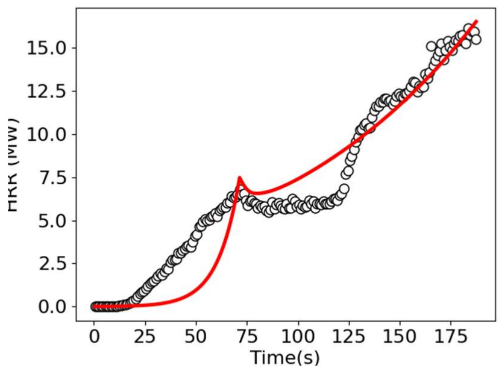

(a) 2 tiers, 4.1 mm/min

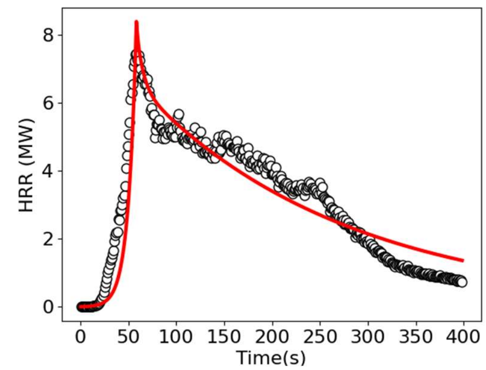

(b) 2 tiers, 6.1 mm/min

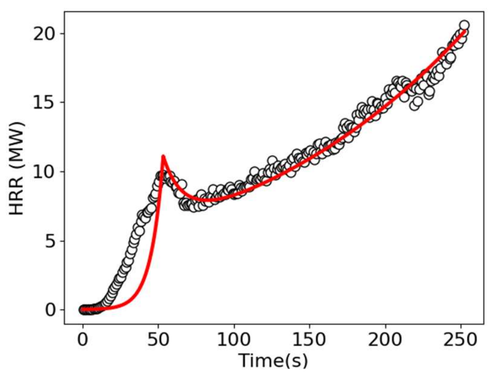

(c) 3 tiers, 12.2 mm/min, Case 3

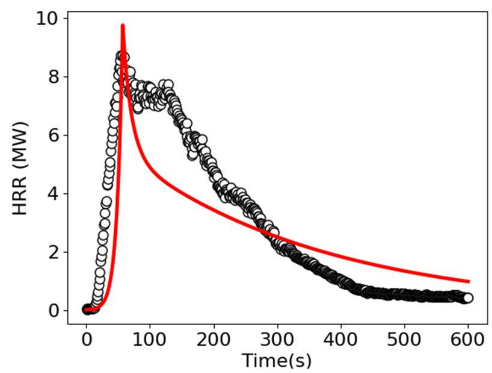

(d) 3 tiers, 14.2 mm/min, Case 3

Figure 22 Comparison of chemical HRR between experimental measurements and modeled results for cartoned meat tray commodity, using the original zone-based model with a single-level optimization framework.

Table 22 Optimized zone model parameters for cartoned meat tray commodity, using the original zone-based model with a single-level optimization framework.

Number of Tiers	WA rate (mm/min)	WA Time (s)	HRR at WA (MW)	p_1 (s)	t_{shift} (s)	p_5 (kg/m^2)	β
2	4.1	71	9.3	11.35	1.06	0.15	0.34
2	6.1	58	10.2	9.00	0.61	0.12	0.23
3	12.2	53	13.4	9.67	0.95	0.13	0.12
3	14.2	57	11.9	10.66	0.06	0.14	0.11

7.2.6 Critical Delivered Fluxes for Different Types of Commodities

The same methodology described in Section 6.1 is applied to estimate the CDF for 5-tier storage across all commodities, using parameters derived from lower-tier tests. To estimate the CDF, linear interpolation is performed to determine the β value at NCDF = 1, based on the relationship between the water evaporation ratio and NCDF for two cases: one controlled and one uncontrolled with the smallest difference in water flux, as shown in Fig. 23.

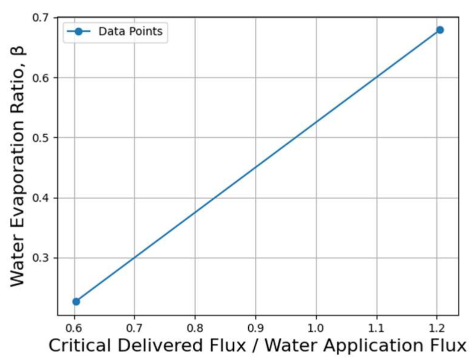

(a) Class 2 commodity, 3 tier

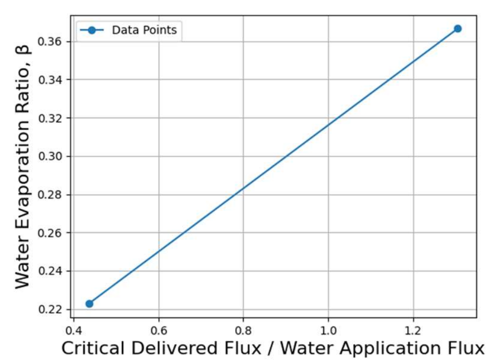

(b) Class 3 commodity, 2 tier

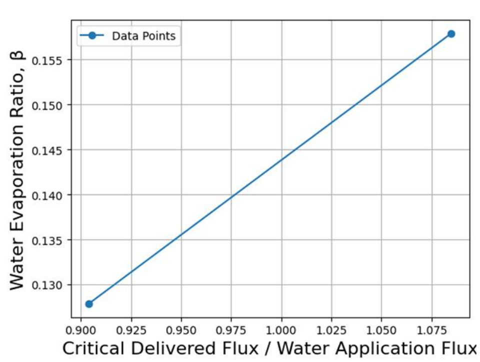

(c) Class 3 commodity, 3 tier

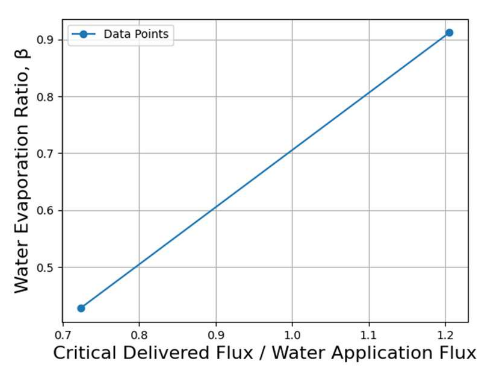

(d) Standard plastic commodity, 2 tier

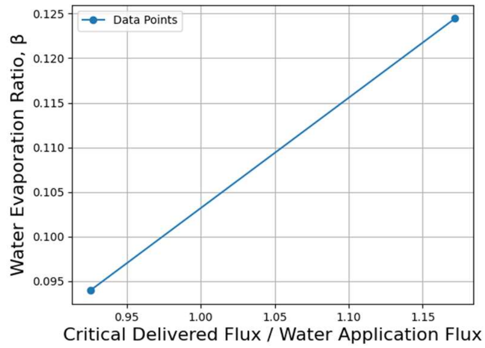

(e) Standard plastic commodity, 3 tier

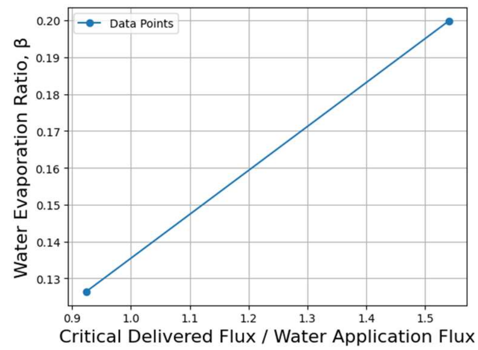

(f) Plastic Pallet commodity, 2 tier

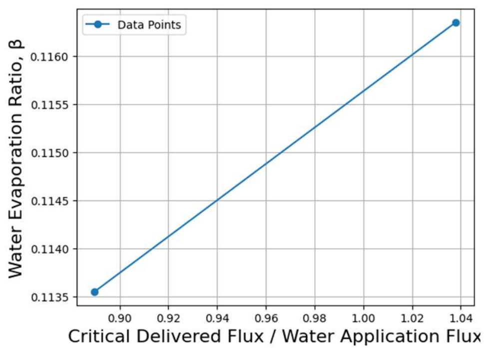

(g) Plastic Pallet commodity, 3 tier

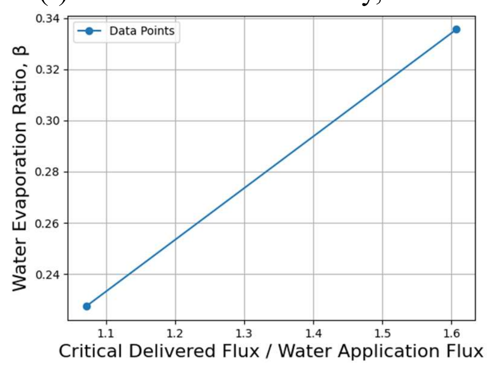

(h) CMT commodity, 2 tier

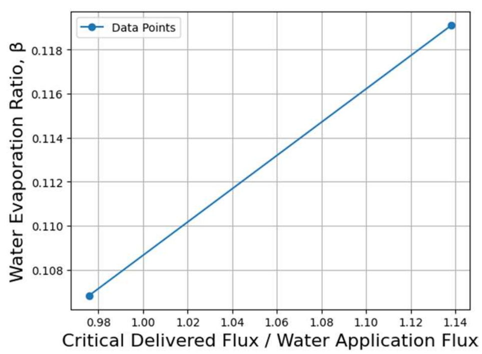

(i) CMT commodity, 3 tier

Figure 23 Correlation between water evaporation ratio and normalized critical delivered flux across different commodities, based on the original zone-based model and the single-level optimization framework (using only two lower-tier tests.

Table 23 summarizes the estimated CDF values for 5-tier storage using the zone model, compared against the CDF values calculated in Xin [12]. Estimations derived from 3-tier storage test data yielded more accurate results than those based on 2-tier data. The overall deviation between model-predicted CDF values using 3-tier data and calculations in Xin [12] remained below 30% for all commodities except plastic pallets — a level of accuracy considered acceptable for industrial fire protection applications. While as few as two 3-tier storage cases proved sufficient to predict 5-tier CDF, the resulting accuracy varied by commodity and was generally lower than the approach in Section 8.1.5, which utilized all available lower-tier data for parameter optimization. For standard plastic and cartoned meat tray commodities, predictions based on 3-tier data already approached the ~30% acceptable threshold, leaving little margin for reliability. Furthermore, the reduced dataset increases sensitivity to parameter estimation and limits the model's capacity to capture test-to-test variability. Together, these limitations underscore the need for continued refinement of the optimization framework to improve robustness and consistency. The larger deviation observed for plastic pallets is attributed primarily to fundamental differences in fire dynamics between cartoned and non-cartoned commodities, as discussed in Section 9.

Table 23 Predicted CDF values for 5-tier storage rack commodities using the zone-based model with parameters calibrated via single-level optimization from two lower-tier tests.

Commodity	Number of Tiers	Predicted value using the model (mm/min)	Calculated value from Yibing (mm/min)
Class 2	3	8.08 (1.47%)	8.2
Class 3	2	10.33 (48.58%)	20.09
	3	16.31 (18.81%)	
Standard Plastics	2	14.23 (40.15%)	
	3	16.73 (29.65%)	23.78
Plastic Pallets	2	17.02 (60.46%)	
	3	18.73 (56.49%)	43.05
Cartoned MT	2	12.9 (52.32%)	
	3	19.80 (26.82%)	27.06

8. Two-level Hierarchical Optimization

The results in Section 7 revealed significant inter-test variability in certain model parameters, motivating a more structured optimization approach. This section introduces a two-level hierarchical optimization framework that separates commodity-specific parameters from test-specific parameters to improve prediction consistency.

8.1 Rationale and Description of the Two-level Hierarchical Optimization

Figure 24 shows the mean values and variability of the four optimized model parameters (p_1, t_{shift}, p_5, and β) across five representative commodity types, calibrated using all available experimental tests for each commodity. The error bars represent the standard error of the mean of the optimized parameter values across tests for the same commodity, providing a measure of the uncertainty in the estimated mean. The coefficient of variation (COV), computed as the ratio of the standard deviation to the mean of the parameter values across tests and expressed as a percentage, is labelled above each bar to provide a scale-independent measure of relative variability. Parameters like p_1 (ignition delay) and p_5 (suppression delay × evaporation flux) exhibit small inter-test variation, as reflected by their small error bars and relatively small COVs, indicating they are predominantly governed by the properties of the commodity material rather than by test-to-test variability. This interpretation is consistent with the discussion of p_5 in Section 3.2. In contrast, t_{shift} and β (water evaporation ratio) show greater variation, as reflected by larger error bar and relatively large COVs, suggesting these parameters are more test-specific.

Examining the mean parameter values across commodity types reveals further physically meaningful trends. The plastic pallet commodity stands out with the highest average p_1 and p_5 values, consistent with its longer ignition delay and elevated suppression resistance, both attributable to its distinct material composition. Class 2 commodities exhibit the highest average β, reflecting a greater water evaporation demand for suppression. In contrast, Class 3 and standard plastic commodities show comparatively lower average values across most parameters, suggesting more moderate fire dynamics. These cross-commodity differences in mean parameter values, combined with the inter-test variability patterns identified in Fig. 24, motivate the need for a structured optimization approach that separates parameters by their physical character.

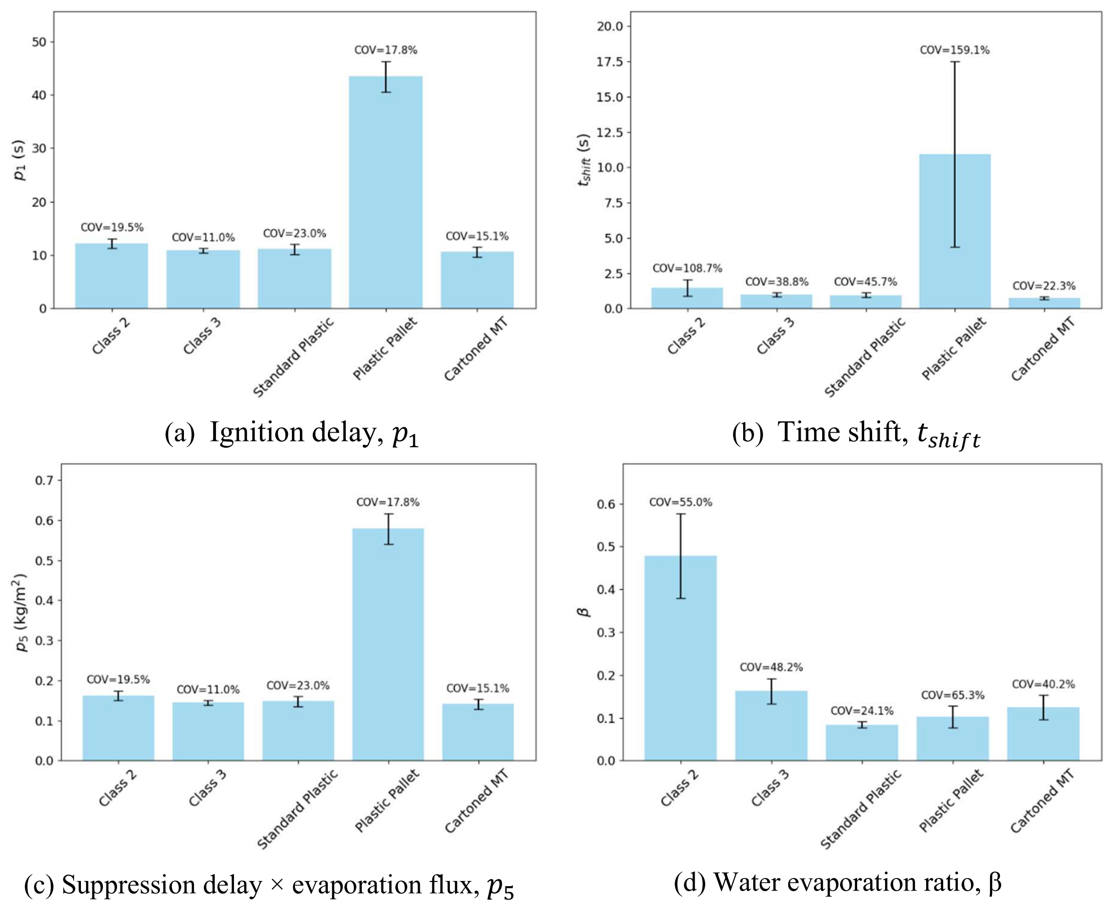

(a) Ignition delay, p_1

(b) Time shift, t_{shift}

(c) Suppression delay × evaporation flux, p_5

(d) Water evaporation ratio, β

Figure 24 Range of optimized model parameters within a single commodity type and across multiple commodity types

In addition, the model, originally developed and validated for Class 2 commodities, has some challenges when it is used for the other class of commodities. In the original model validated for Class 2 commodity, p_4 ($p_4 = \dot{m}_f'' \Delta H_c$) was preset to a fixed value of 0.24 MW/m² estimated from known material properties. However, as shown above, p_4 is a commodity-dependent parameter that directly governs the ignition delay p_1 ($p_1 = \frac{\rho c(T_p - T_a)\delta}{\dot{m}_f'' \alpha_{i,i} \Delta H_c - \dot{m}_f'' \Delta H_p}$) and the heat transfer ratio p_2 ($p_2 = \frac{\alpha_{i-1,i} \dot{m}_f'' \Delta H_c}{\alpha_{i,i} \Delta H_c \dot{m}_f'' - \dot{m}_f'' \Delta H_p}$). Applying a single fixed value of p_4 across all commodity types introduces systematic bias in the estimation of p_1 and p_2, and limits the model's ability to capture the distinct fire behavior of different commodity types. Moreover, A_{ini} represents the initial condition for fire spread in the fuel zones, defined as the area that is burning and generating heat equivalent to that produced by the lighter used to ignite the storage fire. Therefore, it is directly related to the heat output of the lighter and the heat of combustion of the materials involved and is also a commodity-specific parameter.

To make the zone model more robust, a two-level hierarchical optimization has been proposed. A key departure from the original model is the treatment of p_4. Therefore, in the two-level hierarchical optimization framework proposed here, p_4 is classified as a commodity-specific parameter and included in the first-level optimization. This is a key methodological improvement over the original model, enabling the framework to accommodate the diverse material properties of different commodity types and substantially improving predictive performance across the full range of commodities considered in this study. The flow chart of the two-level hierarchical optimization is shown in Fig. 25. In the first level of optimization, the values of p_1, p_5, p_4 and A_{ini} will be optimized for a specific commodity using either 2 tier or 3 tier experimental data as these parameters are commodity specific. Once commodity specific parameters are obtained at the first level optimization, the optimizer will reach at the second level. At the second level of optimization, the values of time shift (t_{shift}) and evaporation ratio (β) will be calculated by minimizing the root mean square error values between experiments and model for each test. Here, the values of time shift and evaporation ratio are test specific parameters.

In this implementation, the fitness equation in both free burn and suppression optimization functions is as per Equation (7), which focuses solely on the RMSE of HRR without the temporal penalty.

$$Fitness = \sqrt{\frac{1}{N}\sum_{i=1}^{N} (HRR_{exp,i} - HRR_{model,i})^2} \quad (7)$$

where the term $HRR_{exp,i}$ is the experimental heat release rate at point i, while $HRR_{model,i}$ refers to the modeled total heat release rate at the same point; N is the number of data points for comparison.

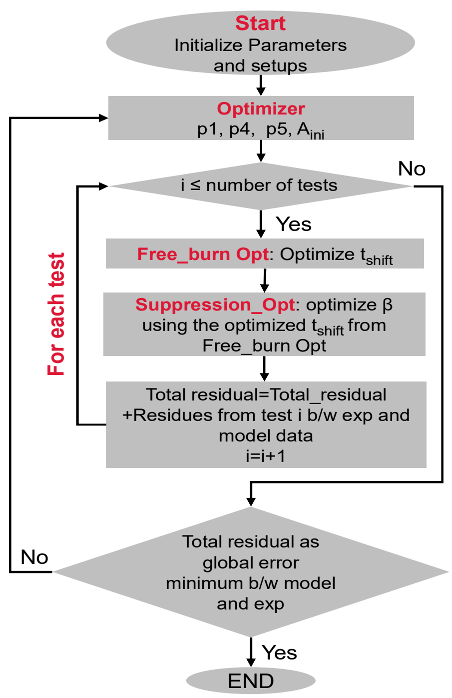

Figure 25 Flow chart of two-level optimization

8.2 Estimation from All Low-tier Experimental Data

8.2.1 Parameters Optimized from Experimental data of Class 2 Commodity

Fig. 26 compares the chemical heat release rate between experimental data and model results for Class 2 commodity based on the optimized parameters. Table 24 summarizes the optimized zone model parameters for Class 2 commodity.

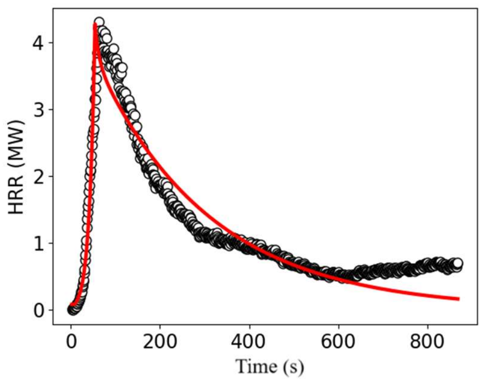

(a) 2 tiers, 4.1mm/min

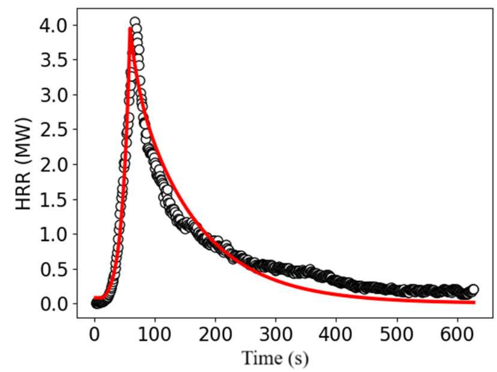

(b) 2 tiers, 8.2 mm/min

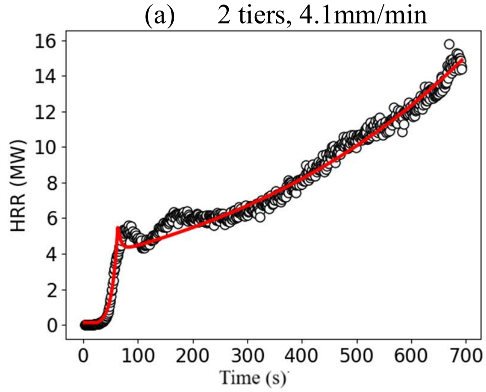

(c) 3 tiers, 4.1mm/min

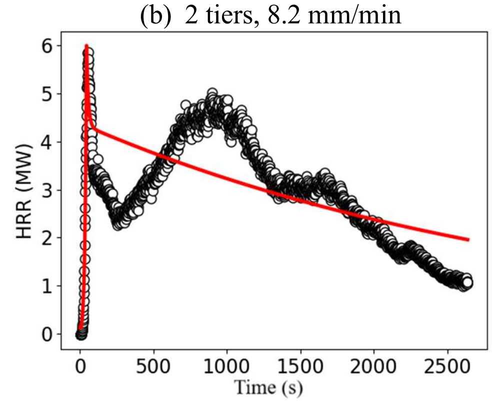

(d) 3 tiers, 6.1mm/min

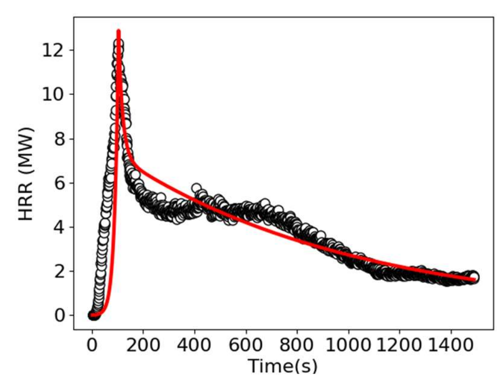

(e) 3 tiers, 8.1mm/min

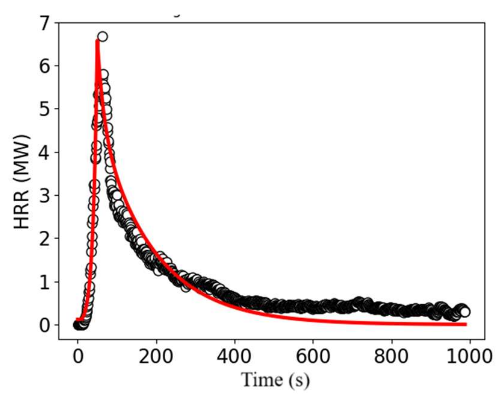

(f) 3 tiers, 12.2 mm/min

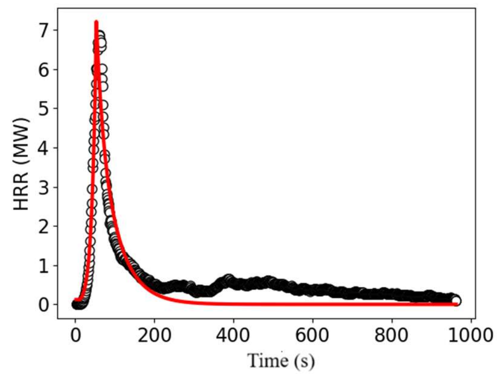

(g) 3 tiers, 18.4 mm/min

Figure 26 Comparison of chemical HRR between experimental measurements and modeled results for Class 2 commodity, using the original zone-based model with the two-level hierarchical optimization framework calibrated on all available lower-tier test data.

Table 24 Optimized zone model parameters for Class 2 commodity, based on the original zone-based model and the two-level hierarchical optimization framework calibrated on all available lower-tier test data.

Test	Number of Tiers	WA rate (mm/min)	WA Time (s)	HRR at WA (MW)	p_1 (s)	p_4 (MW/m^2)	p_5 (kg/m^2)	A_{ini} (m^2)	t_{shift} (s)	β
1	2	4.1	106	5.6	14.56	0.13	0.16	0.32	7.03	0.31
2	2	8.2	102	5.4					12.78	0.14
3	3	4.1	103	7.0					24.00	0.49
4	3	6.1	86	6.0					5.54	0.266
5	3	8.1	135	12.0					5.23	0.27
6	3	12.2	95	8.8					11.33	0.11
7	3	18.4	93	9.2					11.11	0.08

8.2.2 Parameters Optimized from Experimental data of Class 3 Commodity

Fig. 27 shows a comparison of the chemical heat release rate between experimental data and model results for Class 3 commodity, based on the optimized parameters. Table 25 summarizes the optimized zone model parameters for Class 3 commodity.

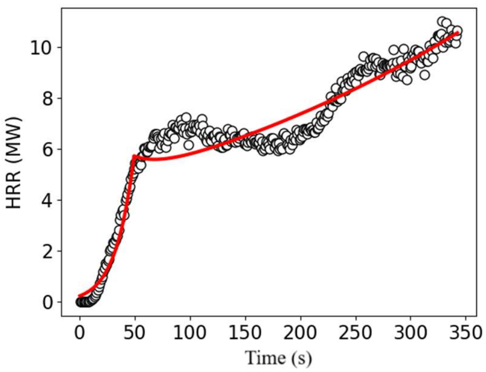

(a) 2 tiers, 4.1 mm/min

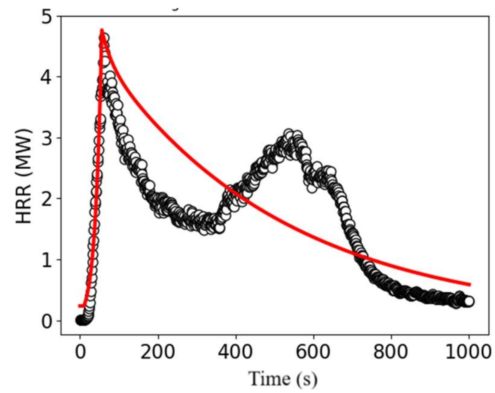

(b) 2 tiers, 6.1 mm/min

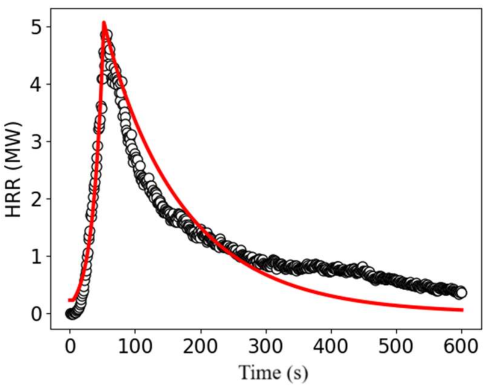

(c) 2 tiers, 12.2 mm/min

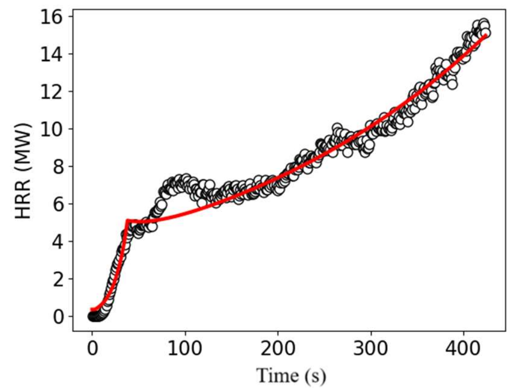

(d) 3 tiers, 6.1 mm/min

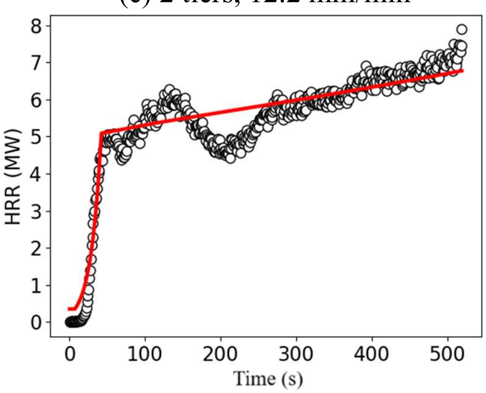

(e) 3 tiers, 10.2 mm/min

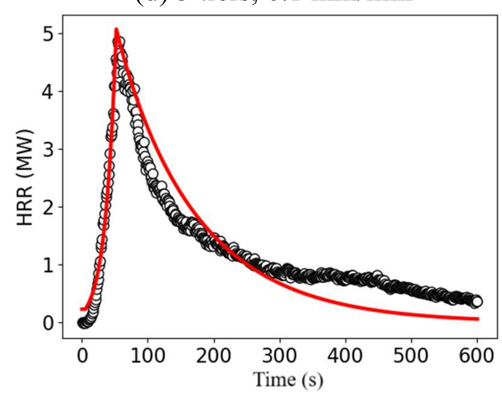

(f) 3 tiers, 12.2 mm/min

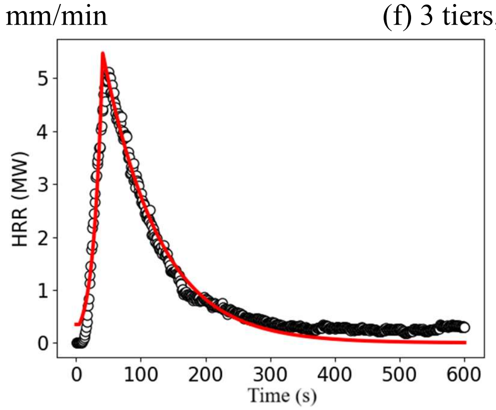

(g) 3 tiers, 18.4 mm/min

Figure 27 Comparison of chemical HRR between experimental measurements and modeled results for Class 3 commodity, using the original zone-based model and the two-level hierarchical optimization framework calibrated on all available lower-tier test data.

Table 25 Optimized zone model parameters for Class 3 commodity, based on the original zone-based model and the two-level hierarchical optimization framework calibrated on all available lower-tier test data.

Test	Number of Tiers	WA rate (mm/min)	WA Time (s)	HRR at WA (MW)	p_1 (s)	p_4 (MW/m^2)	p_5 (kg/m^2)	A_{ini} (m^2)	t_{shift} (s)	β
1	2	4.1	96	7.5	19.75	0.48	0.13	0.24	1.25	0.14
2	2	6.1	60	6.4					11.40	0.10
3	2	12.1	54	6.7					6.37	0.05
4	3	6.1	45	6.7					3.72	0.12
5	3	10.1	58	6.9					8.25	0.06
6	3	12.1	52	7.5					7.27	0.05
7	3	18.2	50	7.0					6.39	0.04

8.2.3 Parameters Optimized from Experimental data of Standard Plastic Commodity

Fig. 28 shows a comparison of the chemical heat release rate between experimental data and model results for standard plastic commodity, based on the optimized parameters. Table 26 summarizes the optimized zone model parameters for standard plastic commodity.

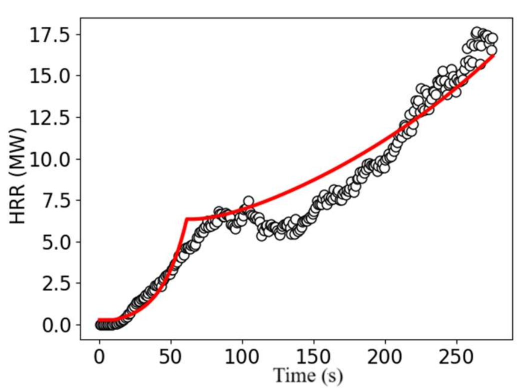

(a) 2 tiers, 4.1 mm/min

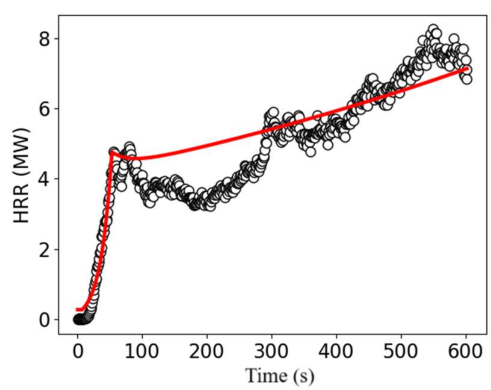

(b) 2 tiers, 6.1 mm/min

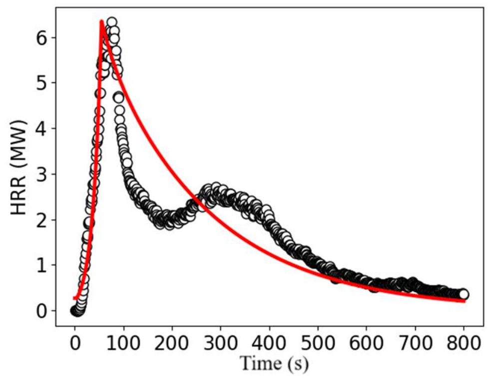

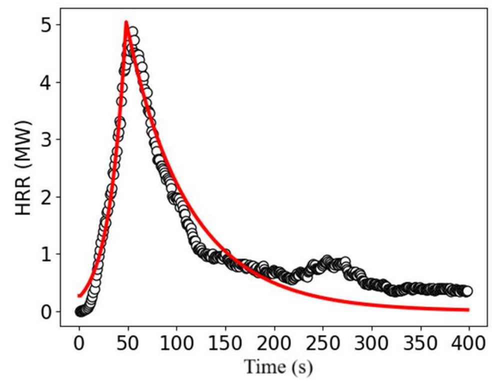

(c) 2 tiers, 10.2 mm/min (d) 2 tiers, 16.3 mm/min

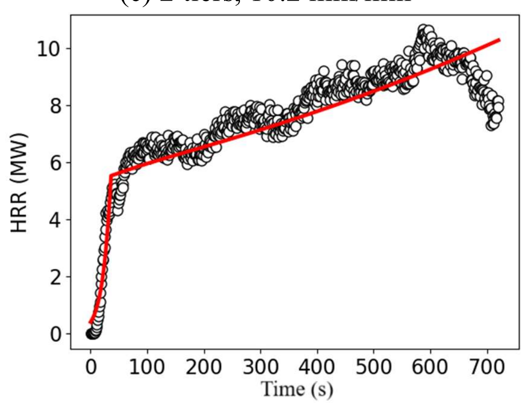

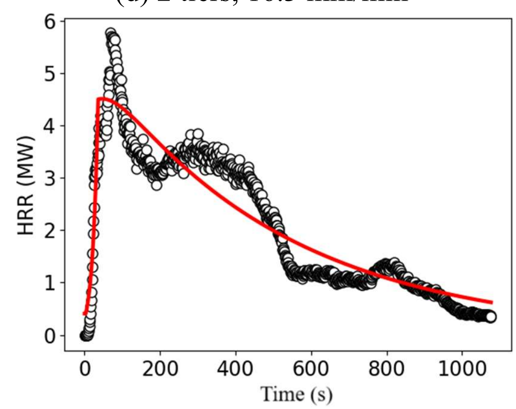

(e) 3 tiers, 12.2 mm/min (f) 3 tiers, 15.5 mm/min

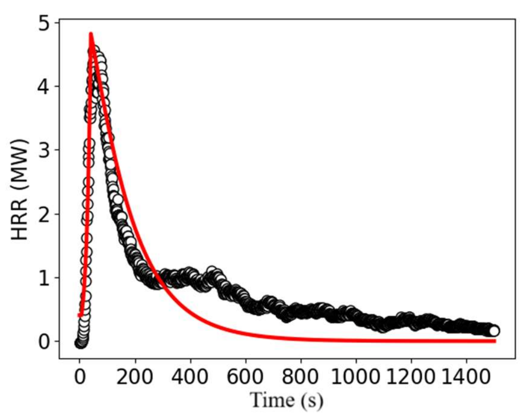

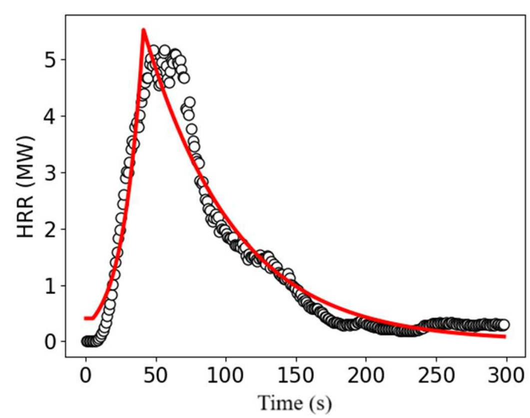

(g) 3 tiers, 18.4 mm/min (h) 3 tiers, 26.5 mm/min

Figure 28 Comparison of chemical HRR between experimental measurements and modeled results for standard plastic commodity, using the original zone-based model and the two-level hierarchical optimization framework calibrated on all available lower-tier test data.

Table 26 Optimized zone model parameters for standard plastic commodity, based on the original zone-based model and the two-level hierarchical optimization framework calibrated on all available lower-tier test data.

Test	Number of Tiers	WA rate (mm/min)	WA Time (s)	HRR at WA (MW)	p_1 (s)	p_4 (MW/m²)	p_5 (kg/m²)	A_{ini} (m²)	t_{shift} (s)	β
1	2	4.1	75	8.5	20.91	0.2	0.17	0.71	10.94	0.17
2	2	6.1	56	6.5					7.73	0.11
3	2	10.1	76	8.7					4.70	0.07
4	2	16.3	54	6.7					2.24	0.05
5	3	12.1	43	7.2					0.01	0.07
6	3	14.2	47	5.9					3.63	0.05
7	3	18.4	51	6.3					7.97	0.05
8	3	26.5	48	7.1					6.14	0.04

8.2.4 Parameters Optimized from Experimental data of Plastic Pallet Commodity

Fig. 29 shows a comparison of the chemical heat release rate between experimental data and model results for plastic pallet commodity, based on the optimized parameters. Table 27 summarizes the optimized zone model parameters for plastic pallet commodity.

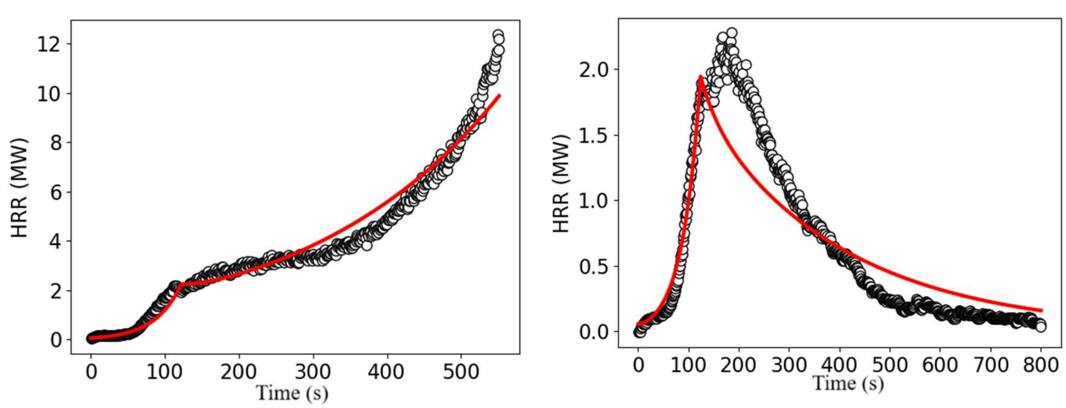

(a) 2 tiers, 6.1 mm/min (b) 2 tiers, 10.2 mm/min

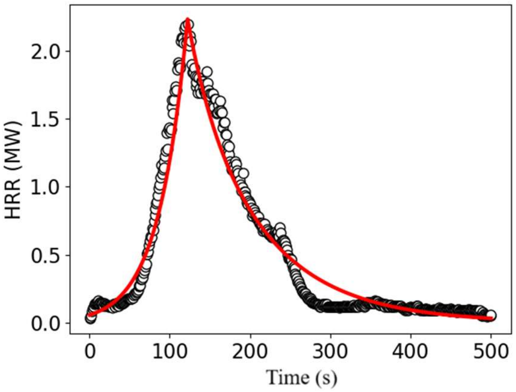

(c) 2 tiers, 16.3 mm/min

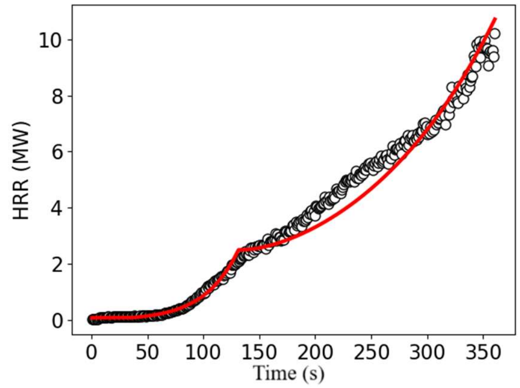

(d) 3 tiers, 6.1 mm/min

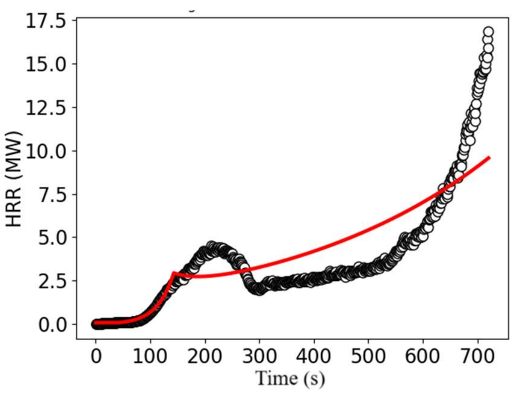

(e) 3 tiers, 10.2 mm/min

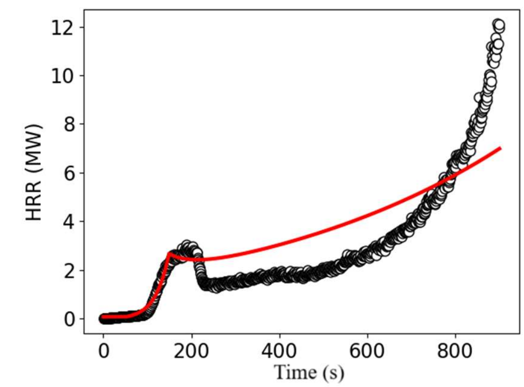

(f) 3 tiers, 12.2 mm/min

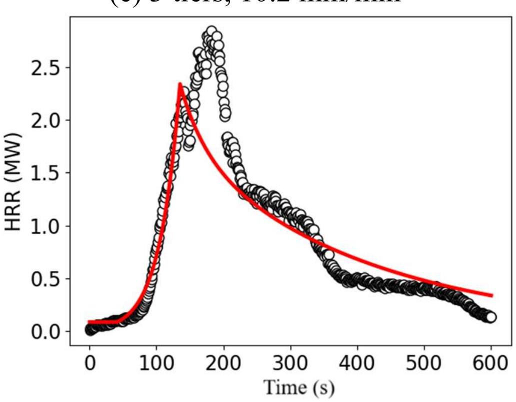

(g) 3 tiers, 14.3 mm/min

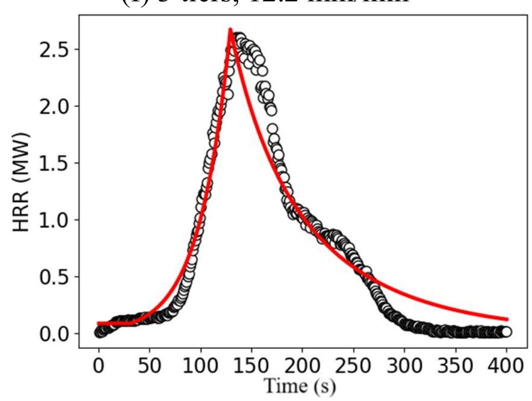

(h) 3 tiers, 24.5 mm/min

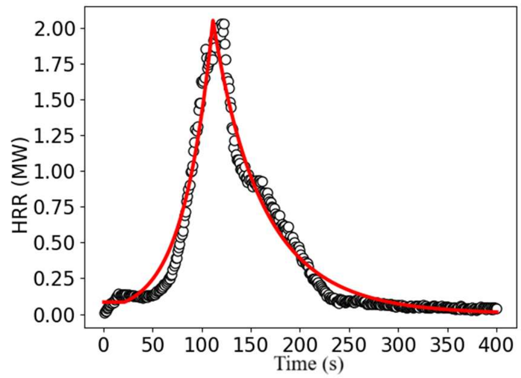

(i) 3 tiers, 40.8 mm/min

Figure 29 Comparison of chemical HRR between experimental measurements and modeled results for plastic pallet commodity, using the original zone-based model and the two-level hierarchical optimization framework calibrated on all available lower-tier test data.

Table 27 Optimized zone model parameters for plastic pallet commodity, based on the original zone-based model and the two-level hierarchical optimization framework calibrated on all available lower-tier test data.

Test	Number of Tiers	WA rate (mm/min)	WA Time (s)	HRR at WA (MW)	p_1 (s)	p_4 (MW/m^2)	p_5 (kg/m^2)	A_{ini} (m^2)	t_{shift} (s)	β
1	2	6.1	112	3	42.83	0.19	0.73	0.15	0.17	0.25
2	2	10.1	129	2.6					7.58	0.18
3	2	16.3	122	3					0.41	0.13
4	3	6.1	144	3.3					36.26	0.36
5	3	10.1	212	4.0					42.58	0.21
6	3	12.2	188	3.6					52.30	0.17
7	3	14.3	140	3.1					42.33	0.17
8	3	24.5	138	3.6					31.96	0.10
9	3	40.8	119	2.8					22.06	0.01

8.2.5 Parameters Optimized from Experimental data of Cartoned Meat Tray (CMT) Commodity

Fig. 30 shows a comparison of the chemical heat release rate between experimental data and model results for CMT commodity, based on the optimized parameters. Table 28 summarizes the optimized zone model parameters for CMT commodity.

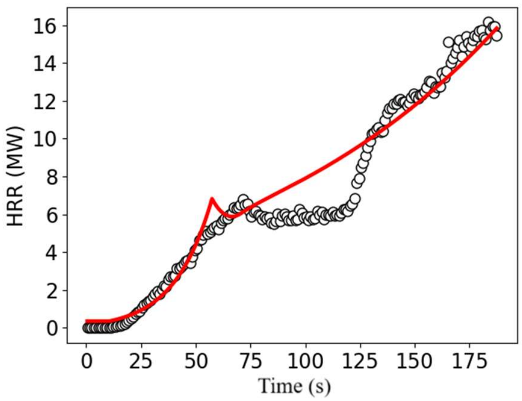

(a) 2 tiers, 4.1 mm/min

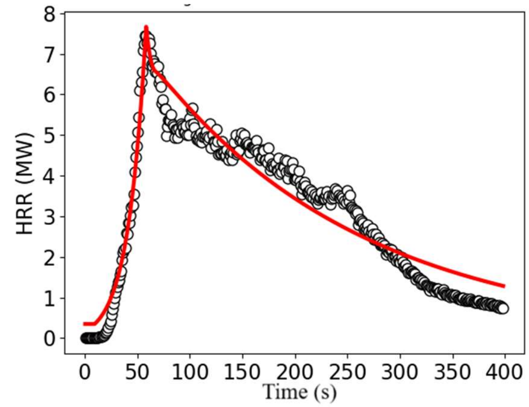

(b) 2 tiers, 6.1 mm/min

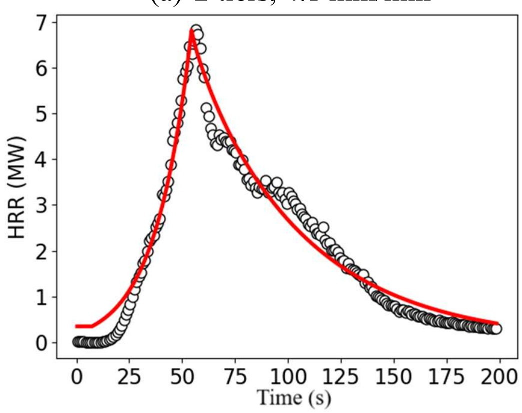

(c) 2 tiers, 10.2 mm/min

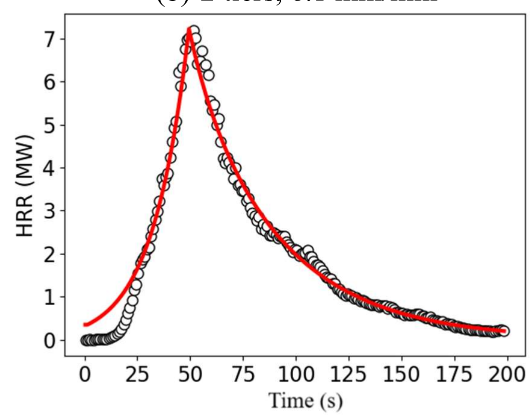

(d) 2 tiers, 16.3 mm/min

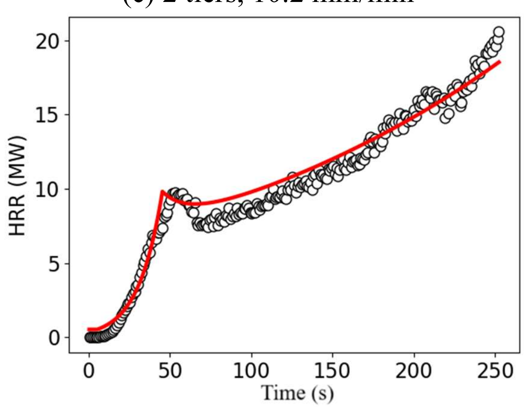

(e) 3 tiers, 12.2 mm/min

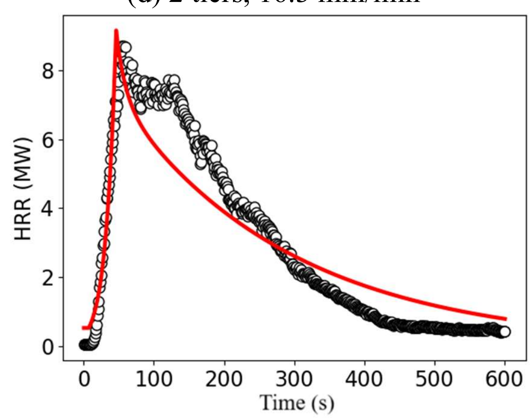

(f) 3 tiers, 14.3 mm/min

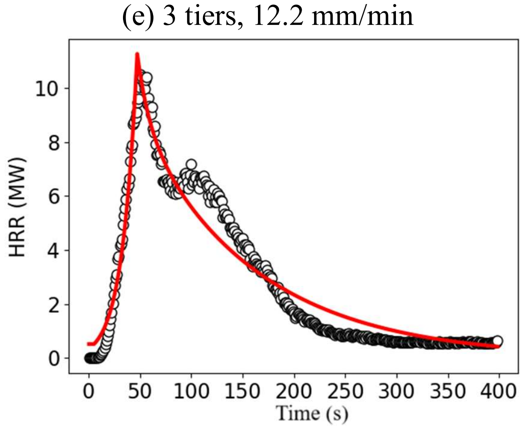

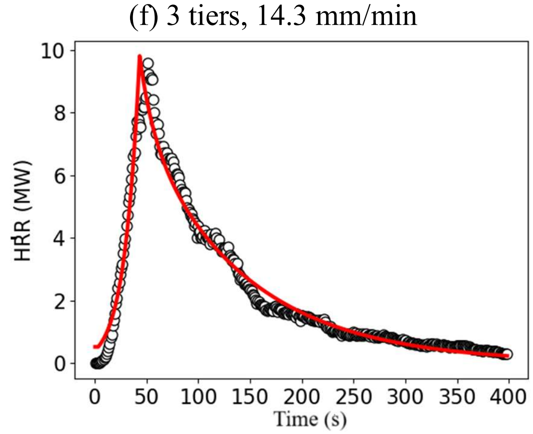

(g) 3 tiers, 15.5 mm/min (h) 3 tiers, 18.4 mm/min

Figure 30 Comparison of chemical HRR between experimental measurements and modeled results for cartoned meat tray commodity, using the original zone-based model and the two-level hierarchical optimization framework calibrated on all available lower-tier test data.

Table 28 Optimized zone model parameters for cartoned meat tray commodity based on the original zone-based model and the two-level hierarchical optimization framework calibrated on all available lower-tier test data.

Test	**Number of Tiers**	**WA rate (mm/min)**	**WA Time (s)**	**HRR at WA (MW)**	p_1 (s)	p_4 (MW/m^2)	p_5 (kg/m^2)	A_{ini} (m^2)	t_{shift} (s)	**β**
1	2	4.1	71	9.3	20.46	0.52	0.56	0.33	11.06	0.99
2	2	6.1	58	10.2					9.89	0.66
3	2	10.1	56	9.3					8.19	0.40
4	2	16.3	51	9.8					1.63	0.23
5	3	12.2	53	13.4					5.92	0.33
6	3	14.2	57	11.9					7.91	0.31
7	3	15.5	50	14.4					5.71	0.29
8	3	18.4	51	13.1					4.48	0.23

8.2.6 Critical Delivered Fluxes for Different Types of Commodities

Fig. 31 shows the correlation between the water evaporation ratio and the NCDF. Across all tests, the evaporation ratio consistently increases with NCDF. However, the trends observed for 3-tier storage configurations differ noticeably from those for 2-tier storages, indicating potential variations in fire suppression dynamics between these configurations, which is consistent with the conclusion in Section 7.1.

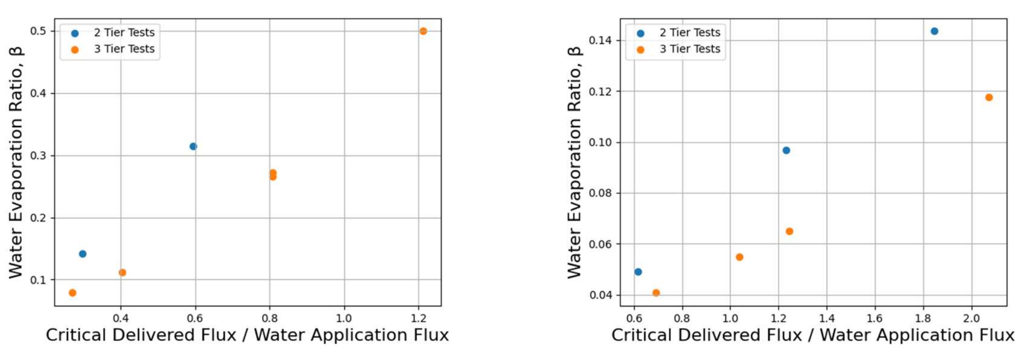

(a) Class 2 commodity (b) Class 3 commodity

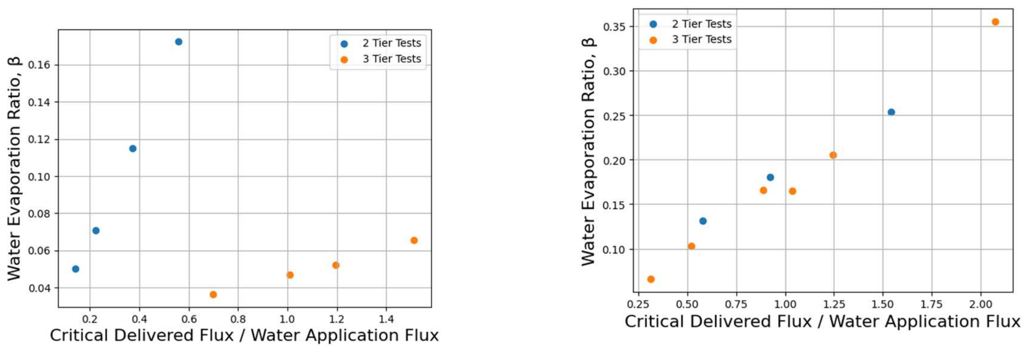

(c) Standard plastic commodity (d) Plastic pallet commodity

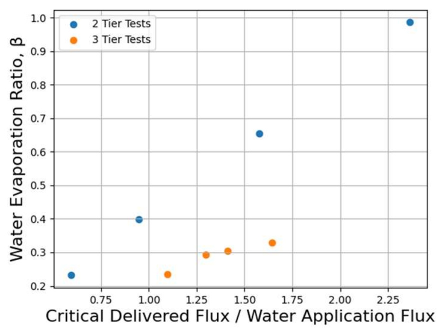

(e) Cartoned MT commodity

Figure 31 Correlation between water evaporation ratio and normalized critical delivered flux across commodity types, based on the original zone-based model and the two-level hierarchical optimization framework calibrated using all available lower-tier test data per commodity type.

The same methodology described in Section 6.1 is applied to estimate the CDF for 5-tier storage across all commodities, using parameters derived from lower-tier tests. To estimate the CDF, linear interpolation is performed to determine the β value at NCDF = 1, based on the relationship between the water evaporation ratio and NCDF, as shown in Fig. 31. Table 29 provides a summary of the estimated CDF for 5-tier storage using the new implementation of the zone model. The results are compared to the calculated CDF values based on test data. The comparison shows that estimations based on the 3-tier storage test data produced more accurate results, compared to those results based on the 2-tier storage test data. For Class 2, standard plastic, and CMT commodities, the model-predicted CDF using 3-tier data was within 10% of the CDF calculated in Xin [12]. However, for Class 3, the model's performance is less reliable. Nevertheless, the deviation from values in Xin [12] remains within 30%, which is generally acceptable for industrial fire protection applications. In the case of Plastic Pallets, the deviation exceeds 30%, primarily due to the same factors later discussed in Section 9.

Table 29 Predicted CDF values for 5-tier storage rack commodities based on the original zone-based model and the two-level hierarchical optimization framework calibrated using all available lower-tier test data per commodity type.

Commodity	**Number of Tiers**	**Predicted value using the model (mm/min)**	**Calculated value from Yibing (mm/min)**
Class 2	2	7.1 (13.41%)	8.2
	3	7.96 (2.92%)	
Class 3	2	12.41 (38.22%)	20.09
	3	16.41 (18.32%)	
Standard Plastics	2	9.58 (59.71%)	23.78
	3	22.95 (3.49%)	
Plastic Pallets	2	17.80 (58.65%)	43.05
	3	18.53 (56.96%)	
Cartoned MT	2	18.57 (31.37%)	27.06
	3	25.36 (6.28 %)	

8.3 Estimations from Two low-tier Experimental Data

In the last section, the CDF of the 5-tier configuration was calculated using parameters optimized from all the lower-tier data. However, in practice, the objective is to minimize the number of tests required while still achieving reliable results. Therefore, in this section, we refine our approach by selecting data from two 2-tier cases or two 3-tier cases—each consisting of one controlled and one uncontrolled scenario with the smallest possible difference in water flux. These limited datasets are used to optimize the parameters, and the resulting CDF is calculated. The same process was repeated for the 2-tier and 3-tier cases, using the same uncontrolled case while varying the controlled case to introduce a relatively larger difference in water flux, in order to examine its impact on the CDF. In the following subsections, odd-numbered cases represent scenarios with the smallest water flux difference for each storage configuration, while even-numbered cases correspond to scenarios with a relatively larger flux difference.

8.3.1 Parameters Optimized from Experimental data of Class 2 Commodity

Fig. 32 shows a comparison of the chemical heat release rate between experimental data and model results obtained using optimized parameters for Class 2 commodity in the 3-tier configuration. Table 30 summarizes the optimized zone model parameters for Class 2 commodity

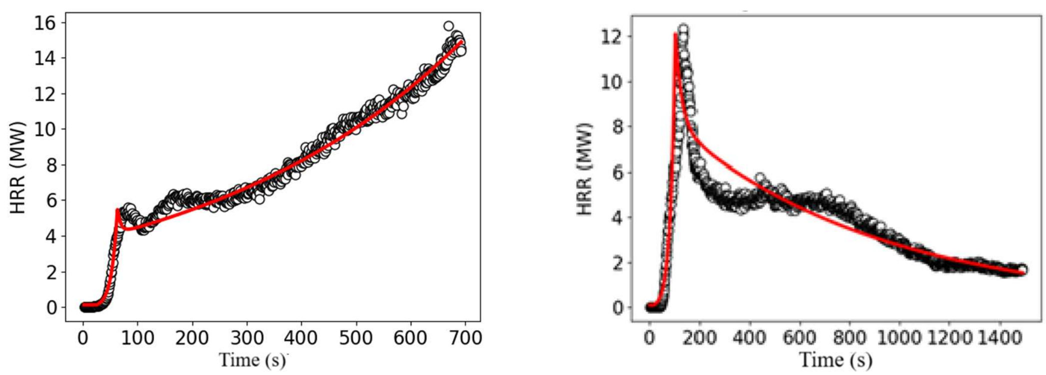

(a) 3 tiers, 4.1 mm/min, Case 1 (b) 3 tiers, 8.1mm/min, Case 1

Figure 32 Comparison of chemical HRR between experimental measurements and modeled results for Class 2 commodity, based on the original zone-based model and the two-level hierarchical optimization framework calibrated using two lower-tier tests.

Table 30 Optimized zone model parameters for Class 2 commodity based on the original zone-based model and the two-level hierarchical optimization framework calibrated using two lower-tier tests.

Case	Number of Tiers	WA rate (mm/min)	WA Time (s)	HRR at WA (MW)	p_1 (s)	p_4 (MW/m^2)	p_5 (kg/m^2)	A_{ini} (m^2)	t_{shift} (s)	β
1	3	4.1	103	7.0	31.93	0.10	0.36	0.55	30.08	0.48
1	3	8.1	135	12					19.48	0.18

8.3.2 Parameters Optimized from Experimental data of Class 3 Commodity

Fig. 33 compares the chemical heat release rate between experimental data and model results obtained using optimized parameters for Class 3 commodity in the 2-tier and 3-tier configurations. Table 31 summarizes the optimized zone model parameters for Class 3 commodity.

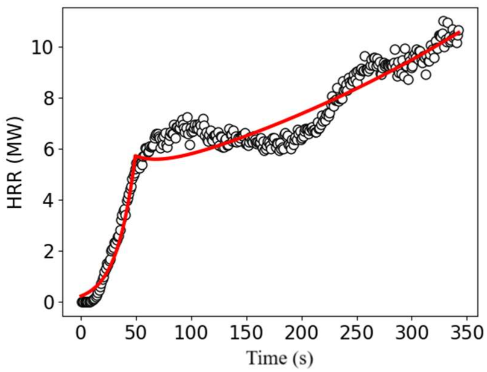

(a) 2 tiers, 4.1 mm/min, Case 1

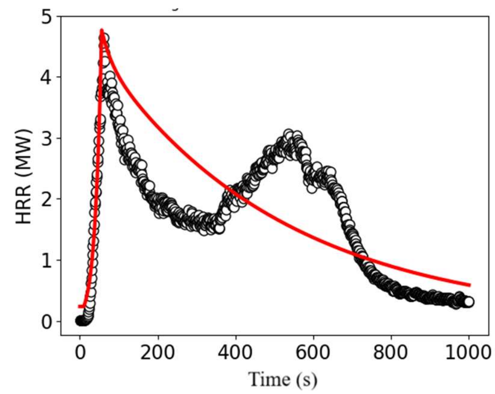

(b) 2 tiers, 6.1 mm/min, Case 1

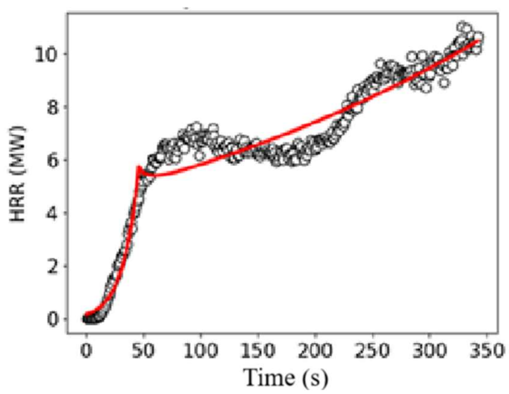

(c) 2 tiers, 4.1 mm/min, Case 2

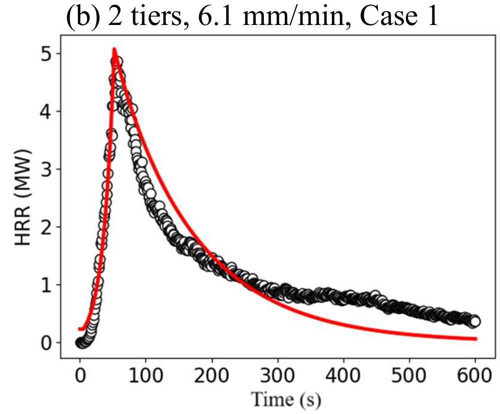

(d) 2 tiers, 12.1 mm/min, Case 2

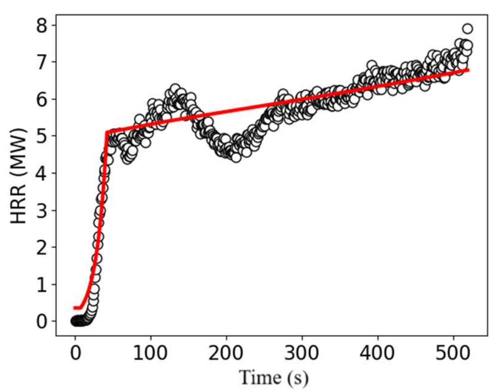

(e) 3 tiers, 10.1 mm/min, Case 3

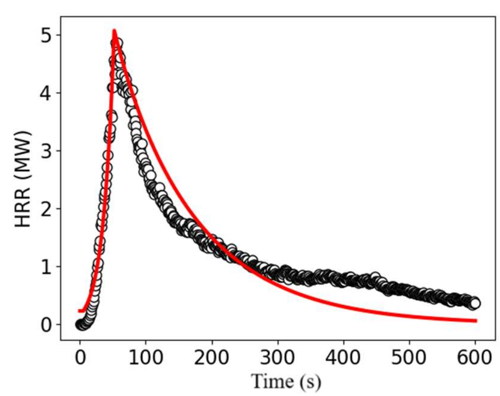

(f) 3 tiers, 12.1 mm/min, Case 3

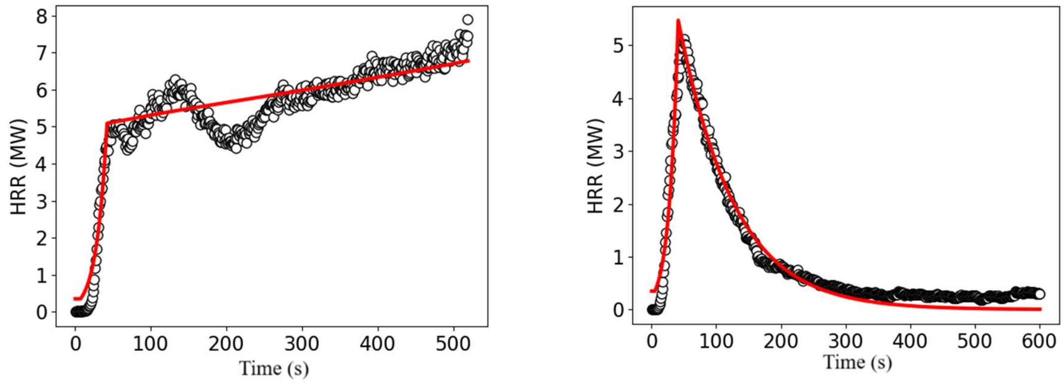

(g) 3 tiers, 10.1 mm/min, Case 4 (h) 3 tiers, 18.2 mm/min, Case 4

Figure 33 Comparison of chemical HRR between experimental measurements and modeled results for Class 3 commodity, based on the original zone-based model and the two-level hierarchical optimization framework calibrated using two lower-tier tests.

Table 31 Optimized zone model parameters for Class 3 commodity based on the original zone-based model and the two-level hierarchical optimization framework calibrated using two lower-tier tests.

Case	Number of Tiers	WA rate (mm/min)	WA Time (s)	HRR at WA (MW)	p_1 (s)	p_4 (MW/m²)	p_5 (kg/m²)	A_{ini} (m²)	t_{shift} (s)	β
1	2	4.1	96	7.5	16.73	0.76	0.17	0.11	0.84	0.25
1	2	6.1	60	6.4					11.49	0.16
2	2	4.1	96	7.5	16.46	0.44	0.24	0.19	1.15	0.40
2	2	12.1	54	6.7					6.69	0.11
3	3	10.1	58	6.9	16.78	0.1	0.1	0.76	6.77	0.06
3	3	12.1	52	7.5					5.07	0.05
4	3	10.1	58	6.9	19.52	0.56	0.14	0.14	3.49	0.07
4	3	18.2	50	7.0					0.97	0.04

As shown in Table 31, although the commodity-specific parameters are intended to remain consistent across all tests for a given commodity, their optimized values differ between the two-tier and three-tier calibrations. For example, p_1 takes values of 16.73, 16.46, 16.78, and 19.52 across the four cases in the two-tier calibration, illustrating how the optimizer adjusts these shared parameters to best fit each dataset. This variation stems from several interrelated factors. The zone-based model operates at reduced physical fidelity and does not explicitly resolve all processes governing fire growth, suppression, and heat transfer. Consequently, the commodity-specific parameters function as effective or lumped representations of complex physical phenomena rather than direct physical quantities. When combined with the limited number of available lower-tier cases, this characteristic makes the optimization process susceptible to overfitting, as the parameters adjust not only to capture genuine physical trends but also to compensate for model deficiencies based on a small dataset, amplifying sensitivity to the specific cases used. Experimental uncertainties arising from measurement errors and variability in material properties further compound this sensitivity, contributing to the observed differences in calibrated values of the commodity-specific parameters across analyses. It should be noted that this behavior is not unique to any single commodity type, but is consistently observed across all commodities examined in this study.

8.3.3 Parameters Optimized from Fire Tests on Standard Plastic Commodity

Fig. 34 shows a comparison of the chemical heat release rate between experimental data and model results obtained using optimized parameters for Standard Plastic commodity in the 2-tier and 3-tier configuration. Table 32 summarizes the optimized zone model parameters for Standard Plastic commodity.

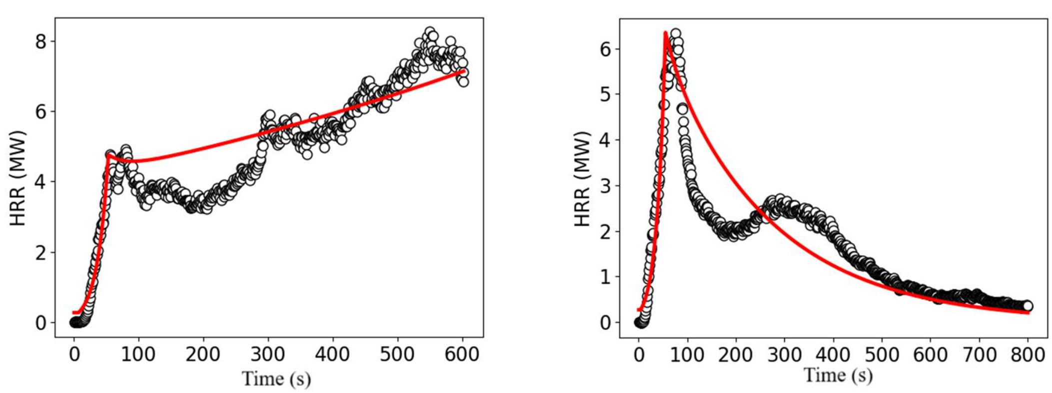

(a) 2 tiers, 6.1 mm/min, Case 1 (b) 2 tiers, 10.2 mm/min, Case 1

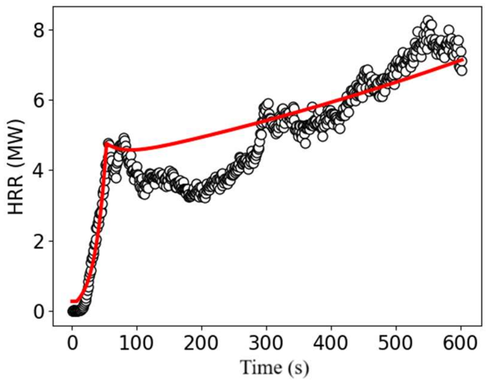

(c) 2 tiers, 6.1 mm/min, Case 2

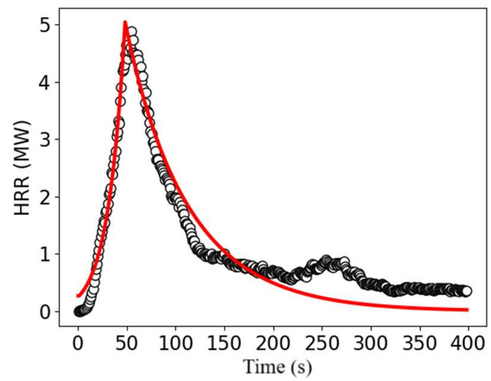

(d) 2 tiers, 16.3 mm/min, Case 2

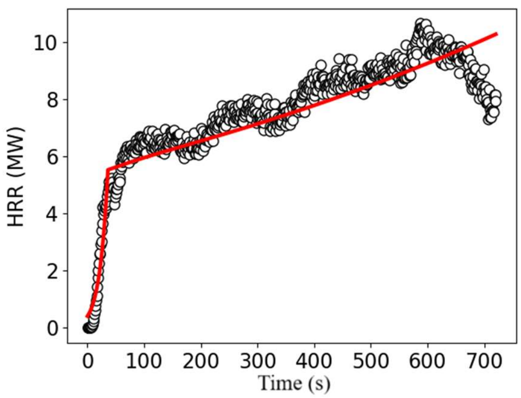

(e) 3 tiers, 12.1 mm/min, Case 3

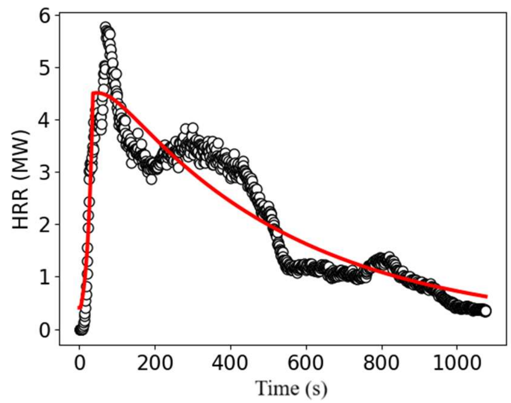

(f) 3 tiers, 14.2 mm/min, Case 3

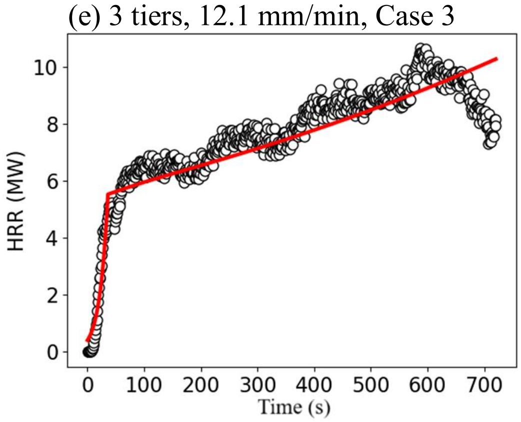

(g) 3 tiers, 12.1 mm/min, Case 4

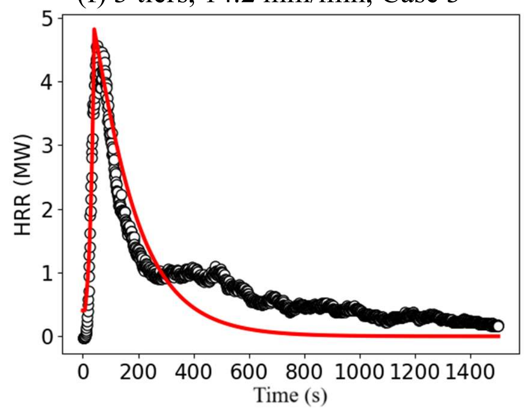

(h) 3 tiers, 18.4 mm/min, Case 4

Figure 34 Comparison of chemical HRR between experimental measurements and modeled results for standard plastic commodity, based on the original zone-based model and the two-level hierarchical optimization framework calibrated using two lower-tier tests.

Table 32 Optimized zone model parameters for standard plastic commodity based on the original zone-based model and the two-level hierarchical optimization framework calibrated using two lower-tier tests.

Case	Number of Tiers	WA rate (mm/min)	WA Time (s)	HRR at WA (MW)	p_1 (s)	p_4 (MW/m^2)	p_5 (kg/m^2)	A_{ini} (m^2)	t_{shift} (s)	β
1	2	6.1	56	6.5	8.39	0.02	0.32	0.30	1.50	0.99
1	2	10.2	76	8.7					0.62	0.46
2	2	6.1	56	6.5	11.04	0.39	0.41	0.05	2.47	0.98
2	2	16.3	54	6.7					1.35	0.27
3	3	12.1	43	7.2	27.02	0.37	0.18	0.55	0.18	0.05
3	3	14.2	47	5.9					5.86	0.04
4	3	12.1	43	7.2	24.49	0.20	0.16	0.86	0.15	0.05
4	3	18.4	51	6.3					8.06	0.04

8.3.4 Parameters Optimized from Experimental data of Plastic Pallet Commodity

Fig. 35 shows a comparison of the chemical heat release rate between experimental data and model results obtained using optimized parameters for Plastic Pallet commodity in the 2-tier and 3-tier configuration. Table 33 summarizes the optimized zone model parameters for Plastic Pallet commodity.

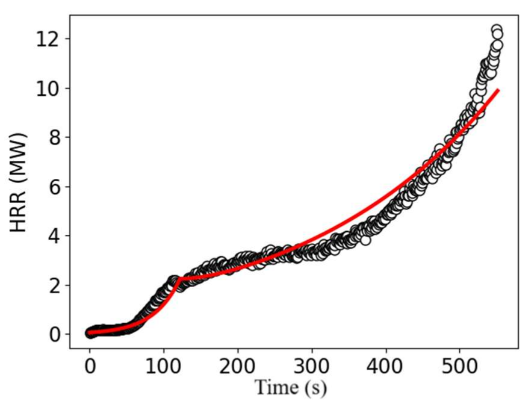

(a) 2 tiers, 6.1 mm/min, Case 1

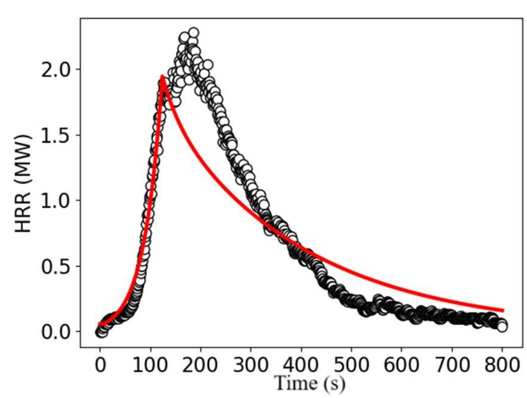

(b) 2 tiers, 10.2 mm/min, Case 1

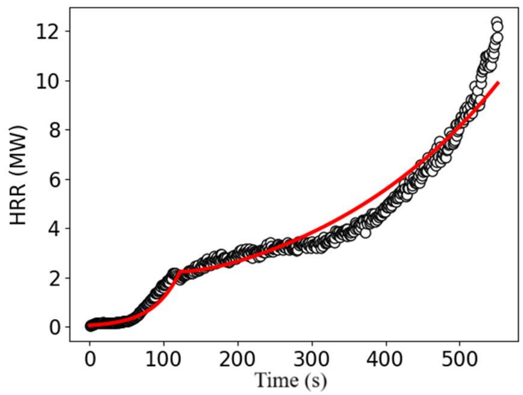

(c) 2 tiers, 6.1 mm/min, Case 2

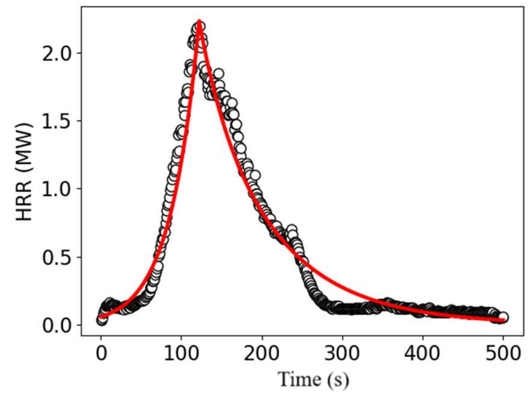

(d) 2 tiers, 16.3 mm/min, Case 2

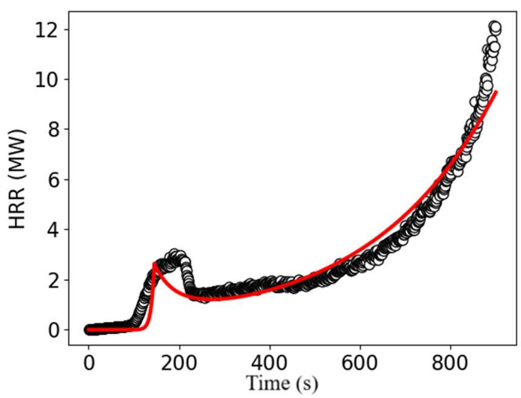

(e) 3 tiers, 12.2 mm/min, Case 3

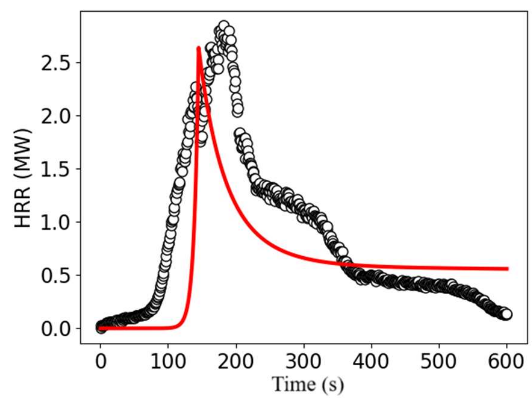

(f) 3 tiers, 14.3 mm/min, Case 3

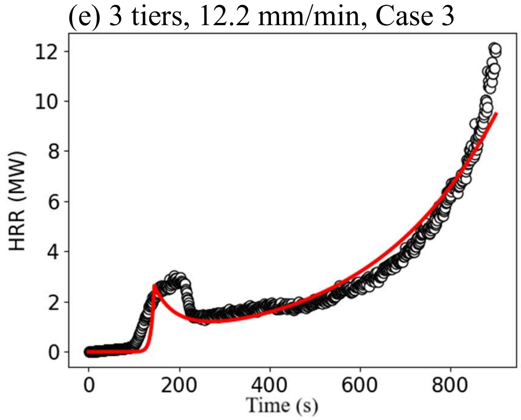

(g) 3 tiers, 12.2 mm/min, Case 4

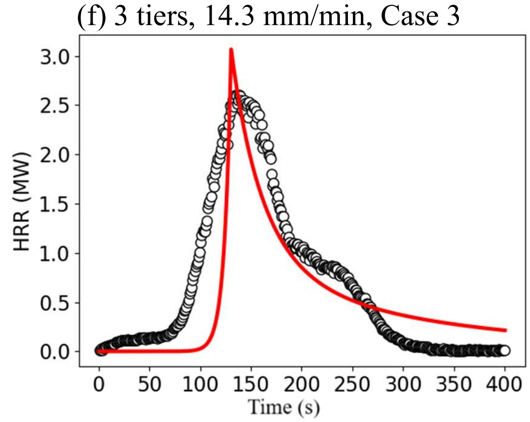

(h) 3 tiers, 24.5 mm/min, Case 4

Figure 35 Comparison of chemical HRR between experimental measurements and modeled results for plastic pallet commodity, based on the original zone-based model and the two-level hierarchical optimization framework calibrated using two lower-tier tests.

Table 33 Optimized zone model parameters for plastic pallet commodity based on the original zone-based model and the two-level hierarchical optimization framework calibrated using two lower-tier tests.

Case	Number of Tiers	WA rate (mm/min)	WA Time (s)	HRR at WA (MW)	p_1 (s)	p_4 (MW/m^2)	p_5 (kg/m^2)	A_{ini} (m^2)	t_{shift} (s)	β
1	2	6.1	112	3	49.59	0.31	0.56	0.09	1.12	0.14
1	2	10.2	129	2.6					0.28	0.11
2	2	6.1	112	3	38.41	0.53	0.41	0.04	0.58	0.14
2	2	16.3	122	3					0.26	0.07
3	3	12.2	188	3.6	32.48	0.01	1.55	0.04	1.23	0.94
3	3	14.3	140	3.1					0.3	0.81
4	3	12.2	188	3.6	19.20	0.17	0.91	0.005	5.99	0.96
4	3	24.5	138	3.6					0.05	0.33

8.3.5 Parameters Optimized from Experimental data of Cartoned Meat Tray (CMT) Commodity

Fig. 36 compares the chemical heat release rate between experimental data and model results obtained using optimized parameters for Cartoned Meat Tray commodity in the 2-tier and 3-tier configurations. Table 34 summarizes the optimized zone model parameters for Cartoned Meat Tray commodity.

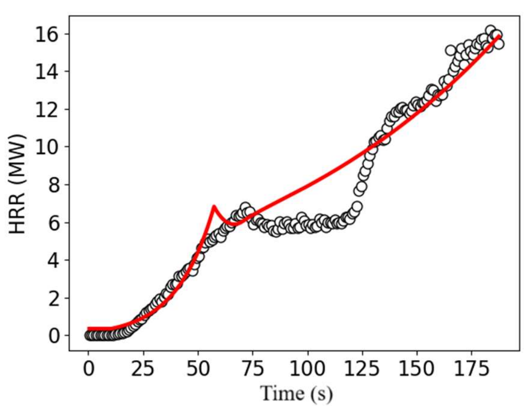

(a) 2 tiers, 4.1 mm/min, Case 1

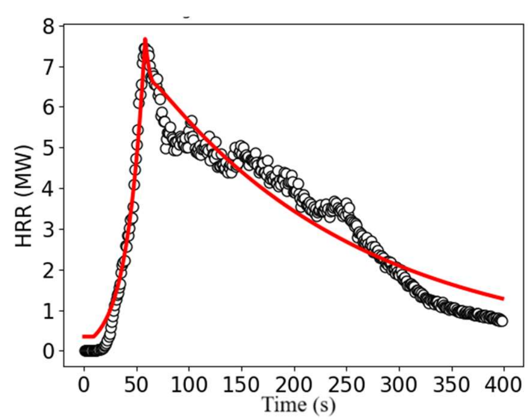

(b) 2 tiers, 6.1 mm/min, Case 1

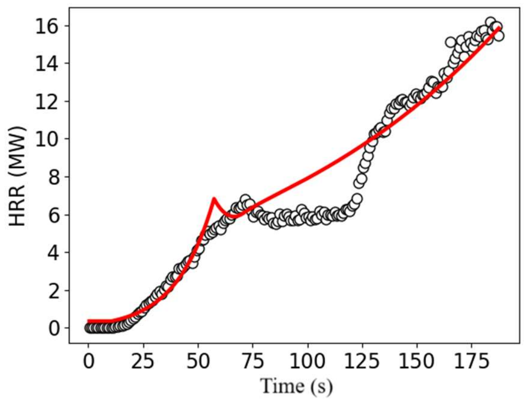

(c) 2 tiers, 4.1 mm/min, Case 2

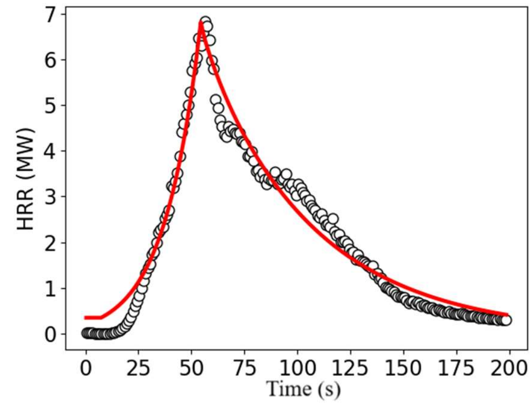

(d) 2 tiers, 10.1 mm/min, Case 2

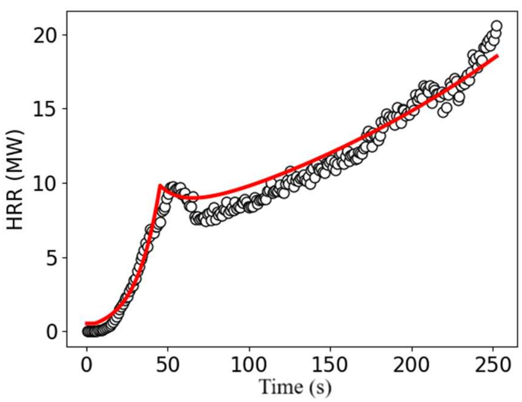

(e) 3 tiers, 12.2 mm/min, Case 3

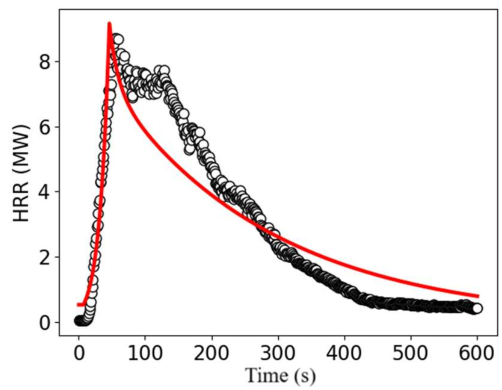

(f) 3 tiers, 14.2 mm/min, Case 3

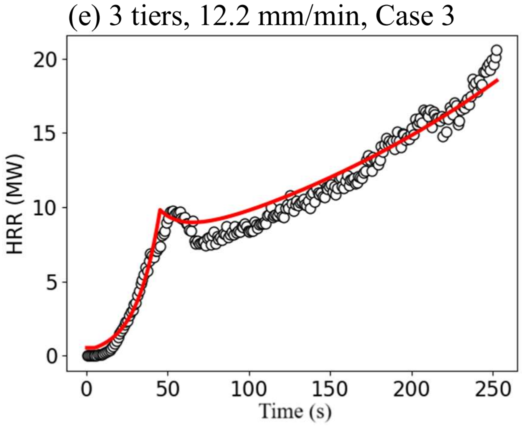

(g) 3 tiers, 12.2 mm/min, Case 4

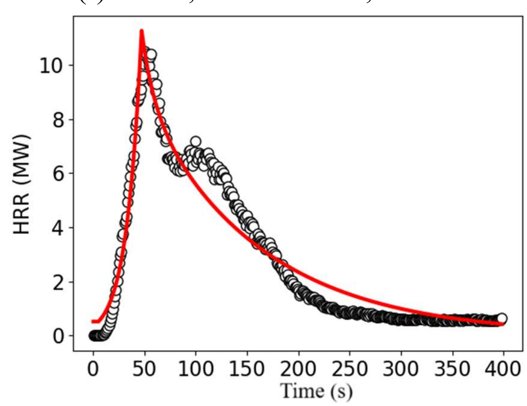

(h) 3 tiers, 15.5 mm/min, Case 4

Figure 36 Comparison of chemical HRR between experimental measurements and modeled results for cartoned meat tray commodity, based on the original zone-based model and the two-level hierarchical optimization framework calibrated using two lower-tier tests.

Table 34 Optimized zone model parameters for cartoned meat tray commodity based on the original zone-based model and the two-level hierarchical optimization framework calibrated using two lower-tier tests.

Case	**Number of Tiers**	**WA rate (mm/min)**	**WA Time (s)**	**HRR at WA (MW)**	p_1 **(s)**	p_4 **(MW/m^2)**	p_5 **(kg/m^2)**	A_{ini} **(m^2)**	t_{shift} **(s)**	**β**
1	2	4.1	71	9.3	14.41	0.83	0.39	0.04	0.66	0.99
1	2	6.1	58	10.2					0.42	0.62
2	2	4.1	71	9.3	16.30	0.18	0.44	0.50	9.07	0.98
2	2	10.1	56	9.3					5.52	0.36
3	3	12.2	53	13.4	21.84	0.59	0.99	0.18	0.56	0.84
3	3	14.2	57	11.9					1.23	0.74
4	3	12.2	53	13.4	20.66	0.17	0.99	0.66	1.21	0.96
4	3	15.5	50	14.4					1.36	0.77

8.3.6 Critical Delivered Fluxes for Different Types of Commodities

As shown in Fig. 37, the relationship between the water evaporation ratio and NCDF is demonstrated for two cases—one controlled and one uncontrolled—with the smallest water flux difference, as indicated by their case numbers in brackets. As the plots for cases with a larger water flux difference showed minimal variation, they were omitted to keep the report concise. The same methodology outlined in Section 6.1 was applied to estimate the CDF for all commodities, using parameters from lower-tier tests to predict higher-tier storage configurations.

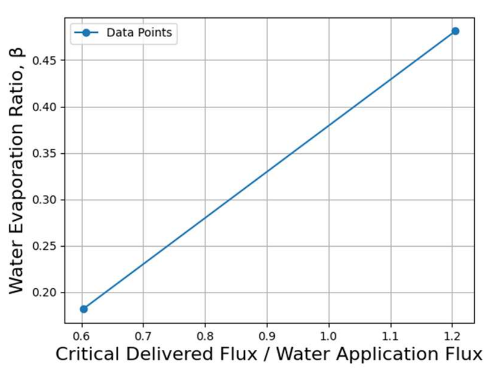

(a) Class 2 commodity, 3 tier, Case 1

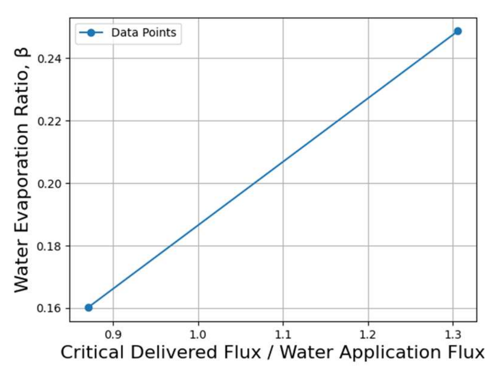

(b) Class 3 commodity, 2 tier, Case 1

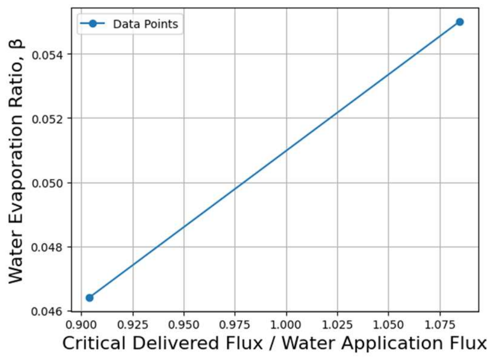

(c) Class 3 commodity, 3 tier, Case 3

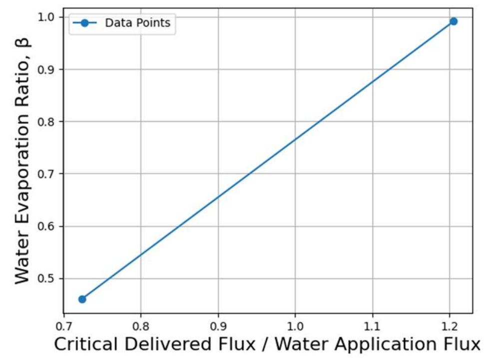

(d) Standard plastic commodity, 2 tier, Case 1

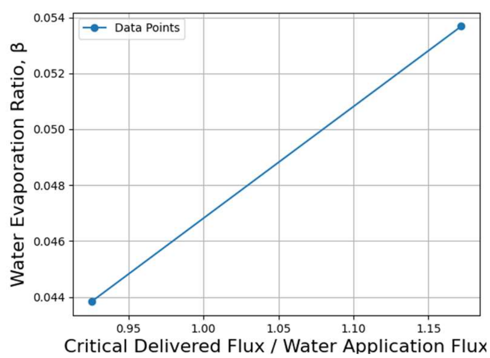

(e) Standard plastic commodity, 3 tier, Case 3

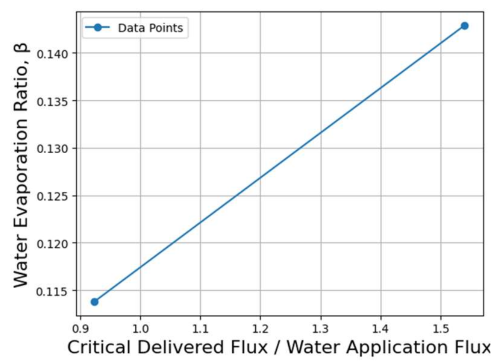

(f) Plastic Pallet commodity, 2 tier, Case 1

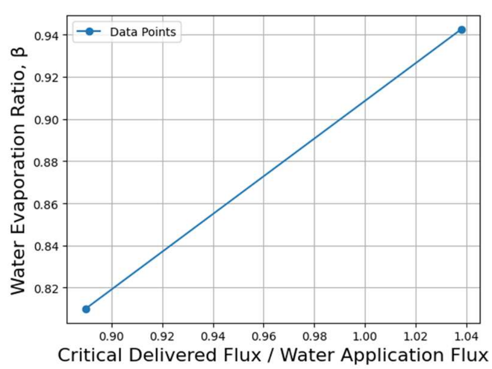

(g) Plastic Pallet commodity, 3 tier, Case 3

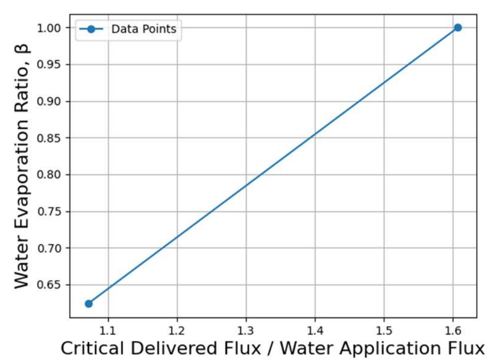

(h) CMT commodity, 2 tier, Case 1

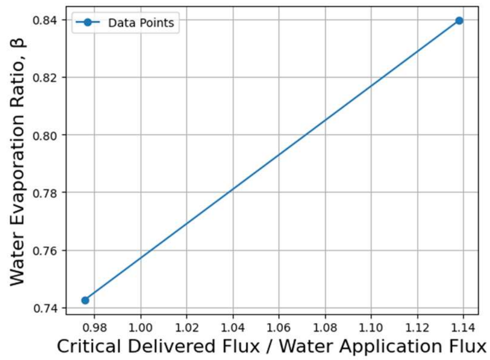

(i) CMT commodity, 3 tier, Case 3

Figure 37 Correlation between water evaporation ratio and normalized critical delivered flux based on the original zone-based model and the two-level hierarchical optimization framework calibrated using two lower-tier tests per commodity and storage tier configuration.

Table 35 summarizes the estimated CDF values for 5-tier storage using the zone model, compared against values calculated in Xin [12]. Using only two tests from 3-tier data, the model reliably predicted the CDF for Class 2, Class 3, Standard Plastic, and Cartoned Meat Tray commodities, with deviations within 30% a range considered acceptable for industrial fire protection applications. However, for Plastic Pallets, predictions based on two tests from both 2-tier and 3-tier data exceeded the 30% threshold. A possible explanation for this discrepancy is discussed in Section 7.1.5.

Furthermore, for most commodities, using 3-tier data revealed that test cases with larger differences in water application flux did not necessarily yield more accurate CDF predictions compared to cases with smaller flux differences, although the variation was generally not substantial.

Table 35 Predicted CDF values for 5-tier storage rack commodities based on the original zone-based model and the two-level hierarchical optimization framework calibrated using two lower-tier tests per commodity and storage tier configuration.

Commodity	**Number of Tiers**	**Predicted value using the model (mm/min)**	**Calculated value from Yibing (mm/min)**
Class 2	3	7.96 (2.92%)	8.2
Class 3	2 (Case1)	10.60 (47.23%)	20.09
	2 (Case2)	11.46 (42.95%)	
	3 (Case3)	15.06 (25.04%)	
	3 (Case4)	15.27 (23.99%)	
Standard Plastics	2 (Case1)	19.55 (17.78%)	23.78
	2 (Case2)	19.62 (17.49%)	
	3 (Case3)	19.71 (17.11%)	
	3 (Case4)	19.39 (18.46%)	
Plastic Pallets	2 (Case1)	15.88 (63.11%)	43.05
	2 (Case2)	16.41 (61.88%)	
	3 (Case3)	23.14 (46.24%)	
	3 (Case4)	22.97(46.64%)	
Cartoned MT	2 (Case1)	15.80 (41.61%)	27.06
	2 (Case2)	15.47 (42.83%)	
	3 (Case3)	23.8 (12.05%)	
	3 (Case4)	24.14 (10.79%)	

9. Model Limitations for Non-Cartoned Commodities and Required Modifications

While the two-level hierarchical optimization framework performed well for cartoned commodities, it did not generalize to non-cartoned commodities such as plastic pallets, which exhibit fundamentally different fire dynamics. This section investigates these limitations and introduces targeted model modifications. Section 9.1.1 presents observations from video analysis that characterize the distinct vertical fire spread behavior of plastic pallet commodity, and the subsequent subsections describe the model adaptations developed in response to these observations.

9.1.1 Experimental Observations from Video Analysis

As discussed in Section 8, the two-level hierarchical optimization framework performed well for all cartoned commodities. Using only two three-tier tests, the model was able to predict the 5-tier CDF with a relative error of less than 30%. However, this zone model did not generalize to non-cartoned commodities, as evidenced by the plastic pallet case examined in this study. The inability to accurately predict the 5-tier CDF for plastic pallets suggests that key differences in fire dynamics between cartoned and non-cartoned commodities are not captured in the original zone model formulation. To address this limitation, A detailed visual review of experimental recordings was conducted to compare the fire dynamics between cartoned commodities tests and plastic pallet commodity tests. The analysis was performed using three-tier tests at the lowest available applied water flux to clearly observe ignition behavior of upper tiers. Relative ignition times between tiers defined with respect to the ignition of the tier below were quantified to systematically characterize vertical fire propagation. The results are summarized in Table 36. The findings indicate that cartoned commodities exhibited rapid vertical fire spread, with ignition delays generally not exceeding approximately 24 s between successive tiers. In contrast, plastic pallet commodity demonstrated substantially slower vertical propagation, with ignition delays reaching up to approximately 100 s. These differences were further reflected in tier-wise burning behavior during suppression. In cartoned commodities, upper tiers ignited quickly and actively contributed to the overall burning. For plastic pallet configurations, however, ignition of upper tiers was significantly delayed, and in all cases the upper tiers did not ignite after water application began. Consequently, burning remained predominantly concentrated in the lower tiers.

Table 36 Tier-to-tier ignition delays observed from video analysis, defined as the ignition time of each tier relative to the preceding tier

Commodity types	Water flux (mm/min)	Tier 2 Ignition (s)	Tier 3 Ignition (s)
Class 2	4.1	24	14
Class 3	6.1	12	8
Standard plastic	12.2	16	10
Plastic pallets	6.1	100	No ignition
Cartoned meat tray	12.2	16	10

The experimentally observed fire behavior of plastic pallet commodities is inconsistent with a key assumption in the original zone-based model: that all tiers ignite simultaneously. Under this assumption, the measured total HRR is distributed among tiers during parameter calibration so that each tier contributes to fire growth from the outset, with lower-tier burning driving rapid upward spread. As a result, the model predicts rapid vertical fire development. Fig. 38 shows the predicted burning area versus time for each tier in the 3-tier plastic pallet configuration at a water flux of 14.3 mm/min, using the original zone-based model. As shown in Fig. 38, the third tier in a three-tier configuration eventually develops the largest burning area. This prediction is a direct consequence of the simultaneous ignition assumption.

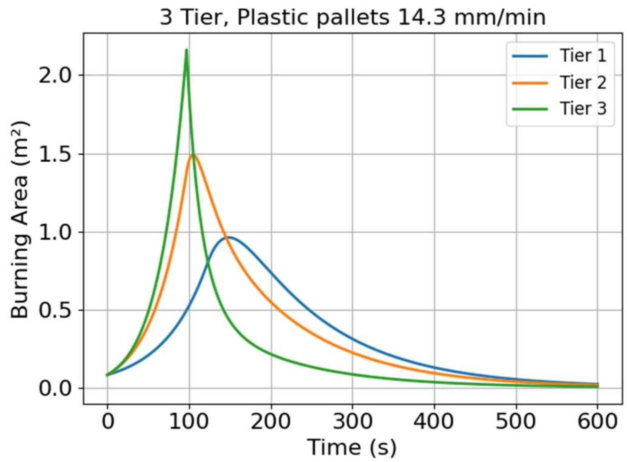

Figure 38 Predicted burning area (m²) versus time (s) for each tier in the 3-tier plastic pallet configuration at a water application flux of 14.3 mm/min using the original zone-based model

To evaluate this behavior against experimental observations, a quantitative comparison was conducted using burning areas estimated from frame-by-frame video analysis. As shown in Fig. 39, visible flame coverage within the porous plastic pallet structure was approximated at selected time instances, considering only flames within the pallet geometry (indicated by yellow color) and excluding those in the flue spaces (indicated by orange color) as a first-order approximation. Using this approach, the relative burning areas of Tiers 2 and 3 were calculated with respect to Tier 1 at the same time instance, and the results are displayed in Figure 40. The experimental data show that burning remains predominantly concentrated in Tier 1, with significantly smaller contributions from Tier 2 throughout the test duration, while Tier 3 does not ignite at any point. In contrast, the model substantially overpredicts upper-tier burning (as shown in Fig. 40), assigning a significant fraction of the total burning area to higher tiers, indicating that the assumed rapid vertical fire spread does not accurately represent the actual fire behavior of plastic pallet commodity.

This discrepancy has significant implications for fire suppression predictions. During parameter calibration, the current model distributes the measured total HRR disparity among all three tiers under the assumption of simultaneous ignition, with the upper tiers assigned a substantial share of the burning contribution. This leads the model to predict that a large portion of the fire is located in the upper tiers, which are reached first by sprinkler water with minimal obstruction and are therefore expected to extinguish rapidly. Suppression of the lower tiers is then assumed to occur after water passes downward, reduced by losses through the upper burning layers. In contrast, experimental observations of plastic pallet tests show that burning remains concentrated primarily in the lower tiers, while upper-tier involvement is much less significant. Because water must penetrate through the upper structure before reaching these lower burning regions, delivery is less efficient due to blockage and water loss. As a result, the actual water demand for suppression is higher than predicted by the model, leading to a systematic underestimation of the CDF for plastic pallet configurations.

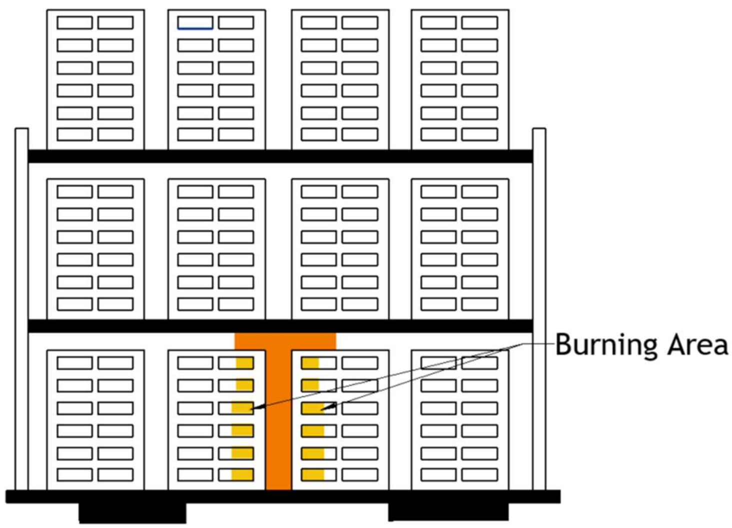

Figure 39 Schematic illustration of burning area identification for plastic pallet commodity based on video analysis.

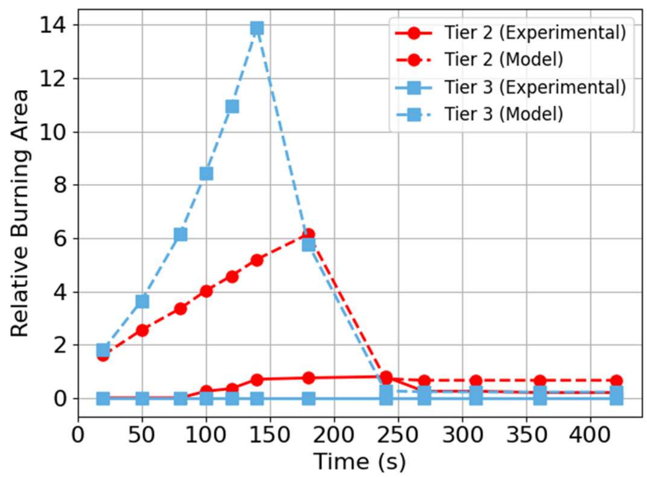

Figure 40 Comparison of model-predicted and experimentally estimated relative burning areas at tier 2 and tier 3 for plastic pallet commodity in 3-tier storage, normalized to the tier 1 burning area.

9.1.2 Model Improvements Based on Experimental Insights

The findings from section 9.1.1 motivated the incorporation of new physical characteristics into the zone-based framework to better represent vertical spread dynamics for each commodity. Two primary modifications were introduced:

Explicit Vertical Ignition Delay. Experimental results from the three-tier plastic pallet tests showed that Tier 2 ignited approximately 100 s after Tier 1, while Tier 3 did not ignite. In contrast, the other commodity types exhibited relatively small inter-tier ignition delays, and ignition consistently propagated to Tier 3. These experimentally observed tier-to-tier ignition delays, summarized in Table 36, were incorporated into the model. For tiers beyond those measured, the Tier 2–Tier 3 ignition delay was applied consistently to all subsequent tiers (e.g., Tier 3–Tier 4 and Tier 4–Tier 5). Incorporating this delay reduces unrealistic early burning in upper tiers and improves agreement with observed vertical fire spread behavior across commodities.

Suppression-Driven Ignition Cut-Off. Video analysis of the plastic pallet tests demonstrated that upper tiers did not ignite once water application began. Accordingly, the model was modified to prevent ignition of higher tiers after the onset of suppression. This modification ensures that the simulated HRR distribution among tiers reflects the experimentally observed behavior, where burning remained primarily confined to the lower tiers after water application. This modification was introduced specifically for the plastic pallet commodity, as all other commodities exhibited rapid vertical fire spread, where the upper tiers typically ignited either before or shortly after water application. Their rapid vertical fire spread is primarily attributed to the presence of exterior cartons in those commodities, which promote flame propagation between tiers.

9.2 Parameters Optimized using Two-level Hierarchical Optimization with tier ignition delay

This section presents the re-estimation of model parameters using 3-tier experimental data, incorporating the two model modifications described in Section 9.1.2: the explicit tier-to-tier ignition delay applied to all commodities and the suppression-driven ignition cut-off applied specifically to the plastic pallet commodity. The analysis follows the same two-level hierarchical optimization framework described in Section 9.3 and is based on two 3-tier experiments, one uncontrolled and one controlled for each type of commodity. This choice is motivated by the observation that 2-tier-based predictions consistently show larger deviations from experimental 5-tier CDF values across all commodity types (as discussed in Sections 7.2.6 and 8.3.6). Moreover, the refinements introduced in Section 10.1.2 are derived directly from 3-tier observations; applying them using 2-tier calibration data would introduce additional uncertainty without providing meaningful new insight. Table 37 summarizes the optimized zone model parameters for the representative commodities obtained from the two 3-tier tests, and Fig. 41 compares the experimental and model-replicated chemical heat release rates for various commodities. The modeled heat release rates successfully capture the distinct trends of all commodities and show close agreement with the experimental data.

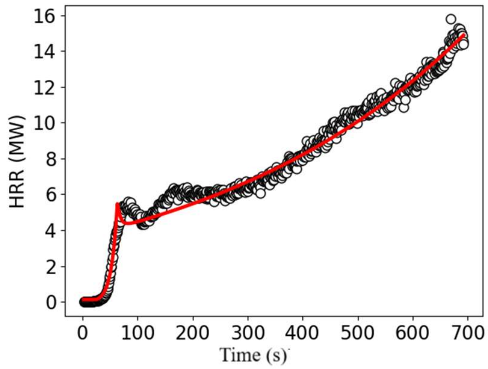

(a) Class 2, 3 tiers, 4.1 mm/min

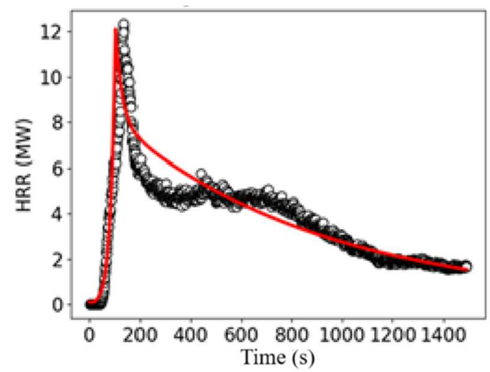

(b) Class 2, 3 tiers, 8.1 mm/min

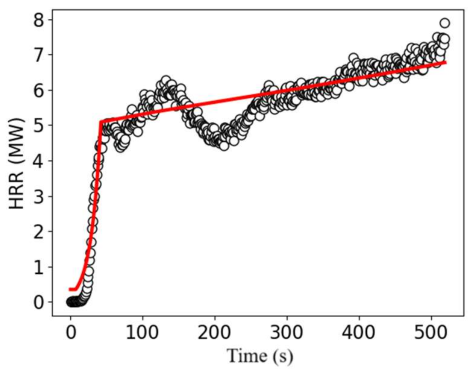

(c) Class 3, 3 tiers, 10.1 mm/min

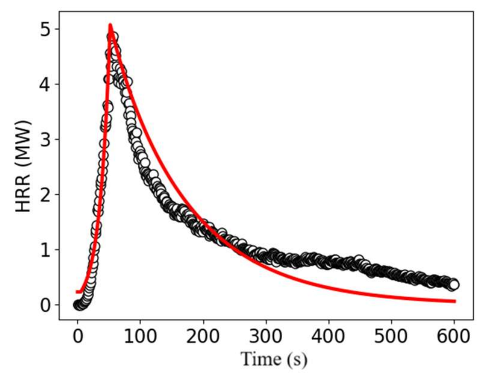

(d) Class 3, 3 tiers, 12.2 mm/min

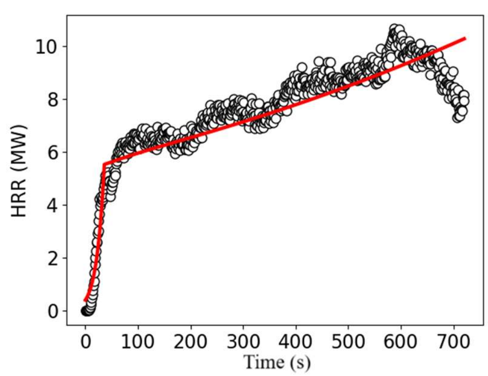

(e) Standard Plastic, 3 tiers, 12.2 mm/min

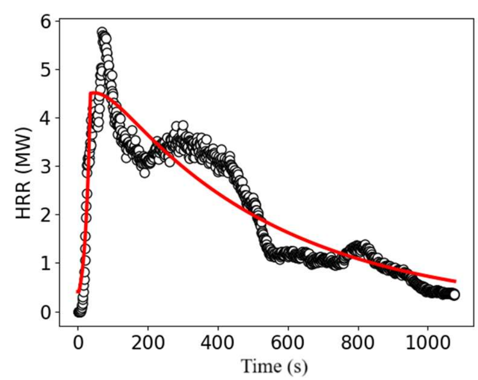

(f) Standard Plastic, 3 tiers, 14.2 mm/min

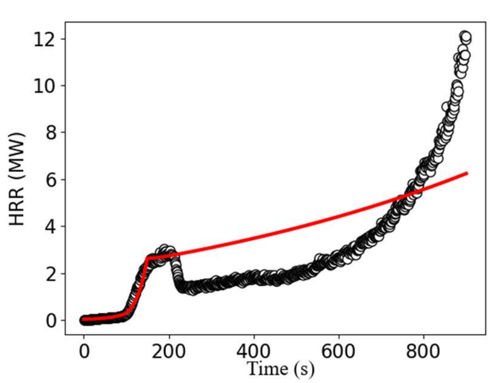

(g) Plastic Pallets, 3 tiers, 12.2 mm/min

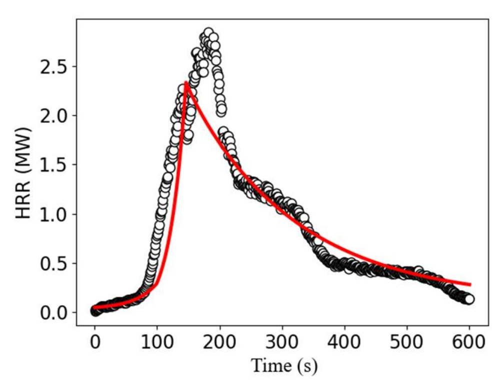

(h) Plastic Pallets, 3 tiers, 14.2mm/min

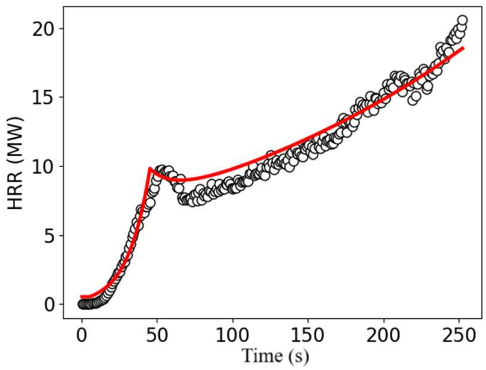

(i) Cartoned MT, 3 tiers, 12.2 mm/min

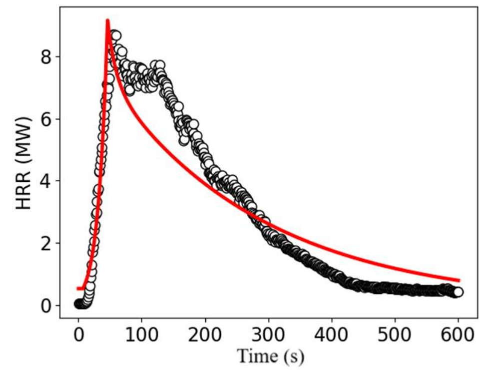

(j) Cartoned MT, 3 tiers, 14.2 mm/min

Figure 41 Comparison of chemical HRR between experimental measurements and modeled results based on the improved zone-based model and the two-level hierarchical optimization framework (The value in the plot caption, expressed in mm/min, is the water application flux)

Table 37 Optimized zone model parameters based on the improved zone-based model and the two-level hierarchical optimization framework

Commodity	**WA rate (mm/min)**	**WA Time (s)**	**HRR at WA (MW)**	p_1 **(s)**	p_4 **(MW/m^2)**	p_5 **(kg/m^2)**	A_{ini} **(m^2)**	t_{shift} **(s)**	**β**
Class 2	4.1	103	7.0	16.17	0.86	0.146	0.006	17.7	0.34
Class 2	8.1	135	12.0	16.17	0.86	0.146	0.006	0.46	0.19
Class 3	10.1	58	6.9	18.98	0.25	0.22	0.04	0.06	0.13
Class 3	12.1	52	7.5	18.98	0.25	0.22	0.4	0.21	0.11
Standard Plastic	12.1	43	7.2	17.05	0.39	0.30	0.6	0.04	0.19
Standard Plastic	14.2	47	5.9	17.05	0.39	0.30	0.6	0.11	0.14
Plastic Pallets	12.2	188	3.6	34.7	0.1	1.2	0.14	0.4	0.38
Plastic Pallets	14.3	140	3.1	34.7	0.1	1.2	0.14	0.3	0.38
Cartoned MT	12.2	53	13.4	24.30	0.58	0.71	0.47	0.19	0.36
Cartoned MT	14.2	57	11.9	24.30	0.58	0.71	0.47	0.48	0.34

9.3 Estimation of Critical Delivered Fluxes for Different Types of Commodities using Two-level Hierarchical Optimization with tier ignition delay

Fig. 42 shows plots that display the correlation between the water evaporation ratio and the NCDF across all lower tier tests for various commodities, the evaporation ratio consistently increases with NCDF.

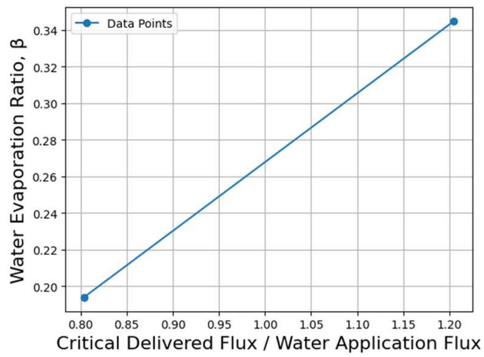

(a) Class 2 commodity, 3 tier

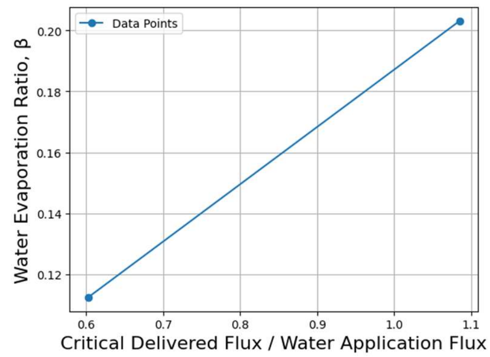

(b) Class 3 commodity, 3 tier

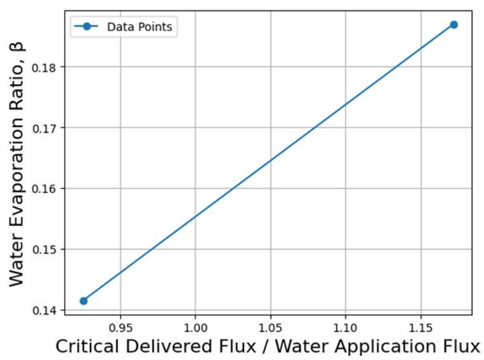

(c) Standard plastic commodity, 3 tier

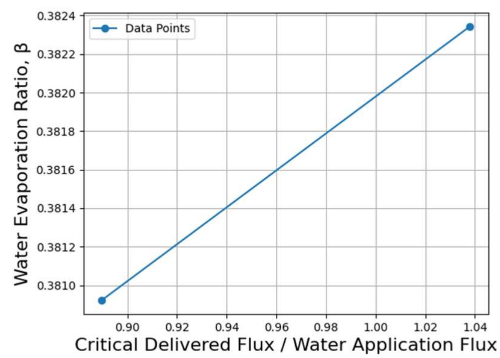

(d) Plastic pallet commodity, 3 tier

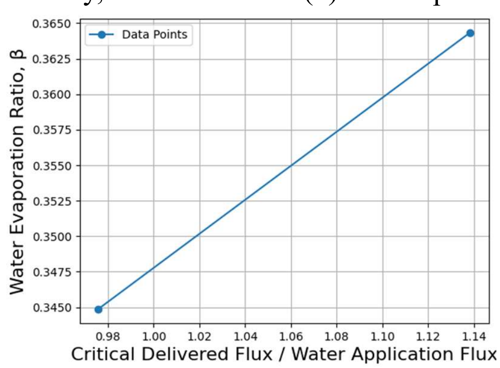

(e) Cartoned MT commodity, 3 tier

Figure 42 Correlation between water evaporation ratio and normalized critical delivered flux across different commodities based on the improved zone model and the two-level hierarchical optimization framework

The same methodology is applied to estimate the CDF for 5-tier storage across all commodities, using parameters derived from lower-tier tests. To estimate the β, linear interpolation is performed to determine the β value at NCDF = 1, based on the relationship between the water evaporation ratio and NCDF, as shown in Fig. 42. Table 38 provides a summary of the estimated CDF for 5-tier storage using the new implementation of the zone model. In Table 38, the values in parentheses in the 'Predicted value' column represent the percentage deviation of the modeled CDF from the experimental CDF. For all representative commodities considered, the model-predicted 5-tier CDF values obtained using the 3-tier experimental data were within reasonable agreement with the CDF values calculated from experiments for tier 5. The deviations were within acceptable limits for industrial fire protection applications, indicating that the model can provide reasonable CDF predictions using only two lower-tier tests.

Table 38 Predicted CDF values for different commodities in 5-tier storage racks based on the improved zone model and the two-level hierarchical optimization framework

Commodity	Number of Tiers	Predicted value using the model (mm/min)	Calculated value from experiment (mm/min)
Class 2	3	7.71 (5.97%)	8.2
Class 3	3	16.53(17.72%)	20.09
Standard Plastics	3	21.14 (11.10%)	23.78
Plastic Pallets	3	40.41 (6.13%)	43.05
Cartoned Meat Tray	3	22.43 (17.11%)	27.06

10.Conclusions

This thesis provides an in-depth analysis and refinement of a zone-based modelling approach for predicting Critical Delivered Flux in commodity fire scenarios. While originally formulated for Class 2 commodities, the model's scope was successfully extended to encompass a wider range of commodities, including Class 3, standard plastics, plastic pallets, and cartoned meat tray commodities. A key methodological advancement was the implementation of a two-level hierarchical optimization framework, which distinguishes between commodity-specific and test-specific parameters, thereby improving the model's flexibility and robustness across diverse cartoned commodities; however, the same approach was not consistently reliable for plastic pallet commodities. Additional analysis revealed distinct vertical fire spread dynamics for plastic pallets, necessitating targeted modifications to the zone-based framework. After incorporating these adjustments, the revised model produced improved CDF predictions with good agreement to experimental observations. This study also examines methods for identifying water application time from test data. Accurate identification is critical, as it defines the transition between free-burn and suppression and impacts parameter calibration from lower-tier experiments, with errors propagating into the predicted CDF for high-tier storage configurations. When direct measurements are unavailable, visual observation of the total HRR curve is the most reliable approach. In addition to water application time, a sensitivity analysis shows that reducing the final test duration has minimal impact on both experimentally derived and model-predicted CDF values.

In the zone model, storage racks are idealized as vertically arranged “fuel zones,” each corresponding to a tier. Fire ignition begins at the bottom zone and propagates upward and laterally, with spread and suppression processes governed by simplified energy and mass conservation equations. The model accounts for key physical phenomena including heat transfer, water suppression effects, and evaporation. To estimate the CDF for high-tier storage configurations, parameters are first optimized using multiple individual lower-tier experiments. The optimized values are then averaged or interpolated and used as model inputs for high-tier storage configurations. CDF is identified through simulations by incrementally increasing the water flux until the threshold condition at which fire growth is just suppressed is reached.

Model performance was validated using experimental data across different commodity types. Results demonstrated strong agreement between predicted and experimental CDFs for most 5-tier storage cases. However, the model was less reliable for plastic pallet commodities, indicating that further refinement is needed to address their distinct fire behavior or their unique interaction with water. Recognizing the need to reduce testing burdens, the study also evaluated a simplified strategy using only two experimental cases (one controlled and one uncontrolled) per configuration. This approach yielded acceptable accuracy for all commodities except plastic pallets, with 3-tier input data generally producing more accurate estimates than 2-tier data. When using 3-tier data, predicted CDFs fell within 30% of reference values for most commodities; however, accuracy varied by commodity and was generally lower than the approach utilizing all available lower-tier data for optimisation. Nonetheless, these results support the model's broader applicability across diverse storage scenarios.

To support model application to materials with unknown burning characteristics, a two-level optimization framework was introduced. At the first level, parameters such as ignition delay (p_1), suppression delay times x evaporation flux (p_5), power flux (p_4), and initial burning area (A_{ini}) were optimized based on commodity properties using lower-tier tests. At the second level, test-specific factors such as time shift (t_{shift}) and water evaporation ratio (β) were fine-tuned to minimize differences between simulated and experimental results. This structured parameterization enhances model consistency while enabling adaptation to a broader range of storage scenarios. The new implementation framework provides parameter estimates that are better grounded in the physical properties of each commodity — most notably through the treatment of p_4 as a commodity-specific parameter rather than a fixed preset value — thereby improving theoretical interpretability. In terms of predictive accuracy, the two-level framework yielded lower CDF deviations for most cartoned commodities when using 3-tier data; however, improvements were marginal or absent for Class 2 commodity, and neither framework reliably captured the fire dynamics of plastic pallets.

Using the two-level hierarchical optimization framework, additional analysis was performed to evaluate the impact of varying test case combinations. Specifically, the same uncontrolled test was paired with different controlled tests to assess the method's sensitivity to case selection. Furthermore, for most commodities, using 3-tier data showed that test pairs with larger water flux differences did not necessarily result in more accurate CDF predictions compared to those with smaller flux differences, although the variation in accuracy was generally minor.

A detailed video analysis of plastic pallet commodity revealed fundamentally different vertical fire spread behavior compared to cartoned commodities, characterized by slower upward propagation and a dominant heat release contribution from the lower storage tiers. These observations provided important physical insight into the burning dynamics of the commodity and were explicitly incorporated into the zone-based modeling framework. By accounting for these distinct vertical spread characteristics from the experiments, the revised model achieved substantially improved agreement between predicted and experimental CDF values for most of the representative commodities, bringing the predictions within an acceptable range of accuracy and enhancing confidence in the model's applicability to noncartoned commodities.

In summary, this work not only verifies the applicability of the zone-based model for evaluating critical delivered flux across different commodities but also improves and extends the existing framework through the development of a structured, hierarchical optimization methodology and by including experimental observations into the model. The enhanced approach strengthens parameter estimation, improves predictive consistency across different commodities, and reduces reliance on extensive experimental testing by leveraging a limited set of representative cases. By integrating these methodological improvements with experimental validation, the study provides a more robust, scalable, and practically applicable tool for estimating CDF, ultimately supporting more informed sprinkler system design and fire protection strategies in modern warehouse environments. Several limitations of the current study warrant acknowledgement. For plastic pallet commodities, the model required targeted modifications to account for distinct vertical spread behaviour, and further validation across a broader range of non-cartoned commodity types is needed. Additionally, the vertical tier ignition delay identified in this work is based on a limited dataset and should be verified with additional experiments. Future work should focus on addressing those limitations.

11.References

[1] National Fire Protection Association (NFPA), Warehouse Structure Fires, NFPA Fire Analysis and Research Division, Quincy, MA, USA, 2025.

[2] International Code Council, International fire code, 2018.

[3] National Fire Protection Association, NFPA 13, Standard for the installation of sprinklers systems, 2016.

[4] F.M. Global, FM Global Property Loss Prevention Data Sheets 8-1, Commodity classification, April 2015.

[5] P.J. Chiarello, J.M.A. Troup, Fire Products Collector Test Procedure for Determining the Commodity Classification of Ordinary Combustible Products, Factory Mutual Research Corporation, 1990 Report No. JI 0ROE5. RR.

[6] M. Arvidson, A. Lönnermark, Commodity Classification Tests of Selected Ordinary Combustible Products (SP Report 2002:03), SP Fire Technology, Borås, Sweden, 2002, p. 12.

[7] CEN, prEN 12845-1: Fixed firefighting systems – Automatic sprinkler systems – Part 1: Design, installation and maintenance. European Committee for Standardization, Brussels.

[8] P.K. Wu, Heat Flux Pipe in Large-Scale Fire Tests, Fire Safety Science, Proceedings of the Eighth International Symposium, International Association for Fire Safety Science, 2005, pp. 1413–1424.

[9] M.J. Gollner, K. Overholt, F.A. Williams, A.S. Rangwala, J. Perricone, Warehouse Commodity Classification from Fundamental Principles. Part I: commodity & Burning Rates, Fire Saf. J. 46 (2011) 305–316.

[10] K. Overholt, M.J. Gollner, F.A. Williams, A.S. Rangwala, J. Perricone, Warehouse Commodity Classification from Fundamental Principles. Part II: flame Height Prediction, Fire Saf. J. 46 (2011) 317–329.

[11] Y. Xin, F. Tamanini, Assessment of Commodity Classification for Sprinkler Protection Using Representative Fuels, Fire Safety Science – in: Proceedings of the Ninth International Symposium, International Association for Fire Safety Science, pp. 527–538.

[12] Xin, Yibing, Effects of storage height on critical delivered flux of representative fuels. Fire Safety Journal 91 (2017): 624-632.

[13] Han, Dong, and Yibing Xin. "Evaluation of a zone-based model for commodity classification using a representative fuel." Proceedings of the Combustion Institute 38.3 (2021): 4655-4663.

[14] Kung H-C, You H-Z, Spaulding RD. “Ceiling flows of growing rack storage fires.” Twenty-first Symposium (International) on Combustion/The Combustion Institute (1986) pp. 121-128.

[15] Storn R, Price K (1997) Differential evolution – a simple and efficient heuristic for global optimization over continuous spaces. Journal of Global Optimization 11:341–359. https://doi.org/10.1023/A:1008202821328